Advanced imaging biomarkers in endometrial cancer

Sigmund Ytre-Hauge

Thesis for the degree of Philosophiae Doctor (PhD)
University of Bergen, Norway
2019

UNIVERSITY OF BERGEN

Advanced imaging biomarkers in endometrial cancer

Sigmund Ytre-Hauge

Thesis for the degree of Philosophiae Doctor (PhD)
at the University of Bergen

Date of defense: 11.12.2019

Year: 2019

Title: Advanced imaging biomarkers in endometrial cancer

Name: Sigmund Ytre-Hauge

Print: Skipnes Kommunikasjon / University of Bergen

Scientific environment

This PhD project is derived from the Department of Clinical Medicine (K1) at the University of Bergen and has been carried out within the context of Bergen Gynecologic Cancer Research Group, Bergen Abdominal Imaging Research Group and Mohn Medical Imaging and Visualization Centre. Research training has also been provided by the Norwegian Research School in Medical Imaging (MedIm).

My main supervisor, Prof. Ingfrid Haldorsen, is the head of Bergen Abdominal Imaging Research Group and a principal investigator at Mohn Medical Imaging and Visualization Centre leading a project entitled "Precision imaging in gynecologic cancer". Haldorsen is also a consultant radiologist at the Department of Radiology at Haukeland University Hospital, where the imaging studies in this project have been conducted.

Bergen Gynecologic Cancer Research Group, comprising around 25 members (including PhD students, research fellows, postdoctoral fellows, medical students, study nurses, technicians and professors), is currently led by Prof. Camilla Krakstad. Former leaders are Prof. Jone Trovik (my co-supervisor) and Prof. Helga Salvesen (my co-supervisor), the latter being the founder of the group. The research group is closely associated with the Department of Gynecology and Obstetrics at Haukeland University Hospital and is also part of Centre for Cancer Biomarkers (CCBIO), a Norwegian Centre of Excellence at the University of Bergen, focusing on translational research, primarily biomarkers and personalized cancer treatment. CCBIO is led by Prof. Lars A. Akslen.

One of the subprojects, exploring MR spectroscopy in endometrial cancer patients, has been carried out in close collaboration with a research group led by Prof. Tone F. Bathen at the Department of Circulation and Medical Imaging at the Norwegian University of Science and Technology (NTNU), Trondheim. Associate professor Øyvind Salvesen at Unit for Applied Clinical Research, Department of Cancer Research and Molecular Medicine, NTNU has provided statistical expertise throughout this PhD project.

Acknowledgements

I would like to thank the University of Bergen for accepting me in their PhD programme, thereby giving me the opportunity to take this long and interesting journey. The staff at the Department of Clinical Medicine has been very helpful with practical aspects.

Funding was provided mainly through The Western Norway Regional Health Authority, but I have also received support from the Department of Radiology at Haukeland University Hospital and from the Norwegian Radiologist Association (The Ødegaards' legacy).

During my time as a resident at the Department of Radiology at Haukeland, Prof. Ingfrid Haldorsen introduced me to gynecological imaging and invited me to join their research group. As my main supervisor, you have been by far the most important pillar in my PhD project, Ingfrid. Not only having a vast knowledge in radiology, deep scientific insights and an enormous working capacity, but also a warm heart and a friendly smile – making every problem seem smaller. I cannot thank you enough for everything you have done – and for the person you are.

Prof. Helga Salvesen was the founder of Bergen Gynecologic Cancer Research Group and a true leading star of our research environment when I started working with my PhD project. I am proud that Helga was my co-supervisor during the first years of my project, and I am very grateful for having experienced Helga's professional attitude, confidence and warmth. When Helga unexpectedly passed away in January 2016, it was a tragic loss to our research group. I would like to thank each member of the group for keeping up your dedicated work in the aftermath of the 2016 winter. In particular, I want to thank Camilla Krakstad, now leading the group steadily, and of course, special thanks to Jone Trovik for willingly replacing Helga as my co-supervisor – in times of heavy burdens. I admire your clear mind and your enthusiasm, Jone. And your good laughter is truly antidepressive!

My colleagues at the Department of Radiology at Haukeland – and more recently, colleagues at the local hospital in Volda, have also meant a lot to me. Especially I would like to thank Jenny Husby for close collaboration in the first subproject of this

thesis, Inger Johanne Magnussen for close collaboration and for being a cornerstone in urogenital imaging at our department for decades, and Prof. Jarle Rørvik for being such a strong voice for imaging research at Haukeland. Sadly, Jarle unexpectedly passed away in 2018 just a few months after our common trip to RSNA, Chicago, where I presented my research. Thanks for always being encouraging, Jarle. From the management at Haukeland, I would like to thank Kari Kuvås and Aslak Aslaksen for their patience and support. The radiographer Eva Øksnes and the physicists Renate Grüner and Erling Andersen have also been very helpful in my PhD project.

All co-authors of the four papers comprising this thesis also deserve many thanks (listed in alphabetical order): Tone F. Bathen, Line Bjørge, Julie A. Dybvik, Morteza Esmaeili, Kristine E. Fasmer, Balaji Ganeshan, Renate Grüner, Ingfrid S. Haldorsen, Jenny Husby, Erling Høivik, Camilla Krakstad, Arvid Lundervold, Inger Johanne Magnussen, Helga B. Salvesen, Øyvind O. Salvesen, Torill E. Sjøbakk, Ingunn M. Stefansson, Jone Trovik, Henrika M. J. Werner and Kathrine Woie.

Special thanks to Morteza and the rest of Tone Bathen's research group for great hospitality in Trondheim during our collaboration on MR spectroscopy. Statistician Øyvind O. Salvesen also deserves special thanks for your patience during long telephone calls and meetings. I might have made it without you, but then, probability is high it would all be erroneous…

It is also important to acknowledge all the women who voluntarily participated in our research projects. Their willingness, even in times of severe disease, are fundamental to our work, and eventually, I hope this group of patients will benefit.

Warm thanks to my mom and dad – for everything! Thanks to my brothers Helge, Vidar and Kristian proving that my genes are capable. (On my own behalf, I have had doubts…) And last, but not least, a big hug to the woman of my life, Synne, and our kids Håkon, Ragni Sofie, Trygve and Solveig. Believe it or not, you were always on my mind :)

HELSE VEST

MMIV

Abstract

Background: Endometrial cancer is the most common gynecological cancer in high-developed regions of the world, and the incidence has been increasing over the last half century, largely driven by a concurrent increase in population obesity. Primary treatment is surgical in most cases, but only limited preoperative risk stratification has been applied in traditional clinical practice. To enable more individualized treatment, improved methods for preoperative tumor characterization are highly warranted.

Aim: To identify and evaluate new imaging markers that may aid in the preoperative risk stratification and tailoring of treatment in endometrial cancer.

Material and methods: The studies included in this thesis are based on collected imaging-, clinical- and histological data from endometrial cancer patients treated at Haukeland University Hospital during April 2009 to November 2013. Standardized MR imaging data were acquired for 216 prospectively included patients with histologically confirmed endometrial cancer. From this cohort, four different subcohorts were included in study I-IV. In **Paper I**, three radiologists independently measured tumor size on conventional MR images for 212 patients. In **Paper II**, metabolic features were extracted from MR spectroscopy performed on 77 patients. In **Paper III**, texture features were extracted from MR images, using a filtration-histogram technique in 180 patients. In **Paper IV**, CT imaging data were retrospectively collected and texture features extracted for 155 patients. In all studies, the respective imaging markers were evaluated as predictors of histopathological high-risk features and survival.

Results: The interobserver variability for MRI-measured tumor size is very low (ICC 0.78-0.85) (**Paper I**). AP diameter greater than 2 cm independently predicts deep

myometrial invasion (OR 6.7, p<0.001) and CC diameter greater than 4 cm independently predicts lymph node metastases (OR 4.9, p=0.009) when adjusting for conventional MRI reading results and risk status based on preoperative endometrial biopsy (**Paper I**). CC tumor diameter has an independent impact on recurrence- and progression-free survival (adjusted HR 1.04, p=0.009) (**Paper I**).

Tumor tissue has significantly higher MR spectroscopy-derived ratios for tCho/Creatine, tCho/Water and tCho/Noise than normal myometrial tissue (p<0.001 for all) (**Paper II**). High tumor tCho/Water ratio is also significantly associated with high histological tumor grade in endometrioid tumors (p=0.02) (**Paper II**). No significant associations are found between tumor tCho-levels and recurrence- and progression-free survival (**Paper II**).

When performing texture analysis of MR images, high tumor entropy in ADC-maps independently predicts deep myometrial invasion (OR 3.2, p<0.001), and high MPP in T1c images independently predicts high-risk histological subtype (OR 1.01, p=0.004) when adjusting for MRI-measured tumor volume, conventional MRI reading results and biopsy risk status (**Paper III**). Furthermore, high kurtosis in T1c images independently predicts reduced recurrence- and progression-free survival (adjusted HR 1.5, p<0.001) (**Paper III**).

When performing texture analysis of CT images, high tumor entropy independently predicts deep myometrial invasion (OR 3.7, p=0.008) and cervical stroma invasion (OR 3.9, p=0.02) when adjusting for MRI-measured tumor volume, conventional MRI reading results, age and biopsy risk status (**Paper IV**). High value of MPP (MPP5>24.2) independently predicts high-risk histological subtype (OR 3.7, p=0.01) (**Paper IV**). High tumor kurtosis tends to independently predict reduced recurrence- and progression-free survival (adjusted HR 1.1, p=0.06) (**Paper IV**).

Conclusions: Tumor size can be measured on preoperative conventional MRI with very low interobserver variability. Large tumor size predicts deep myometrial invasion,

lymph node metastases and poor outcome in endometrial cancer, and thus, imaging markers based on tumor size may improve preoperative risk stratification (**Paper I**).

High choline levels, measured by MR spectroscopy, differentiate tumor tissue from normal tissue in endometrial cancer patients, but do not have significant prognostic value in our study (**Paper II**).

MRI-derived tumor texture parameters predict deep myometrial invasion, high-risk histological subtype, and reduced recurrence- and progression-free survival in endometrial cancer (**Paper III**). CT-derived tumor texture features predict deep myometrial invasion and cervical stroma invasion in endometrial cancer, and also tend to predict high-risk histological subtype and survival (**Paper IV**). The image texture features entropy, kurtosis and MPP seem to reflect tumor heterogeneity and may aid in preoperative risk assessment (**Paper III and IV**).

List of publications

I. Ytre-Hauge S, Husby JA, Magnussen IJ, Werner HM, Salvesen ØO, Bjørge L, Trovik J, Stefansson IM, Salvesen HB, Haldorsen IS. Preoperative tumor size at MRI predicts deep myometrial invasion, lymph node metastases, and patient outcome in endometrial carcinomas. International Journal of Gynecological Cancer 2015; 25:459-466.

II. Ytre-Hauge S, Esmaeili M, Sjobakk TE, Grüner R, Woie K, Werner HM, Krakstad C, Bjørge L, Salvesen ØO, Stefansson IM, Trovik J, Bathen TF, Haldorsen IS. In vivo MR spectroscopy predicts high tumor grade in endometrial cancer. Acta Radiol 2018; 59:497-505.

III. Ytre-Hauge S, Dybvik JA, Lundervold A, Salvesen ØO, Krakstad C, Fasmer KE, Werner HM, Ganeshan B, Høivik E, Bjørge L, Trovik J, Haldorsen IS. Preoperative tumor texture analysis on MRI predicts high-risk disease and reduced survival in endometrial cancer. Journal of Magnetic Resonance Imaging 2018; 48:1637-1647.

IV. Ytre-Hauge S, Salvesen ØO, Krakstad C, Trovik J, Haldorsen IS. Tumor texture features from preoperative CT predict high-risk disease in endometrial cancer. Submitted to Acta Radiologica June 2019.

Contents

9. REFERENCES

STUDY I-IV

APPENDIX

1 Abbreviations

1H	Proton (1H is the most common isotope of hydrogen with one proton and no neutrons.)
2D	2-dimensional
3D	3-dimensional
ADC	Apparent diffusion coefficient
AP	Anteroposterior
AUC	Area under the curve
Ax	Axial
Ax obl	Axial oblique
b1000	b-value of 1000 (measure for degree of diffusion weighting in DWI)
BMI	Body mass index
CA-125	Cancer antigen 125
CC	Craniocaudal
ce	Contrast-enhanced
CI	Confidence interval
Cor	Coronal
CSI	Chemical shift imaging
CT	Computed tomography

CTTA	CT texture analysis
DCE	Dynamic contrast-enhanced
DNA	Deoxyribonucleic acid
DWI	Diffusion weighted imaging
EC	Endometrial cancer
ER	Estrogen receptor
ESGO	European Society of Gynaecological Oncology
ESMO	European Society of Medical Oncology
ESUR	European Society of Urogenital Radiology
F	Fluorine
FDG	Fluorodeoxyglucose
FIGO	International Federation of Gynecology and Obstetrics
FS	Fat saturated
GDF-15	Growth differentiation factor 15
HNPCC	Hereditary nonpolyposis colorectal cancer
HR	Hazard ratio
ICC	Intraclass correlation coefficient
IrRC	Immune-related Response Criteria
KRAS	Kirsten rat viral sarcoma homolog
L1CAM	L1 cell adhesion molecule

LVSI	Lymphovascular space invasion
MDC	Minimal detectable change
min	Minutes
ml	Milliliter
mm	Millimeter
msec	Millisecond
MoMaTEC	Molecular Markers in Treatment of Endometrial Cancer
MPP	Mean of positive pixels
MR	Magnetic resonance
MRI	Magnetic resonance imaging
MRS	Magnetic resonance spectroscopy
MRTA	MR texture analysis
n	Number
OR	Odds ratio
p	Probability
PERCIST	Positron Emission tomography Response evaluation Criteria In Solid Tumors
PET	Positron-emission tomography
PR	Progesterone receptor
PRESS	Point-resolved spectroscopy
RECIST	Response Evaluation Criteria In Solid Tumors

REK	Regional etisk komité (Regional ethics commitee)
ROC	Receiver operating characteristic
ROI	Region of interest
s	Seconds
Sag	Sagittal
SD	Standard deviation
SLN	Sentinel lymph node
SNR	Signal-to-noise ratio
SSF	Spatial scale filter
T	Tesla
T1	Refers to T1-weighting of MR images, i.e. scan parameters set to enable visualization of differences in longitudinal magnetization recovery
T1c	T1-weighted images with intravenous contrast (in this thesis equivalent to VIBE +C)
T2	Refers to T2-weighting of MR images, i.e. scan parameters set to enable visualization of differences in transverse magnetization decay
TA	Acquisition time
tCho	Total choline-containing metabolites
TE	Echo time
TP53	Tumor protein 53

TR	Repetition time
TrueFISP	True fast imaging with steady state precession
TSE	Turbo spin-echo
TV	Transverse
TVUS	Transvaginal ultrasound
USPIO	Ultrasmall particles of iron oxide
VIBE	Volumetric interpolated breath-hold examination
VIBE +C	VIBE with intravenous contrast
WHO	World Health Organization
X^2	Chi square

2 Introduction

2.1 EPIDEMIOLOGY

Cancer arising from the epithelial lining of the uterine cavity, i.e. the endometrium, is the most common gynecological malignancy in developed countries (1, 2). Overall, in these countries, endometrial cancer is the fourth most common cancer in women, after breast, colorectal and lung cancer. In Norway, approximately 700 new cases are diagnosed each year (3). The age-standardized incidence rate in Norway has been steadily increasing during the last half century, at least until the last decade (Figure 1). A similar increase of incidence has also been observed in the rest of Western Europe and in North America, and the obesity epidemic is believed to be the main driver of this increase (2, 4).

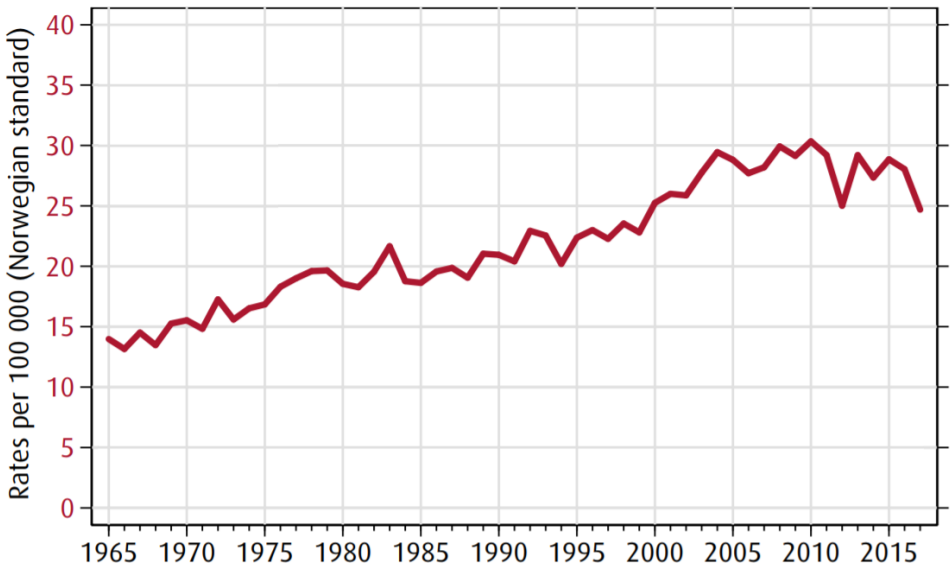

Figure 1: *Increasing age-standardized incidence rate (Norwegian standard population) of uterine cancer* over the last half century. Figure adapted from Cancer in Norway 2017(3).*

** Includes endometrial cancer and uterine sarcomas, the latter comprising only about 3% of uterine corpus cancers and having a relatively stable incidence rate (5, 6).*

Endometrial cancer is predominantly a disease of elderly women. Approximately 85% of cases are diagnosed in postmenopausal women (2). In Norway during 2013-2017, the age-specific incidence rate was highest in the age group 75-79 years, and the median age at the time of diagnosis was 68 years (3).

Typically presenting with abnormal vaginal bleeding, endometrial cancer is often diagnosed at an early stage and generally has a good prognosis. The five-year relative survival was 84% in Norway in the period 2013-2017 (3). However, with advancing disease stage at the time of diagnosis, the prognosis is substantially worsened. While patients with localized disease have an excellent prognosis (95% five-year relative survival), patients with regional- and distant spread have reported five-year relative survival of only 59% and 40%, respectively (3).

2.2 ETIOLOGY, PATHOGENESIS AND RISK FACTORS

No definite or isolated cause of endometrial cancer has been identified. However, alterations in estrogen metabolism seem to play an important role in the pathogenesis, in particular for endometrial cancer of endometrioid subtype. The main risk factor is exposure to excess and unopposed endogenous or exogenous estrogens associated with obesity, insulin resistance, early age at menarche, nulliparity, late-onset menopause, older age and use of tamoxifen (2). Increased estrogen levels, without opposing progesterone, induces endometrial proliferation, which may lead to hyperplasia and eventually cancer (7). Traditionally, a dualistic classification into Bokhman type I and type II endometrial cancer has been used (8). Type I cancers being estrogen-dependent, typically low-grade endometrioid tumors in obese patients and having a good prognosis, contrary to type II cancers comprising non-endometrioid, high-grade tumors with a worse prognosis. Although relevant for understanding endometrial cancer pathogenesis, this classification has been less used in recent years, as more clearly defined histological criteria enable a more detailed and consistent risk stratification.

Furthermore, endometrial cancer characterization has been complemented by more refined classifications based on genetic alterations (9).

The vast majority of endometrial cancers occur sporadically, but approximately 5% are caused by inherited genetic changes (10). Most important, Lynch syndrome, i.e. hereditary nonpolyposis colorectal cancer (HNPCC), is an autosomal dominant inherited cancer susceptibility syndrome, which predisposes for several cancer types including endometrial cancer. In fact, women with HNPCC have a lifetime risk of up to 71% of developing endometrial cancer (10). Cowden's syndrome is another autosomal dominant inherited condition which is associated with up to 28% lifetime risk of developing endometrial cancer (11). In general, women with hereditary endometrial cancer are diagnosed at younger age, often in their forties (12, 13).

2.3 HISTOPATHOLOGY

As in most cancers, histopathological examination is the cornerstone for establishing the diagnosis of endometrial cancer. The endometrioid subtype accounts for about 80% of cases (14). The term endometrioid refers to endometrial-type glands of varying differentiation. According to the WHO classification system (15), endometrioid carcinoma of grade 1 consists of well-formed glands with ≤5% solid areas; grade 2 tumor has less differentiated glands and 6-50% solid areas; whereas a grade 3 tumor has poorly differentiated, distorted gland structure and >50% solid growth. The non-endometrioid subtype comprises tumors that are all considered high-grade tumors: i.e. serous carcinomas (3-10% of cases), clear cell carcinomas (2-3% of cases), carcinosarcomas (<2% of cases) and undifferentiated carcinomas (15). Importantly, these histological distinctions may be difficult, and studies have reported substantial discordance even between experienced pathologists, e.g. in distinguishing high-grade endometrioid tumors from non-endometrioid tumors (16, 17). Also the distinction between low-grade endometrioid cancer and endometrial hyperplasia (not

malignancy) is difficult with reportedly substantial interobserver variability among pathologists (18).

2.4 CLINICAL FEATURES

2.4.1 Symptoms of endometrial cancer

Abnormal vaginal bleeding is one of the presenting symptoms in about 90% of all endometrial cancer patients (2). Due to this conspicuous symptom being frequent, endometrial cancer is often diagnosed at an early stage – as women with abnormal vaginal bleeding tend to seek health care without much delay. In a postmenopausal setting, vaginal bleeding should always lead to further investigation, as it is reportedly caused by endometrial cancer in 5-10% of cases, and also other gynecological cancers may present as vaginal bleeding (19). With increasing age and presence of other risk factors, the endometrial cancer risk is even higher. In premenopausal women, abnormal vaginal bleeding is also an important symptom. However, this diagnosis is much more challenging, as only 0.33% of patients with premenopausal abnormal vaginal bleeding are diagnosed with endometrial cancer (20). Patients with advanced disease may also, due to large pelvic tumor burden or metastatic disease, present with abdominal or pelvic pain, abdominal distention, lower-extremity edema or weight loss.

2.4.2 Biopsy and curettage

In most cases, endometrial cancer can be easily diagnosed with an office-based biopsy kit, e.g. the Pipelle (with reported sensitivity 91-99%) (21). If sufficient material is obtained, a preliminary diagnosis including histological subtype and grade can be determined. If endometrial biopsy is inconclusive, the slightly more invasive and anaesthesia-requiring procedure; dilatation and curettage can be performed. In addition to histological subtype and grade, the fractionated curettage gives a preliminary assessment of cervical tumor involvement. A third option, is a visual guided biopsy

using hysteroscopy. This method yields higher accuracy than blind curettage (22, 23), but is more resource-demanding. Although a biopsy, regardless of method, is needed for diagnosis and useful for initial risk stratification, substantial discordance is reported when comparing histological subtype and grade in preoperative biopsy with the hysterectomy specimen. A large study comparing low-risk histology (endometrioid grade 1 or 2) and high-risk histology (endometrioid grade 3 or non-endometrioid) in biopsies and hysterectomy specimen found a discordance rate of 16% between biopsy and hysterectomy specimen (24).

2.4.3 Sonography

Transvaginal ultrasonography (TVUS) is routinely used as a first-line imaging method to investigate abnormal vaginal bleeding. Being highly available, inexpensive and without patient side-effects, TVUS is an important diagnostic tool for the gynecologist. Particularly in postmenopausal women, sonographic assessment of the endometrium is useful, reportedly yielding 96% sensitivity and 61% specificity for detection of endometrial cancer, when using a 5 mm threshold to define abnormal endometrial thickening (25). In premenopausal women there is cyclical variation in endometrial thickness, and thus, no valid threshold exists for ruling out malignancy. However, TVUS may identify benign causes of bleeding e.g. polyps and myomas. Regarding local tumor extent in endometrial cancer, recent advances in ultrasound technology have enabled experienced sonographers to achieve accuracies for myometrial and cervical invasion assessments comparable to that reported for magnetic resonance imaging (MRI) (26). TVUS still has some limitations, though, as visibility may be reduced due to myomas, acoustic shadows etc, and the method is also inherently operator-dependent.

2.4.4 Radiological diagnostics

In routine clinical practice, most endometrial cancer patients undergo a preoperative computed tomography (CT) scan of the thorax, abdomen and pelvis for detection of lymph node metastases and distant spread. Pelvic MRI is also established as a routine preoperative examination at most centers, as this method, in general, is considered the superior modality for assessment of local pelvic tumor extent (27). Additional aspects of MRI are elaborated in chapter 2.5. 18F-fluorodeoxyglucose positron emission tomography/computed tomography (18F-FDG PET/CT) is increasingly used in endometrial cancer patients. 18F-FDG PET/CT seems superior for detection of metastatic lymph nodes and distant spread in endometrial cancer (28-30). However, metastatic lymph nodes or metastatic lesions of very small size are more likely to be PET-negative. One 18F-FDG PET/CT study reported sensitivities of 93% for lesions ≥10 mm, 67% for lesions 5-9 mm and as little as 17% for lesions ≤ 4 mm (30).

2.4.5 Serum markers and tumor tissue markers

In routine diagnostic work-up of endometrial cancer, no blood sample analyses are yet implemented in decision-making. However, several studies suggest serum cancer antigen (CA)-125 (also used for detection and treatment monitoring in ovarian cancer) as a potential preoperative risk stratification tool in endometrial cancer (31-34). High levels of calprotectin and growth differentiation factor (GDF)-15 have also been linked to an aggressive endometrial cancer phenotype (35, 36).

The traditionally used histological markers related to subtype and grade are long known prognostic biomarkers in endometrial cancer. Along with the International Federation of Gynecology and Obstetrics (FIGO) staging parameters, these have been used to decide on optimal treatment strategy and for prognostication. However, it is shown that 15-20% of presumed low-risk patients will develop recurrent disease, whereas approximately 50% of presumed high-risk patients will not (2). Hence, several

histological and molecular biomarkers have been studied aiming to improve risk stratification in endometrial cancer. Histological lymphovascular space invasion (LVSI) (37), DNA ploidy status (38), estrogen- and progesterone receptor (ER/PR) expression (39, 40), L1CAM expression (41), TP53 expression (42) and KRAS amplification (43) are all biomarkers reported to have independent prognostic value. Recently, LVSI has been included in risk stratification guidelines from the European Society for Medical Oncology (ESMO) (44). The other markers mentioned above are, at present, not implemented in routine clinical practice. However, large prospective studies are ongoing (e.g. MoMaTEC2/NCT00598845) in order to determine whether new markers should be recommended for routine clinical implementation.

2.5 MAGNETIC RESONANCE IMAGING IN ENDOMETRIAL CANCER

2.5.1 Conventional MRI

MRI has long been considered the imaging method of choice for preoperative staging of endometrial cancer (45-47). With its high soft-tissue contrast, high spatial resolution with minimal effect on image quality caused by surrounding skeletal parts and calcifications, MRI is well suited for oncological imaging in the pelvic region. Two perpendicular T2-weighted acquisitions, angled along the long- and short axes of the uterine body, are routinely performed. T1-weighted images with intravenous contrast are also normally included in the protocol, and the recommended contrast delay is 2 min ± 30 s, which is reported as optimal for assessment of deep myometrial invasion (46). Tumor tissue is usually isointense or moderately hyperintense (relative to the myometrium) on T2-weighted images, and on contrast-enhanced T1-weighted images tumor tissue is hypointense compared to the highly vascularized myometrium (Figure 2). Additional acquisitions perpendicular to the axis of the endocervical channel may improve assessment of cervical tumor invasion. Although conventional MRI has limited sensitivity to detect lymph node metastases, the European Society of Urogenital Radiology (ESUR) also recommend T1- and T2-weighted images up to the levels of

the kidneys for retroperitoneal lymph node assessment (46). Routinely, patients fast for 3-6 hours prior to MRI, and a peristaltic inhibitor (glucagon or butyl-scopolamine) is administered intramuscularly or intravenously shortly before scanning in order to reduce peristalsis artifacts.

The preoperative staging includes assessment of deep myometrial invasion (<50% vs. ≥50%), cervical stroma invasion, extrauterine tumor growth and presence of lymph node metastases. Contrast-enhanced MRI has been considered superior to TVUS, CT and unenhanced MRI for assessment of local tumor extent (45, 48, 49). However, with advances in ultrasound technology some recent publications report comparable results for TVUS and MRI (26). To some extent, though, all conventional imaging methods seem to be hampered by non-perfect accuracies for the staging

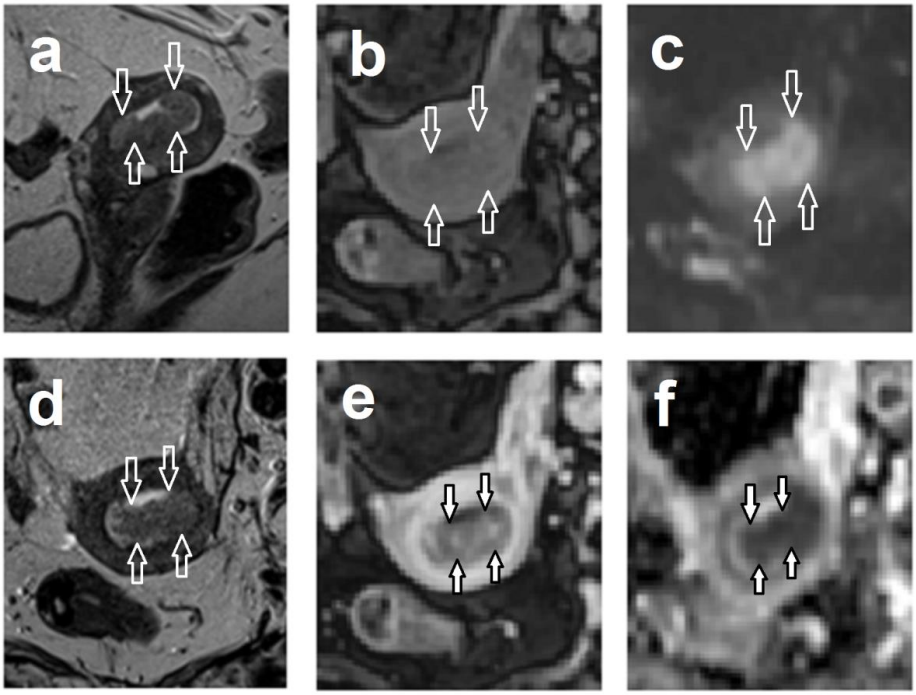

Figure 2: *FIGO stage 1b endometrial carcinoma (arrows), endometrioid grade 2, in a 76-year-old woman.* ***a*** *Sagittal T2.* ***b*** *Axial oblique T1 before contrast.* ***c*** *Axial oblique DWI b1000.* ***d*** *Axial oblique T2.* ***e*** *Axial oblique T1 after contrast (2 min).* ***f*** *Axial oblique ADC-map.*
ADC, apparent diffusion coefficient; DWI, diffusion-weighted imaging; FIGO, the International Federation of Gynecology and Obstetrics.

parameters and limitations in reliability (27), a fact that has motivated further research on new imaging techniques and new approaches for image interpretation.

2.5.2 Diffusion-weighted MRI

Diffusion-weighted imaging (DWI) is often included in routine MRI examinations in endometrial cancer patients. Especially if MRI contrast agents are contraindicated, DWI can be useful in preoperative staging, as it aids in the assessment of myometrial invasion (50). The technique depicts tissue microstructure, as the image contrast is derived from the random motion of water molecules, which is restricted in tissue with high cell density. Endometrial cancers are typically hyperintense in high b value (i.e. highly diffusion-weighted) images, and have corresponding low values on the apparent diffusion coefficient (ADC) maps (Figure 2CF). As ADC values can be quantitatively measured in regions of interest (ROIs), several studies have proposed cutoffs for differentiation of malignant/benign/normal tissue and also for risk stratification in endometrial cancers (51-55).

2.5.3 Dynamic contrast-enhanced (DCE)-MRI

DCE-MRI is a functional imaging technique, in which tissue perfusion and vascular permeability can be visualized and quantitatively measured. Thus, an angiogenic tumor profile may be obtained in vivo (56). DCE-MRI-derived tumor parameters are reportedly associated with specific clinical and histological phenotypes in endometrial cancer and may also predict poor outcome (57, 58). However, the complexity of these image analyses and the post-processing required, warrant further exploration and standardization prior to possible future clinical implementation.

2.5.4 MR spectroscopy (MRS)

MRS is another functional MRI technique, enabling non-invasive in vivo quantification of specific tissue metabolites. Most commonly, proton (1H)-MRS is performed, exploiting the physical phenomenon that protons in different molecules resonate at slightly different frequencies in high magnetic fields. Although being established as a valuable adjunct to conventional MRI in several cancer types (e.g. brain, prostate and breast cancer) (59), MRS in endometrial cancer is largely unexplored. However, a few small studies have reported MRS-measured choline (60-62), lipids (63) and lactate (64) in endometrial cancers to be associated with specific phenotypes.

2.5.5 MRI with new contrast agents

A study using a lymph node-specific contrast agent composed of ultra-small particles of iron oxide (USPIO) reported substantially higher sensitivity (with no loss of specificity) for lymph node metastases than conventional MRI in endometrial cancer (65). Also in other cancer types (e.g. cervical and prostate cancer) encouraging results were reported a decade ago. Unfortunately, withdrawal of clinical approval of the contrast agent (ferumoxtran-10) has limited its use, also for research purposes. However, a recent reintroduction in the Netherlands with a large study on prostate cancer patients (66), hopefully will open the avenue for further research on the use of USPIO in gynecological cancers.

2.6 RADIOMICS

With advances in computer technology and information technology during the last decade, substantial efforts have been put into computer-assisted extraction of quantitative features from radiological imaging data; often referred to as radiomics. This approach is not limited to MRI, rather it seeks integration of multimodal imaging

data, and may yield complex models determining cancer aggressiveness (67). Going beyond the human eye and brain at image interpretation, exploration of tumor texture and tumor heterogeneity may reveal new insights relevant for tumor characterization and therapy. Such studies on endometrial cancer patients are scarce; however, a few publications have used radiomic approaches in MR- and PET-images, and report novel imaging biomarkers for prediction of high-risk disease (68, 69).

Texture analysis, a method for quantification of heterogeneity in images, is an important element of radiomics, and this method is increasingly employed in clinical research. In oncological imaging, a typical approach would be to perform tumor delineation (i.e. selecting a ROI) in the acquired images – either a 2-dimensional (2D) ROI in a single, representative image slice or a 3-dimensional (3D) ROI comprising a whole tumor lesion in a multi-slice image stack. The voxels in the ROI would then be analyzed by a computer algorithm aiming at extracting features (e.g. entropy, kurtosis, skewness etc.) which could reflect biologically relevant information. Numerous publications have reported CT-derived texture features to be associated with tumor aggressiveness, treatment response and/or patient outcome in various cancer types, e.g. in colorectal (70), pancreatic (71), lung (72) and metastatic melanoma (73). However, at present, no study on CT texture analysis in endometrial cancer has been published.

2.7 STAGING

In 2009 an update of the endometrial cancer FIGO staging system was published (74), and at present, this is still the current staging system (Table 1). Endometrial cancer is surgically staged, although the term *surgicopathological staging* often is used (27), pinpointing that the final disease stage is usually not determined until the histopathological assessment after primary surgery (usually encompassing hysterectomy) is finalized.

Table 1. FIGO 2009 staging system for endometrial cancer.

Stage	*Criteria*
IA	Tumor confined to the corpus uteri, <50% myometrial invasion
IB	Tumor confined to the corpus uteri, ≥50% myometrial invasion
II	Tumor invades cervical stroma, but does not extend beyond the uterus
IIIA	Tumor invades the uterine serosa and/or adnexae
IIIB	Vaginal and/or parametrial tumor involvement
IIIC1	Pelvic lymph node metastases
IIIC2	Para-aortic lymph node metastases
IVA	Tumor invades bladder and/or bowel mucosa
IVB	Distant metastases, including intra-abdominal metastases and/or inguinal lymph node metastases

Table adapted from Pecorelli 2009 (74).

FIGO, the International Federation of Gynecology and Obstetrics.

2.8 TREATMENT

2.8.1 Surgery

Surgery is the cornerstone of primary treatment in endometrial cancer. Hysterectomy and bilateral salpingo-oophorectomy is the standard treatment for presumed stage I disease and is curative in most cases (2). The rationale for removal of

the adnexae is multifaceted: as part of staging to rule out ovarian metastases, to decrease estrogen production and thus possibly decrease estrogen as cancer driver and to prevent ovarian cancer (44). In young patients with low-risk disease, however, ovarian preservation may be discussed. Even fertility preserving management is sometimes an option in selected patients (75). Minimally invasive techniques (laparoscopy or robot-assisted surgery) are increasingly employed and are associated with shorter hospital stays and fewer postoperative complications (76). If stage II disease is suspected, radical hysterectomy (including paracervical and parametrial structures) has traditionally been recommended. However, a recent study found no survival benefit of radical hysterectomy compared with simple hysterectomy, and additionally, there was a higher rate of perioperative and late adverse events associated with radical hysterectomy (77). Thus, current European guidelines do not recommend radical hysterectomy as routine treatment in suspected stage II endometrial cancer, however it should be considered in cases of obvious involvement of the parametrium (44). If preoperative biopsy indicates serous carcinoma or clear cell carcinoma with a serous component, omentectomy is additionally recommended – even in apparent stage I disease (44).

Lymphadenectomy is an integral part of the comprehensive surgical staging of endometrial cancer and provides a basis for prognostication and triage of patients for adjuvant therapy. However, prospective clinical trials have not shown a survival advantage associated with systematic lymphadenectomy in early-stage disease (78, 79), and the extent of lymphadenectomy performed varies between institutions (2). In apparent stage II disease, lymphadenectomy is in general recommended, and in more advanced disease (stage III-IV), complete macroscopic tumor debulking and comprehensive staging is recommended (44). In apparent stage I disease, however, there is some controversy on how and when to employ lymphadenectomy. Norwegian guidelines (revised in 2015) (80) subdivide stage I disease into three categories based on risk of recurrence (Table 2), which are identical to the ESMO classification published in 2013 (81). In the low-risk group, no lymph node sampling is recommended unless enlarged lymph nodes (short axis >10 mm) are identified, whereas in the intermediate-risk and high-risk groups, lymph node sampling is advised.

Furthermore, in the high-risk group both pelvic and para-aortic lymphadenectomy is recommended (80). Translated into clinical practice, these recommendations implicate a major role of the preoperative biopsy (histological type and grade) and on preoperative imaging (depth of myometrial invasion), possibly supported by intraoperative findings, when deciding whether or not lymphadenectomy should be performed. Awareness of the increased risk of complications associated with lymphadenectomy (82), and the known limitations of preoperative conventional imaging and even biopsy assessments, makes lymphadenectomy still an issue of controversy. Extensive research is undertaken to explore new biomarkers aiming at improving patient triage to lymphadenectomy, to which the studies comprising this thesis also is a contribution.

Table 2. Risk of recurrence in stage I endometrial cancer.

	FIGO IA	**FIGO IB**
Endometrioid grade 1-2	Low risk	Intermediate risk
Endometrioid grade 3	Intermediate risk	High risk
Non-endometrioid	High risk	High risk

Table adapted from the Norwegian Gynecological Oncology Group guidelines 2015 (80).

FIGO, the International Federation of Gynecology and Obstetrics.

Sentinel lymph node (SLN) mapping has received increasing interest in endometrial cancer in recent years (83). The concept is intriguing, as it – at least theoretically – minimizes the treatment related morbidity, while maintaining the benefit of surgical staging. However, some elements of the technique (e.g. site of injection) are not fully standardized, and the importance of detecting lymph nodes with small metastases and isolated tumor cells (i.e. if SLN dissection is combined with

pathological ultrastaging) is unclear (44). Nevertheless, evidence is accumulating that SLN dissection may be useful in the management of endometrial cancer (84, 85).

2.8.2 Adjuvant therapy

According to the Norwegian guidelines referred to in Table 2, apparent stage I disease with low- and intermediate risk of recurrence should be treated with surgery alone. For apparent high-risk stage I disease and stage II and above, adjuvant therapy is recommended (80). As decisions on adjuvant therapy can be made after primary surgical treatment with the final histopathology report available, the preoperative pelvic imaging findings guides adjuvant therapy only if confirmed at surgicopathological staging. However, if distant metastases are suspected at preoperative imaging, such findings will triage patients into further investigations; either abdominal/regional biopsies during surgery or image guided biopsy for verification of suspected distant metastasis. If disseminated disease is confirmed, adjuvant therapy is recommended. Available adjuvant therapies are chemotherapy, radiation (external radiotherapy or vaginal brachytherapy) and hormonal therapy. In Norway, chemotherapy is the most used adjuvant treatment; recommended for high risk stage I and all stage II-IV. Radiation therapy is rarely given to stage I (as no survival benefit is documented), but is recommended for stage II when only simple hysterectomy has been performed. For stage III-IV radiation therapy is mainly given for palliative treatment. In other parts of Europe, radiation therapy is more widely used as part of adjunctive therapy.

At present, no specific imaging markers are implemented in algorithms guiding the choice of adjuvant therapy in endometrial cancer. However, advances in molecular tumor profiling, functional imaging techniques and radiomics, may in the future enable more tailored treatment – possibly also targeted therapies.

Regarding treatment monitoring, imaging has been a cornerstone for decades, with well established criteria based on conventional imaging, e.g. Response Evaluation

Criteria In Solid Tumors (RECIST), based solely on size of tumor lesions, published in 2000 and revised in 2009 (86). In recent years, as novel therapies and new imaging techniques have been introduced, more adapted response evaluation criteria have also been proposed, e.g. the Choi criteria in gastrointestinal stromal tumors treated with tyrosine kinase inhibitors, the Immune-related Response Criteria (IrRC) adapted for immune therapy and the Positron Emission tomography Response evaluation Criteria In Solid Tumors (PERCIST) incorporating metabolic changes in tumor lesions assessed by PET imaging (87).

3 Specific background and aims of the study

3.1 SPECIFIC BACKGROUND

Endometrial cancer is the most common gynecological cancer in high-developed regions of the world, and the incidence has been increasing over the last half century, largely driven by a concurrent increase in population obesity (1, 2). Staging of endometrial cancer is surgical, and the treatment strategy and prognosis are traditionally based on the FIGO stage and histological subtype and grade determined from the hysterectomy specimen (35, 74). To enable more individualized surgical treatment, improved methods for preoperative risk stratification are highly warranted. Imaging is mandatory in the diagnostic work-up of endometrial cancer, and provides information important for the preoperative decision-making, e.g. whether or not to perform lymphadenectomy. MRI is the preferred modality for assessment of local tumor extent (27, 47). However, conventional MRI has shortcomings in predicting FIGO stage (88), and interobserver variability between radiologists also represents a source of inaccuracy (89). Thus, we aim at identifying novel, robust and accurate imaging markers that may aid in the preoperative risk stratification and tailoring of treatment in endometrial cancer.

3.2 AIMS OF THE STUDY

1. To explore associations between preoperative tumor size measured on MR images and the surgical pathological staging parameters: deep myometrial invasion, cervical stroma invasion and lymph node metastases. Secondly, to assess the interobserver variability for the different tumor size measurements and to explore their prognostic value (**Paper I**).

2. To explore whether preoperative MR spectroscopy-derived tumor choline levels are associated with clinical/histological features or survival in endometrial cancer (**Paper II**).

3. To explore whether tumor texture features from preoperative MRI are related to known prognostic factors (deep myometrial invasion, cervical stroma invasion, lymph node metastases, and high-risk histological subtype) and to outcome in endometrial cancer patients (**Paper III**).

4. To explore whether tumor texture features from preoperative CT are related to known prognostic histopathological factors (deep myometrial invasion, cervical stroma invasion, lymph node metastases and high-risk histological subtype) and to outcome in endometrial cancer patients **(Paper IV)**.

4 Materials and methods

4.1 PATIENTS AND DATA COLLECTION

The studies included in this thesis are based on collected data from endometrial cancer patients treated at Haukeland University Hospital during April 2009 to November 2013. In this time period, patients referred with suspected endometrial cancer had clinical examination, transvaginal ultrasound and biopsy and underwent preoperative pelvic 1.5T MRI using a standardized imaging protocol (Table 3). Images were prospectively transferred to a research database and subsequently de-identified. The research imaging archive was administered by the Department of Radiology at Haukeland University Hospital. Clinical, histological and follow-up data were collected by review of patient hospital records and from correspondence with responsible physicians if follow-up was continued outside hospital. These data were recorded in a separate database administered by the Department of Obstetrics and Gynecology at Haukeland University Hospital. Patients with a final diagnosis different from endometrial cancer after surgical pathological staging were excluded from both databases. Follow-up data have been registered until January 2017. Patient status has been recorded as either “alive and well”, “alive with active disease”, “dead from other cause”, “dead with disease, but not due to active disease” or “dead from disease”. Data on recurrence and/or progression have been recorded as either “no recurrence”, “recurrence from presumed cured disease”, “stable metastatic disease” or “progressive metastatic disease”. These recordings have enabled *recurrence- and progression-free survival* to be used as endpoint in the current studies. All patients signed an informed consent form prior to the collection of data, and the studies were conducted under institutional review board approved protocols (REK Vest #2009/2315; 2015/2333).

In **Paper I,** a total of 252 patients who had undergone MRI were assessed. In 36 patients, the surgical pathological staging did not confirm endometrial cancer, and these were excluded. Additionally 4 patients were excluded due to incomplete FIGO staging (only curettage in 3 patients having substantial co-morbidity and tumor reduction surgery in 1 patient). Thus, the final study cohort in **Paper I** comprised 212

consecutive endometrial cancer patients with complete FIGO staging, imaged during April 2009 to November 2013 (Figure 3).

In **Paper II**, 95 patients with confirmed endometrial cancer at subsequent staging, underwent MR spectroscopy (MRS) and were prospectively included in the MRS imaging database. Of these, 15 patients were excluded due to poorly defined tumors, considered difficult to reliably analyze, and 3 patients were excluded due to poor spectral quality. Thus, the final study cohort comprised 77 patients (a subgroup of the study cohort in Paper I (Figure 3)) who underwent MRS in addition to conventional MRI during June 2009 to January 2012.

In **Paper III**, 216 consecutive endometrial cancer patients underwent MRI during April 2009 to November 2013. Of these, 33 were excluded due to small or poorly defined tumors, and 3 due to major image artifacts. Thus, 180 patients were included for MR texture analysis. This study cohort was largely overlapping with the study cohort in Paper I (Figure 3).

In **Paper IV**, the clinical imaging records of the 180 patients in Paper III were retrospectively examined. In total, 169 patients had available CT images. Of these, 14 were excluded due to poorly defined tumors, considered ineligible for reliable texture analysis. Thus, 155 patients were included for CT texture analysis in Paper IV (a subgroup of the study cohort in Paper III (Figure 3)). The CT imaging of these 155 patients was performed during April 2009 to November 2013, and these imaging data were retrospectively collected from different local hospitals in Western Norway (the majority from Haukeland University Hospital). Contrary to the MR imaging data in Paper I-III, the CT imaging data in Paper IV were not originally intended for research purposes, and thus, we are unable to report specific information on scanner types and settings or contrast media administration (i.e. types, amounts) in Paper IV.

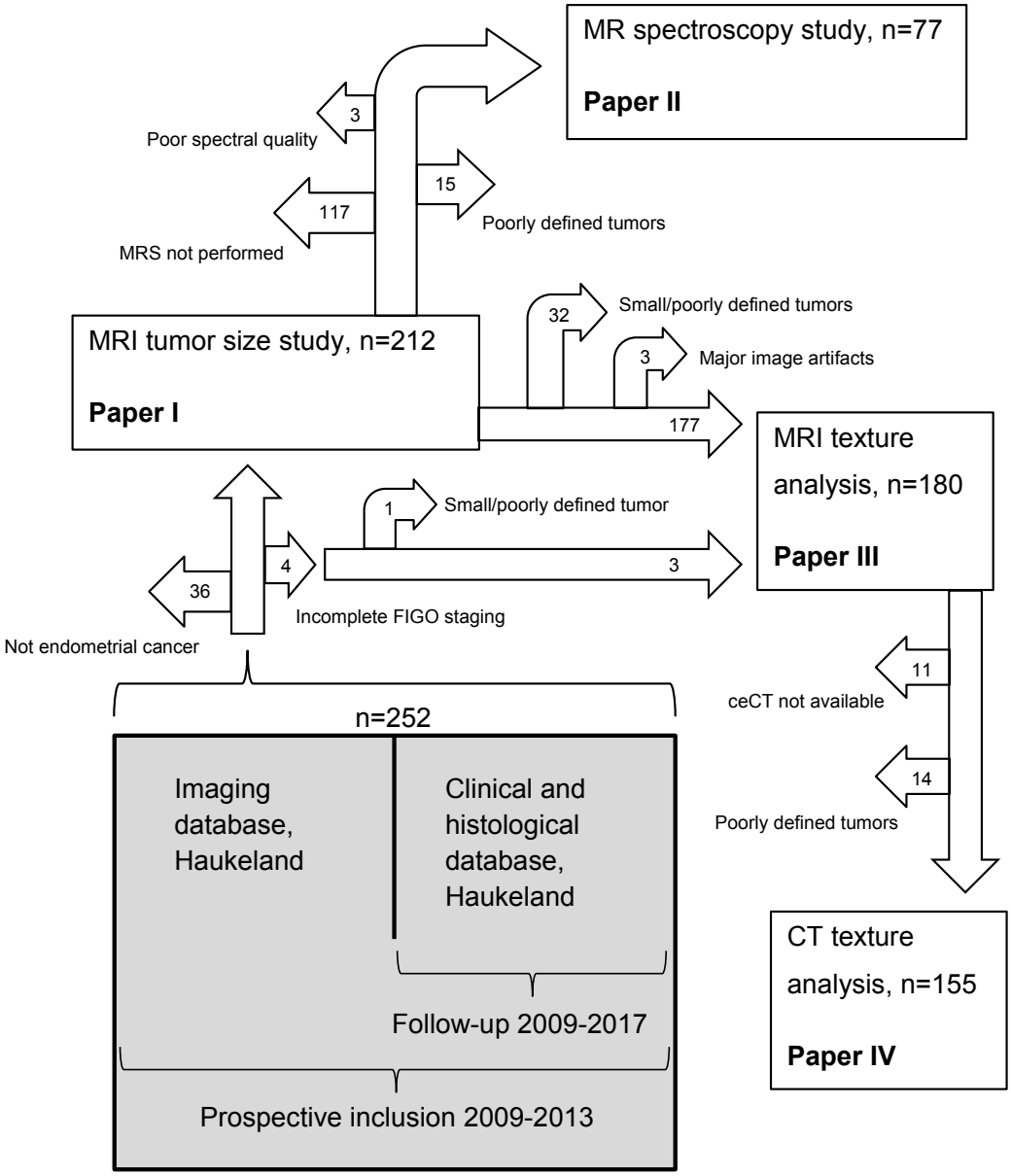

Figure 3: *Flowchart showing patient inclusion and exclusion in study I-IV in this thesis.*

Table 3. MR imaging protocols

Sequence	Plane	TR/TE (msec)	Section thickness (mm)	Matrix	Field of view (mm)	TA
Pelvic conventional:						
T2 TSE	Sag	4920/95	3	256×256	180×180	4:03 min
* T2 TSE	Ax obl	6310/95	3	256×256	180×180	3:04 min
FS T1 VIBE	Ax obl	7.23/2.55	2	192×192	250×250	0:35 min
* FS T1 VIBE +C (2 min delay)	Ax obl	7.23/2.55	2	192×192	250×250	0:35 min
Abdominal conventional:						
T1	Axial	128/4.76	6	256×256	380×380	0:36 min
T2 TrueFISP	Axial	3.59/1.51	4	256×256	380×380	0:48 min
T2 TrueFISP	Cor	3.57/1.51	4	192×192	300×300	0:12 min
Pelvic DWI:						
DWI b0_1000	Ax obl	3100/79	5	128×128	300×300	2:38 min
* ADC-map	Ax obl		5	128×128	300×300	
Pelvic 1H-MRS:						
CSI_PRESS	Ax obl	690/120	6.7 (nominal voxel size (isotropic))	12×12×12		11:36 min

*Sequences used for MRI texture analysis.

1H, proton; ADC, apparent diffusion coefficient; Ax obl, axial oblique (i.e. perpendicular to the long axis of the uterus); C, intravenous contrast; Cor, coronal; CSI, chemical shift imaging; DWI, diffusion-weighted imaging; FS, fat saturated; PRESS, point-resolved spectroscopy; Sag, sagittal; T1, T1-weighted imaging; T2, T2-weighted imaging; TA, acquisition time; TE, echo time; TR, repetition time; TrueFISP, true fast imaging with steady state precession; TSE, turbo spin-echo; VIBE, volumetric interpolated breath-hold examination.

4.2 IMAGE ANALYSES

4.2.1 Conventional MRI reading

The conventional MR images in **Paper I**, comprising T2-weighted images, diffusion-weighted images including ADC-maps and contrast-enhanced T1-weighted images, were de-identified and read independently by three observers who were blinded for tumor stage, histological diagnosis and patient outcome. Observer 1 and 2 were consultants with more than 10 years of experience with pelvic MRI. Observer 3 included two junior radiologists (both having approximately 4 years of experience with pelvic MRI); one read the first 105 MRI examinations and the other read the following 107 examinations. All observers reported the imaging findings in a standardized form (see Appendix). The maximum tumor diameters were measured in three orthogonal planes: anteroposterior (AP) and transverse (TV) diameter on axial oblique (perpendicular to the long axis of the uterus) contrast-enhanced T1-weighted images and craniocaudal (CC) diameter on sagittal T2-weighted images (Figure 4).

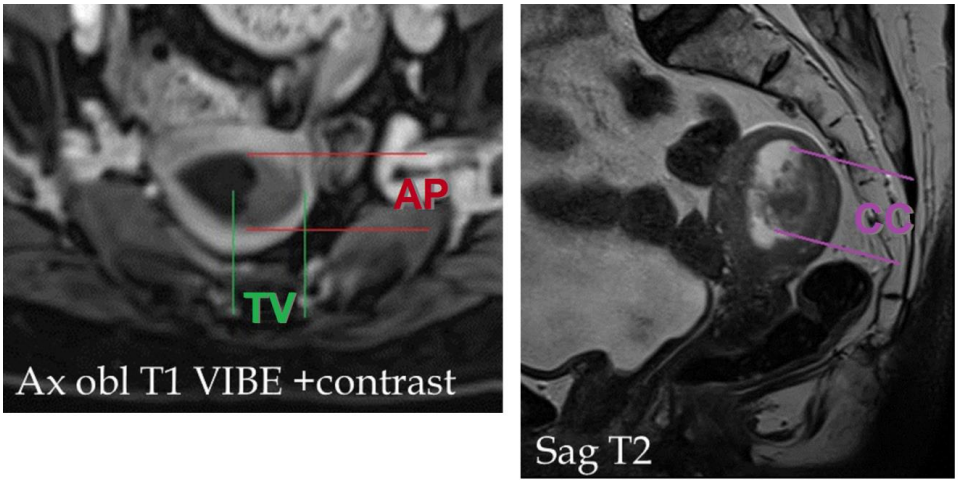

Figure 4: *Transverse (TV) and anteroposterior (AP) tumor diameters measured on axial oblique contrast-enhanced T1-weighted image (left) and craniocaudal (CC) tumor diameter measured on sagittal T2-weighted image (right) in a 64-year-old woman with FIGO stage 1b endometrial carcinoma (endometrioid grade 1).*

Tumor volume was estimated using the following equation: AP diameter × TV diameter × CC diameter × 0.5. Presence of deep myometrial invasion (tumor invading half or more of the myometrium), cervical stroma invasion (disruption of the low-signal intensity cervical stroma on T2-weighted images), and enlarged lymph nodes (largest short-axis diameter ≥10 mm) were also recorded. Before reading the MR images in the study cohort, each observer independently read five cases, which then were discussed to achieve a common understanding of the image reading criteria applied. The five pilot cases were not included in the study cohort.

A consensus score was established for the registered parameters using the majority score for categorical variables and the median value for continuous variables. These data have also been used for comparison in **Paper II-IV**.

4.2.2 MR spectroscopy (1H-MRS)

All patients in **Paper II** underwent localized multivoxel point-resolved spectroscopy (PRESS) with a 12 × 12 × 12 matrix manually placed to cover the tumor region in all planes. Images were de-identified and assessed on a Syngo workstation by one radiologist (with 5 years of experience in pelvic MRI) and one spectroscopist (with 6 years of experience in MRS) who were blinded for tumor stage, histological diagnosis and patient outcome. The radiologist manually selected representative voxels from tumor tissue and adjacent normal tissue (myometrium), respectively (Figure 5). The spectroscopist assessed the spectral quality of the selected voxels. After excluding patients with small or poorly defined tumors, considered hard to reliably analyze (n=15), and patients with poor spectral quality (with tCho SNR < 2) in tumor voxels (n=3), a total of 77 patients were included in the study. Spectral data were analyzed using the java-based software jMRUI v5.2 for quantification of total choline-containing compounds (tCho) at 3.22 ppm, creatine at 3.03 ppm, water at 4.7 ppm and average noise level at 8.0-9.0 ppm. Three tCho ratios were generated: tCho/Creatine, tCho/Water and tCho/Noise.

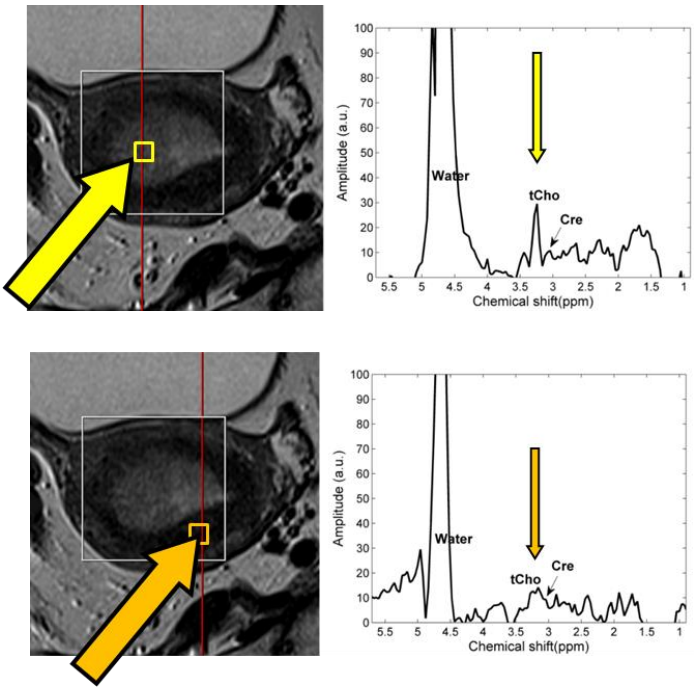

Figure 5: *T2-weighted MR images showing tumor voxel (yellow arrow) and non-tumor (myometrium) voxel (orange arrow) from a 55-year-old woman with FIGO stage 1a endometrial cancer (endometrioid, grade 1). Corresponding MR spectra are shown to the right. Notice the high choline level (tCho peak) in tumor compared with non-tumor tissue.*

4.2.3 Texture analysis of MR- and CT images

In **Paper III and IV** de-identified contrast-enhanced T1-weighted images (n=180), T2-weighted images (n=180), ADC-maps (n=177) and contrast-enhanced CT images (n=155), were exported to the commercially available research software TexRAD (TexRAD Ltd, part of Feedback Plc, Cambridge, UK). Regions of interest (ROIs) were drawn on the slice displaying the largest cross-sectional tumor area, separately on the respective image series, aiming at including all viable tumor tissue. The ROIs were processed using a filtration-histogram technique based on Laplacian of Gaussian spatial bandpass filtering, in which image elements of different sizes were enhanced corresponding to spatial scale filter (SSF) from 2-6 mm, i.e. fine (2 mm), medium (3-5 mm) and coarse texture (6 mm) (Figure 6). Based on texture

quantification in tumor ROIs, the parameters mean, standard deviation (SD), entropy, mean of positive pixels (MPP), skewness and kurtosis were calculated. Unlike CT images with standardized pixel values (measured in Hounsfield units), T1-weighted and T2-weighted MR images do not have standardized pixel values. Furthermore, the mean intensity does not reflect heterogeneity per se, and thus, the parameters mean and MPP in native (SSF=0) images (which equals mean, as no pixels in native MR images have negative values), was omitted in further analyses of all MR images.

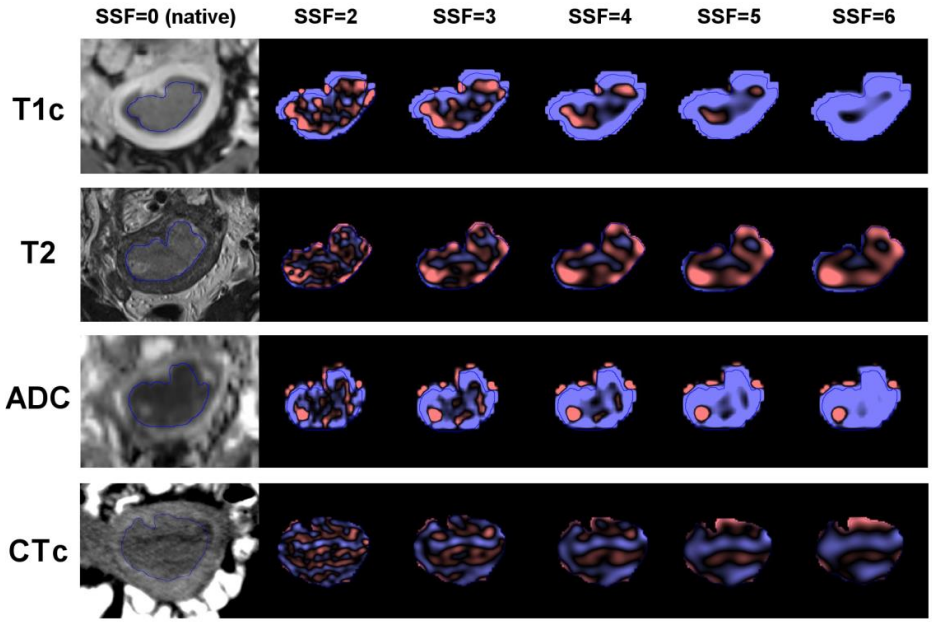

Figure 6: *Endometrial carcinoma manually segmented (blue line) on contrast-enhanced T1-weighted MR image, T2-weighted MR image, ADC-map and contrast-enhanced CT image from the same 52-year-old postmenopausal woman diagnosed with FIGO stage 1b disease (endometrioid, grade 1). Successive filtered images (spatial scale filter [SSF] 2-6) to the right.*

4.3 STATISTICAL METHODS

4.3.1 Sample size

To assess the risk of type II errors in our analyses, an estimation of recommended cohort size was done by X^2 test using the software East4 2005 (Cytel Software Corp). To achieve 90% power of detecting a 20% higher occurrence of a biomarker in one risk category versus another (e.g. 25% in patients with lymph node metastases versus 5% in patients with no lymph node metastases) at a 5% significance level, 101 patients were needed. Furthermore, to reach 90% power to detect a 30% difference in 5-year survival (e.g. 90% for patients with normal levels of a biomarker versus 60% for patients with abnormal levels of a biomarker) at a 5% level of significance, 65 patients were needed, assuming a positive to negative ratio of the markers of 1:3. Thus, **Paper II** (n=77) had a somewhat small study cohort (no more eligible cases were available in the imaging database), while **Paper I** (n=212), **III** (n=180) **and IV** (n=155) had adequate study cohorts.

4.3.2 Normality testing

All image-derived variables were tested for normality by the Kolmogorov-Smirnov and Shapiro-Wilk tests. The majority of the variables did not have normal distribution, thus non-parametric tests were used for further statistical analyses in **Paper I-IV**.

4.3.3 Associations between image-derived variables and clinical and histopathology-based variables

Image-derived variables in **Paper I-IV** were analyzed in relation to clinical and histological tumor and patient characteristics using Mann-Whitney U test, Kruskal-Wallis H test, Jonckheere-Terpsta trend test, Pearson X^2 test, and binary logistic

regression analysis. Receiver operating characteristic (ROC) analyses were performed to assess the diagnostic value of the image-derived variables in **Paper I, III and IV**. ROC analyses were also applied to determine the best cutoff values for tumor size (**Paper I**) and MRI- and CT texture variables (**Paper III and IV**) selecting the highest Youden index, and thereby achieving the best separation between groups. McNemar test was used for pairwise analysis of differences in sensitivity, specificity and accuracy among image-derived variables, i.e. comparing tumor size measurements with conventional MRI reading (**Paper I**) and MRI texture variables to conventional MRI reading (**Paper III**). To assess whether image-derived variables were *independent* predictors of high-risk endometrial cancer, multivariable binary logistic regression analyses were performed including the following covariates: preoperative biopsy risk status (low risk defined as endometrioid grade 1-2 versus high risk defined as endometrioid grade 3 and non-endometrioid) (**Paper I, III and IV**), conventional MRI findings (**Paper I, III and IV**) and patient age (**Paper IV** only).

Spearman's bivariate correlation test was used to explore correlations between the different image-derived variables (**Paper II, III and IV**). In **Paper II**, comparison of MR spectroscopic features in tumor tissue and normal tissue was performed with related-samples Wilcoxon signed rank test.

4.3.4 Interobserver variability

In **Paper I**, intraclass correlation coefficient (two-way random model, calculated from single measurement and based on absolute agreement) was used to assess the reliability of tumor size measurements. Minimal detectable change (MDC = 1.96 × standard error of the mean × √2) for the measured diameters was also reported. In **Paper II-IV** the interobserver variability was not assessed.

4.3.5 Survival analyses

In **Paper I, III and IV**, differences in time to recurrence (for patients considered cured by primary treatment) or progression (for patients known to have residual disease after primary treatment) among patient groups defined by image-derived biomarkers were assessed by the Mantel-Cox (log-rank) test. A similar method was used in **Paper II**, but here the Mantel-Cox (log-rank) *linear trend* test was applied on MR spectroscopy-derived continuous variables stratified into quartiles. In **Paper I and IV** consecutive patient groups with similar survival were merged in the Mantel-Cox tests and the corresponding Kaplan-Meier plots.

In **Paper I, III and IV**, the Cox proportional hazards model was used in univariable and multivariable analyses to study the effect on recurrence- and progression-free survival of image-derived continuous variables. In the multivariable analyses we aimed to adjust for relevant prognostic information available preoperatively, and included the following covariates: preoperative biopsy risk status (**Paper I, III and IV**), conventional MRI findings (**Paper III and IV**) and patient age (**Paper IV** only).

4.3.6 Determination of significance level

In **Paper I and II**, all reported P values were generated by two-sided tests and considered significant when <0.05.

In **Paper III**, a customized modification of Bonferroni correction was applied, in which the number of effective tests was arbitrarily estimated as 25 (from originally 87 texture variables being extensively correlated), leading to P values <0.002 (in two-sided tests) being considered significant. In **Paper IV**, 36 CT derived texture variables were generated. With adjustment for inter-variable correlations, the significance level was set to 0.0025. With this significance level for the 36 individual tests, a random allocation (without replacement) of the 36-variate texture variables to outcome group had approximately 5% chance of at least one significant result.

In the *multivariable* analyses in **Paper III and IV**, a traditional significance level of 0.05 was used.

5 Main results

In **Paper I**, we investigate the relationship between preoperative MRI measured tumor size and the surgical pathological staging parameters deep myometrial invasion, cervical stroma invasion and lymph node metastases – and survival – in a cohort of 212 consecutive patients with histologically confirmed endometrial cancer. When adjusting for risk status based on preoperative endometrial biopsy and other tumor size variables, we find that AP tumor diameter independently predicts deep myometrial invasion (p=0.001), and that CC tumor diameter tends to independently predict lymph node metastases (p=0.06).

Based on ROC curves, the following tumor size cutoff values are identified: AP diameter greater than 2 cm predicts deep myometrial invasion (unadjusted odds ratio (OR) 12.4, p<0.001; adjusted OR 6.7, p<0.001) and CC diameter greater than 4 cm predicts lymph node metastases (unadjusted OR 6.2, p<0.001; adjusted OR 4.9, p=0.009) (adjusted ORs when including conventional MRI reading results [indicating presence of deep myometrial invasion and lymph node metastases, respectively] and risk status based on preoperative endometrial biopsy). Large tumor size is also associated with reduced recurrence- and progression-free survival. When adjusting for risk status based on preoperative endometrial biopsy and other tumor size variables, CC tumor diameter has an independent impact on recurrence- and progression-free survival (adjusted hazard ratio (HR) 1.04, p=0.009). The interobserver variability for the different size measurements was very low (ICC 0.78-0.85).

In **Paper II**, we quantify levels of choline-containing metabolites (tCho) from in vivo magnetic resonance spectroscopy (MRS) of 77 endometrial cancer patients. The overall aim is to explore whether tumor tCho-levels are associated with clinical/histological patient and tumor characteristics and patient outcome. We also compare tCho-levels in tumor tissue and normal tissue (myometrium). We find that high tumor tCho/Water ratio is significantly associated with histological tumor grade in endometrioid tumors (p=0.02), and that tumor tissue has significantly higher ratios

for tCho/Creatine, tCho/Water and tCho/Noise than normal myometrial tissue ($p<0.001$ for all). No significant associations are found between tumor tCho-levels and recurrence- and progression-free survival.

In **Paper III**, we extract texture features from tumor ROIs in MR images, using a filtration-histogram technique, in 180 endometrial cancer patients, and explore whether these tumor texture features are related to known prognostic features (deep myometrial invasion, cervical stroma invasion, lymph node metastases, and high-risk histological subtype) and to outcome (recurrence- and progression-free survival). The multivariable analyses included risk status from preoperative biopsy, conventional MRI reading results and MRI measured tumor volume – in addition to the highest ranked MRI derived texture features. We find that high tumor entropy in apparent diffusion coefficient (ADC) maps independently predicts deep myometrial invasion (OR 3.2, $p<0.001$ for entropy at filter level 6), and high MPP in T1c images independently predicts high-risk histological subtype (OR 1.01, $p=0.004$ for MPP at filter level 4). Furthermore, high kurtosis in T1c images independently predicts reduced recurrence- and progression-free survival (HR 1.5, $p<0.001$ for kurtosis at filter level 2).

In **Paper IV**, we apply the same methods as in Paper III to extract texture features from tumor ROIs from contrast-enhanced CT images in 155 endometrial cancer patients. These are also analyzed in relation to known prognostic features (deep myometrial invasion, cervical stroma invasion, lymph node metastases, and high-risk histological subtype) and to outcome (recurrence- and progression-free survival). The multivariable analyses included risk status from preoperative biopsy, conventional MRI reading results, MRI measured tumor volume and patient age – in addition to the highest ranked CT derived texture features. We find that high tumor entropy (at filter level 6) independently predicts deep myometrial invasion (OR 3.7, $p=0.008$) and cervical stroma invasion (OR 3.9, $p=0.02$). High MPP (at filter level 5) tends to independently predict high-risk histological subtype (OR 1.01, $p=0.10$), and when a cutoff based on the highest Youden index is applied, MPP5>24.2 independently predicts high-risk histological subtype in the same multivariable model (OR 3.7,

p=0.01). None of the CT derived texture features independently predicts lymph node metastases. High tumor kurtosis tends to independently predict reduced recurrence- and progression-free survival (HR 1.1, p=0.06 for kurtosis at filter level 5).

6 Discussion

6.1 METHODOLOGICAL CONSIDERATIONS

6.1.1 Patient series

The patient cohorts studied in this thesis originate from a population-based hospital cohort (Haukeland University Hospital). As elaborated in chapter 4.1, MRI data from newly diagnosed endometrial cancer patients at Haukeland University Hospital have been consecutively and prospectively included in an imaging database for research purposes since 2009. Haukeland is the main hospital in Hordaland County and serves approximately 10% of the Norwegian population. Age distribution, incidence and stage distribution has been demonstrated to be similar in endometrial cancer patients in Hordaland and in Norway as a whole (3). Patients referred for treatment of endometrial cancer are routinely submitted to MRI investigation, thus, in general, only patients with contraindications to MRI (e.g. severe claustrophobia or dementia) do not undergo MRI. Of 360 endometrial cancer patients treated at Haukeland who consented to be included in the clinical research database for the period April 2009 - November 2013, preoperative MRI was performed for 216 patients in accordance with a standardized protocol at Haukeland. Many of the other patients had MRI examinations performed at other local hospitals, but these images were not used in the current studies. The study cohorts in **Paper I-IV** are similar to the total endometrial cancer population in age, histological type and FIGO stage distribution (Table 4). It is clear, however, that the advanced image analyses in **Paper II-IV** are not applicable to very small tumors, which explains the somewhat lower proportion of stage IA cancers in these cohorts (Table 4). Eligibility criteria for selecting patients to the final study cohorts of the respective studies are given in chapter 4.1.

Table 4. Patient and tumor characteristics for the whole endometrial cancer population treated at Haukeland University Hospital during April 2009 to November 2013 and the respective study cohorts in **Paper I-IV**.

	Total EC-population (n=360)	**Original EC study cohort (no exclusions) (n=216)**	**Paper I (n=212)**	**Paper II (n=77)**	**Paper III (n=180)**	**Paper IV (n=155)**
Median age (years)	67	66	66	66	67	68
FIGO stage						
I (not specified)	1%	0	0	0	0	0
IA	51%	54%	55%	38%	48%	47%
IB	21%	22%	23%	34%	25%	27%
II	8%	10%	10%	10%	12%	10%
IIIA	1%	0	0	0	0	0
IIIB	2%	1%	1%	1%	2%	2%
IIIC1	6%	6%	6%	9%	7%	7%
IIIC2	3%	4%	4%	7%	4%	4%
IV (not specified)	1%	0	0	0	0	0
IVA	2%	<1%	0	0	<1%	1%
IVB	3%	1%	<1%	1%	2%	2%
Incomplete FIGO staging	<1%	<1%	0	0	0	0
Histological subtype						
Endometrioid	76%	81%	81%	79%	79%	78%
Clear cell	4%	3%	3%	4%	3%	3%
Serous	12%	10%	10%	9%	11%	10%
Carcinosarcoma	5%	4%	4%	7%	5%	6%
Adenosquamous	<1%	0	0	0	0	0
Undifferentiated/others	3%	2%	2%	1%	2%	3%
Histological grade						
Grade 1	51%	50%	51%	39%	45%	43%
Grade 2	28%	29%	29%	34%	32%	32%
Grade 3	17%	18%	17%	26%	21%	23%
Ungraded	4%	3%	4%	0	1%	2%

FIGO stage refers to the International Federation of Gynecology and Obstetrics stage according to 2009 criteria.

EC, endometrial cancer.

6.1.2 Imaging protocols

In **Paper I-III** standardized protocols were used for image acquisition, which makes our imaging data homogenous and potentially increases reproducibility. Furthermore, in **Paper I and III**, the acquisition of the T2-weighted and contrast-enhanced T1-weighted MR images were based on guidelines from the European Society of Urogenital Imaging (ESUR) published in 2009 (46), which implies that images are expected to be similar to those at comparable institutions. However, when performing MRI texture analysis (**Paper III**), scanner specific settings in image reconstruction (e.g. intensity adjustment, edge enhancement, smoothing etc.) may theoretically affect the results, as the ESUR guidelines did not give details at this level. ESUR guidelines also did not give specific recommendations on acquisition of diffusion-weighted images analyzed in **Paper III**. However, our protocol was similar to those reported in comparable previous studies (51, 90, 91). Furthermore, reported tumor ADC values for endometrial cancer tissue are quite similar in spite of differences in the employed diffusion imaging protocols (with b values of 0/800, 0/1000 and 0/500/1000) (88). **Paper II** had a relatively small study cohort, and the MRS acquisitions were performed on a 1.5T scanner, which is known to yield a lower signal-to-noise ratio compared to 3T or higher fields (92). Thus, the paucity of significant findings in this study should be interpreted with caution.

In **Paper IV**, CT images were retrospectively collected from different local hospitals in Western Norway, and thus, were not acquired using a standardized protocol. However, all patients were imaged in a routine clinical setting as part of the diagnostic workup of endometrial cancer, and although the imaging data in the study were somewhat heterogeneous, the positive findings may suggest that this method is rather quite robust.

6.1.3 Image analyses

The tumor size measurements in **Paper I**, comprising three orthogonal tumor diameters and subsequent estimation of tumor volume (AP × TV × CC × 0.5), can be considered as a routine method in oncological image interpretation. Similar methods

are also previously employed in endometrial cancer MRI studies (93, 94). The MR spectroscopy acquisitions in **Paper II** were performed with a multivoxel technique, which increases post-processing options, i.e. selected tumor areas can be analyzed retrospectively. The post-processing software and method used for spectral fitting in our study, are well established in research (95, 96). Limiting our metabolite of interest to choline (total choline-containing metabolites (tCho)) only, was decided after literature review and for practical purposes. An inherent limitation of *in vivo* MR spectroscopy is that metabolite levels are quantified as relative concentrations rather than absolute. Thus, we generated the ratios tCho/Creatine, tCho/Water and tCho/Noise, which is in line with previous MRS studies (61, 62, 97). In **Paper III and IV**, tumor texture analysis was performed on MR- and CT images, respectively, using the software TexRAD, which is an established research software which has been featured in more than 100 PubMed listed publications. This image post-processing tool, employing a filtration-histogram technique for texture analysis, has previously yielded predictive and prognostic imaging biomarkers in several cancer types (98). It is clear, however, that the feature extraction provided in TexRAD (six features only: mean, standard deviation, skewness, entropy, mean of positive pixels and kurtosis) covers only a small part of the wider range of available texture features (99).

6.1.4 Reproducibility and reliability

In general, the results in this thesis are limited by imaging data derived from a single institution (except **Paper IV**), analyses being performed by a single observer (except **Paper I**) and not yet being internally or externally validated. Additionally, *intra*observer variability has not been assessed. Thus, validation across observers, centers and platforms are warranted. Particularly the complex image analyses in **Paper II-IV** should be reproduced in different cohorts using *a priori* cutoffs prior to potential implementation in clinic.

6.2 DISCUSSION OF RESULTS

6.2.1 Interobserver variability

Conventional MRI reading in endometrial cancer patients includes evaluation of local pelvic tumor extent (depth of myometrial invasion, cervical stroma invasion, extrauterine tumor extension, etc.) and presence of lymph node metastases on a strict anatomical basis (45). For diagnosing deep myometrial invasion, the interobserver agreement varies from fair to good in different studies (89). For cervical stroma invasion and lymph node metastases, the same studies report moderate to good interobserver agreement. This knowledge about substantial interobserver variability as a source of inaccuracy has also motivated an exploration of new imaging biomarkers, potentially less hampered by interobserver variability, in endometrial cancer. In **Paper I**, we found the interobserver variability of tumor size measurements on MRI to be very low (ICC 0.78-0.85), and furthermore, there was no significant difference in diagnostic performance among experienced and non-experienced readers. Thus, tumor size measurements on MRI seem to represent an attractive alternative as robust imaging biomarkers complementing staging parameters derived from conventional reading.

In **Paper II-IV**, we explored more complex imaging biomarkers, all of which were quantitative in nature. Not including intra- or interobserver analyses in these studies is clearly a limitation. In **Paper II**, the subjectivity in selecting voxels for spectroscopic analysis putatively represents the main source of variability. The further steps in the assessment, including spectral fitting and quantification of metabolites, were performed according to a fixed and automated algorithm, expected to reduce intra- and inter-observer variability. Similarly, in **Paper III and IV** the manual image slice selection and tumor delineation, although based on fixed criteria, are potential sources of variability. The fixed algorithm in the subsequent image texture analysis, however, is expected to yield highly reproducible results. On the other hand, when comparing different studies with complex, multi-step image analyses, even small variations in software settings (e.g. jMRUI in **Paper II** and TexRAD in **Paper III-IV**) may affect the results. An additional challenge with TexRAD is that the image filtration

technique is not open-source, and thus, the results are difficult to validate based on other software platforms.

6.2.2 Tumor size measurements on MR images

In **Paper I** three observers independently measured tumor size in three orthogonal planes on MR images with very low interobserver variability. Furthermore, the study demonstrated significant associations between tumor size and high-risk endometrial cancer, in accordance with a study by Todo et al (94) reporting high volume index (defined as maximum AP × TV × CC tumor diameter measured on MRI) to be associated with deep myometrial invasion. Unlike Todo et al, we aimed at exploring the respective tumor diameters as individual variables. In a multivariable model including preoperative risk status based on endometrial biopsy, AP tumor diameter was the only size variable independently predicting deep myometrial invasion. Based on ROC curve analysis, a cutoff of 2 cm was proposed. Using the surgicopathological staging as the gold standard, this relatively simple size criteria (AP tumor diameter >2 cm) achieved comparable accuracy (sensitivity, specificity) to conventional MRI reading for identification of deep myometrial invasion: 79% (66%, 86%) versus 74% (70%, 77%), respectively. The specificity for AP tumor diameter >2 cm (86%) was significantly higher than that of conventional reading (77%; p=0.02, McNemar test), whereas accuracy and sensitivity was not significantly different.

In daily radiologic practice, scoring depth of myometrial invasion (<50% or ≥50%) on MRI is a continuing challenge. The present study also illustrates this, demonstrating disagreement between three radiologists in as much as 46% (98/212) of the patients. In this subgroup, AP diameter >2 cm had significantly higher accuracy than conventional MRI consensus reading for identification of deep myometrial invasion: 76% versus 64% (p=0.05, McNemar test). Specificity was also significantly higher: 88% versus 69% (p=0.01, McNemar test), whereas sensitivity was equal at 56%. A potential clinical application of this finding could be the following reading strategy: If the radiologist is in doubt when scoring depth of myometrial invasion, the (AP) tumor size cutoff should aid in deciding the depth of myometrial invasion.

In the literature, a macroscopic tumor diameter greater than 2 cm in hysterectomy specimens has been reported to independently predict lymph node metastases and survival (100), but results in other studies are equivocal (101, 102). Another study based on macroscopic inspection of the hysterectomy specimen, reported a maximum tumor diameter greater than 3.75 cm (measured by the pathologist) to independently predict deep myometrial invasion, distant recurrence and death (103). In our study, median (consensus) CC diameter was 3.1 cm, whereas median AP diameter was 1.6 cm and median TV diameter 2.6 cm. In the vast majority of patients, the CC diameter was the largest tumor diameter, so our proposed cutoff of CC diameter >4 cm (based on ROC curve analysis for prediction of lymph node metastases) seems to be in line with Chattopadhyay et al (103). Even if tumor measurements on macroscopic fresh tissue are not directly comparable to tumor measurements on MRI, large tumor size as a predictor of high-risk endometrial cancer seems to be broadly supported in the present literature.

In a survival analysis using recurrence- and progression-free survival as endpoint, we also found CC diameter to be an independent prognostic factor. The combination of CC diameter >4 cm and AP diameter >2 cm was proposed as an easily applicable criteria for preoperative risk stratification. In current literature, comparable survival data is scarce, and we suggest further exploration of tumor size parameters along with other potential biomarkers available in a preoperative setting.

6.2.3 Choline-levels measured by MR spectroscopy

Choline is a marker of active proliferation and cell membrane turnover, and numerous MRS studies have demonstrated that choline metabolism is altered in various cancers (104). In **Paper II**, we explored whether tumor choline levels, quantified by in vivo MRS, were associated with high-risk features of endometrial cancer. Additionally, we compared choline levels in tumor tissue and the adjacent normal myometrium. The ratios tCho/Creatine, tCho/Water and tCho/Noise were consistently higher in tumor tissue than in normal myometrium. In line with this, previous studies have reported that MRS tCho quantifications can differentiate endometrial cancers from benign lesions

(60-62). Also, in vitro studies have shown that the choline-metabolite profile in cancer tissue is highly different from that observed in normal or benign tissue (105-107). Our study also showed that high tumor tCho/Water ratio was significantly associated with high tumor grade in endometrioid tumors (p=0.02, Jonckheere-Terpstra trend test). However, none of the tCho ratios could differentiate non-endometrioid from endometrioid tumors, and when analyzing all tumors together, high tCho/Water only tended (p=0.08, Mann-Whitney U test) to predict high-risk histological subtype (endometrioid grade 3 or non-endometrioid). Zhang et al. also found no significant association between tCho/Water and tumor grade in 38 endometrial cancer patients (61) and Han et al. reported no significant association between tCho/Noise and tumor grade in 33 endometrial cancer patients (62).

Considering that our study also did not find significant predictors of deep myometrial invasion, cervical stroma invasion, lymph node metastases or recurrence- and progression-free survival, the immediate clinical value of MRS, at present, seems somewhat limited. On the other hand, the method is clearly able to extract tumor-specific metabolic information, and with methodological refinements it may potentially aid in preoperative risk stratification. Relatively small patient cohorts and somewhat heterogeneous approaches in currently available publications imply that definite conclusions may not be drawn.

6.2.4 Texture analysis of MRI and CT

In **Paper III and IV**, we have demonstrated that texture features extracted from preoperative MRI and CT are significantly associated with high-risk disease and poor outcome in endometrial cancer. In multivariable analyses including endometrial biopsy status, conventional MRI reading results and tumor volume (estimated by MRI), the texture features remained significant and independent predictors of deep myometrial invasion, cervical stroma invasion, high-risk histological subtype and recurrence/progression-free survival (Table 5 and 6). Our findings are in line with other endometrial cancer studies also reporting image texture features as predictors of high-

risk disease (68, 69) – although not being directly comparable. In a broader context, our results also support a more general hypothesis stating that tumor heterogeneity, whether at the genetic, histological or macroscopic level, may reflect tumor aggressiveness (67). In recent years, with the introduction of radiomics, a shift towards computer-assisted extraction of quantitative features from radiological imaging data, rather than the traditional subjective assessments and simple measurements, has emerged. A review article from 2016 with the illustrative title *"Images are more than pictures, they are data"* elaborates on this topic (99). Numerous publications have reported image texture analysis as a promising tool in the diagnostic workup in several cancer types (70-73, 108-110), i.e. supporting accurate diagnosis, preoperative risk stratification or assessment of treatment response.

High entropy in ADC maps (**Paper III**) and high entropy in ceCT (**Paper IV**) were the highest ranked predictors of deep myometrial invasion in the respective studies (Table 5). Furthermore, high entropy in ceCT also independently predicted cervical stroma invasion (**Paper IV**). High kurtosis in T1c images (**Paper III**) and high kurtosis in ceCT (**Paper IV**) were the highest ranked prognostic features in the respective studies, both using recurrence- and progression-free survival as endpoint (Table 6).

Table 5. Uni- and multivariable logistic regression for prediction of deep myometrial invasion, cervical stroma invasion, lymph node metastases and high-risk histological subtype at surgical staging from MRI- and CT derived tumor texture parameters.

			Univariable		Multivariable	
	Tumor texture parameters	n	Unadjusted OR (95% CI)	p	Adjusted OR (95% CI)	p
Deep myometrial invasion	ADC_Entropy6	175	4.7 (2.8-7.8)	<0.001	3.2 (1.7-6.1)[a]	<0.001[a]
	ceCT_Entropy6	153	6.7 (2.8-16.0)	<0.001	3.7 (1.4-9.7)[b]	0.008[b]
	Predictor with cutoff[g]					
	ADC_Entropy6 ≥4.49	69/175	12.0 (5.8-24.7)	<0.001	6.2 (2.5-15.1)[a]	<0.001[a]
	ceCT_Entropy6 ≥4.84	71/153	3.9 (2.0-7.7)	<0.001	2.4 (1.1-5.2)[b]	0.02[b]
Cervical stroma invasion	T2_MPP4	178	0.995 (0.99-1.00)	0.03	0.996 (0.99-1.00)[c]	0.11[c]
	ceCT_Entropy6	153	4.4 (1.5-12.8)	0.006	3.9 (1.2-12.4)[d]	0.02[d]
	Predictor with cutoff[g]					
	T2_MPP4 <137	49/178	4.0 (1.8-9.0)	<0.001	3.6 (1.5-8.7)[c]	0.005[c]
	ceCT_Entropy6 ≥4.85	68/153	4.6 (1.8-11.8)	0.001	4.5 (1.6-12.6)[d]	0.004[d]
Lymph node metastases	T1c_Entropy6	154	3.1 (1.5-6.6)	0.003	1.7 (0.7-4.3)[a]	0.26[a]
	ceCT_Kurtosis5	131	1.3 (1.1-1.7)	0.01	1.1 (0.8-1.5)[b]	0.75[b]
	Predictor with cutoff[g]					
	T1c_Entropy6 >5.31	49/154	6.0 (2.1-16.9)	<0.001	2.6 (0.7-9.9)[a]	0.16[a]
	ceCT_Kurtosis5 >0.16	61/131	6.0 (1.6-22.4)	0.007	3.4 (0.8-14.0)[b]	0.09[b]
High-risk histological subtype[h]	T1c_MPP4	178	1.01 (1.00-1.01)	0.001	1.01 (1.00-1.01)[e]	0.004[e]
	ceCT_MPP5	153	1.01 (1.00-1.03)	0.02	1.01 (1.00-1.03)[f]	0.10[f]
	Predictor with cutoff[g]					
	T1c_MPP4 >123	80/178	3.1 (1.6-5.7)	<0.001	3.9 (1.7-9.4)[e]	0.002[e]
	ceCT_MPP5 >24.2	96/153	4.7 (2.2-10.2)	<0.001	3.7 (1.3-10.1)[f]	0.01[f]

[a] Adjusted for MRI-measured tumor volume, conventional MRI reading and biopsy risk status[h].
[b] Adjusted for MRI-measured tumor volume, conventional MRI reading, age and biopsy risk status[h].
[c] Adjusted for MRI-measured tumor volume, conventional MRI reading and cervical tumor involvement status in the preoperative endocervical curettage.
[d] Adjusted for MRI-measured tumor volume, conventional MRI reading, age and cervical tumor involvement status in the preoperative endocervical curettage.
[e] Adjusted for MRI-measured tumor volume and biopsy risk status[h].
[f] Adjusted for MRI-measured tumor volume, age and biopsy risk status[h].
[g] Cutoffs are determined by ROC curve analysis selecting the highest Youden index.
[h] High-risk histological subtype is defined as endometrioid grade 3 or non-endometrioid subtype as opposed to low-risk histological subtype defined as endometrioid grade 1 and 2.

Texture features are annotated with number indicating spatial scale filter (SSF).

ADC, apparent diffusion coefficient (map); ceCT, contrast-enhanced CT; CI, confidence interval; CT, computed tomography; MPP, mean of positive pixels; OR, odds ratio; T1c, contrast-enhanced T1-weighted (images); T2, T2-weighted (images).

Table 6. Uni- and multivariable Cox regression analysis for prediction of recurrence- and progression-free survival in endometrial cancer.

Outcome	Predictor	n	Univariable		Multivariable	
			Unadjusted HR (95% CI)	p	Adjusted[a] HR (95% CI)	p
RPFS (**Paper III**)	T1c_Kurtosis2	180	1.7 (1.3-2.3)	<0.001	1.5 (1.2-2.0)	<0.001
	MRI tumor volume	180	1.01 (1.00-1.01)	<0.001	1.01 (1.00-1.01)	0.007
	High-risk biopsy[b]	177	4.3 (2.3-8.0)	<0.001	3.4 (1.8-6.4)	<0.001
	Predictor with cutoff[c]					
	T1c_Kurtosis2 ≥0.26	91/180	3.2 (1.6-6.4)	<0.001	2.2 (1.1-4.5)	0.03
RPFS (**Paper IV**)	ceCT_Kurtosis5	155	1.2 (1.1-1.2)	<0.001	1.1 (1.0-1.2)	0.06
	MRI tumor volume	155	1.01 (1.00-1.01)	<0.001	1.01 (1.00-1.01)	0.01
	High-risk biopsy[a]	152	3.6 (1.9-6.9)	<0.001	2.6 (1.3-5.2)	0.01
	Age	155	1.03 (1.00-1.07)	0.06	1.02 (0.98-1.05)	0.33
	Predictor with cutoff[c]					
	ceCT_Kurtosis5 ≥1.00	39/155	2.9 (1.5-5.5)	0.002	1.8 (0.9-3.8)	0.10

[a] All variables grouped by vertical leaders are included in each multivariable analysis. (When analyzing texture variables with cutoff, the continuous variable is replaced by the corresponding categorical variable in the same analysis.)
[b] High-risk biopsy is defined as endometrioid grade 3 or non-endometrioid subtype as opposed to low-risk comprising endometrioid grade 1 and 2.
[c] Cutoffs are determined by Kaplan-Meier analyses, in which consecutive groups (quartiles) with similar survival are merged: For T1c_Kurtosis2 the *median* value was selected as cutoff, and for ceCT_Kurtosis5 the *75-percentile* value was selected as cutoff.

Texture features are annotated with number indicating spatial scale filter (SSF).

ceCT, contrast-enhanced computed tomography; CI, confidence interval; HR, hazard ratio; MRI, magnetic resonance imaging; RPFS, recurrence- and progression-free survival; T1c, contrast-enhanced T1-weighted (images).

Entropy is a measure of random irregularity and kurtosis is related to the peakedness of the pixel distribution curve in ROIs. In general, high entropy and high kurtosis in tumor images reflect increased histological heterogeneity (71), which in turn is often related to irregular tissue architecture induced by tumor-induced angiogenesis, hypoxia and necrosis (111). Thus, our findings support that intratumor heterogeneity is associated with tumor aggressiveness and reduced survival, which is also reported in several pan-cancer studies assessing genetic heterogeneity in a variety of cancer types (112, 113). In **Paper III**, high MPP in T1c images independently predicted high-risk histological subtype (Table 5), and in **Paper IV**, MPP>24.2 also independently predicted high-risk histological subtype (Table 5). MPP is a TexRAD specific feature defined as the mean value of positive pixels. In CT images MPP can be calculated from

unfiltered as well as filtered images. In MRI, however, the feature MPP is relevant only in filtered images (as native MR images have no negative pixel values), i.e. when objects of a given size in the images are enhanced, by which pixels are recoded into a range of positive values or negative values according to their native values, as elaborated in a review by Miles et al. (98). Consequently, MPP is a measurement of brightness in the highlighted objects in the ROIs, and the impact of dark objects in the ROIs (e.g. nonenhancing fluid collections in T1c images) is reduced. In a study of non-small cell lung cancer, Ganeshan et al. (72) found significant associations between MPP in ceCT tumor ROIs and histological markers of tumor hypoxia and angiogenesis. A recent study of pancreatic cancer also found MPP in ceCT tumor ROIs to be significantly associated with overall survival (71). In the only previous study on MRTA in endometrial cancer, Ueno et al. included MPP of DCE images and ADC maps among 10 other texture features in the prediction of lymphovascular space invasion (68). Although inherently dependent on the imaging modality and sequence, and even if the biological correlate of MPP is somewhat unclear, it seems to have a potential as an imaging biomarker, which our findings also support.

In current literature, most studies on image texture analysis have relatively small patient numbers, and are typically retrospective and could be regarded as proof-of-principle studies. The need for further validation of texture features as imaging biomarkers is obvious. To potentially increase the clinical applicability of texture features, we also suggest aiming at developing more integrative risk prediction models, tentatively including elements from different imaging modalities as well as other biomarkers available preoperatively (e.g. histological and molecular biopsy markers, serum markers and relevant clinical information). Eventually, prospective studies with a priori cutoff values of the included biomarkers should be undertaken.

6.2.5 Diagnostic performance of imaging markers and their prognostic value

For prediction of deep myometrial invasion and lymph node metastases, we have summarized the diagnostic performance of relevant imaging markers in **Paper I-IV** in Table 7. ROC curve analyses in the respective cohorts show that markers based

on tumor size measurements on conventional MR images (**Paper I**) and texture features from MR images (**Paper III**) have the highest AUC for prediction of DMI as well as LNM. MR spectroscopy-based markers (**Paper II**) have the lowest AUC in both analyses. In this context, it should be mentioned that these AUC values do not give information regarding the predictors' independency from established risk factors.

For prediction of recurrence- and progression-free survival (Table 8), MRI-measured tumor size (**Paper I**) and texture features derived from MRI and CT (**Paper III and IV**) are clearly more interesting imaging markers than those derived from MR spectroscopy (**Paper II**). Choline levels in tumor (as measured by the ratios tCho/Creatine, tCho/Water and tCho/Noise) do not seem to reflect survival, whereas the highest ranked size and texture features yield HRs around 3 (unadjusted) when appropriate cutoffs are applied.

Methodologically, among the image derived markers explored in this thesis, tumor size measurement on MR images would probably, at present, be the most feasible marker in daily radiological practice. Interestingly, these markers are also among the highest ranked for prediction of high-risk disease and poor outcome (Table 7 and 8), and they are proven highly reliable (**Paper I**).

Although our studies were not designed for head-to-head comparison of MRI versus CT, it seems reasonable to infer that, in general, MRI texture features are more strongly associated with high-risk endometrial cancer including poor outcome, than CT texture features (Table 6-8). However, if MRI is unavailable, it is worth noting that texture analysis of ordinary diagnostic CT images may provide added value in the preoperative risk stratification.

Table 7. Diagnostic performance of imaging markers for prediction of deep myometrial invasion and lymph node metastases.

Paper	Method	Predictor	n	AUC
		Deep myometrial invasion		
I	MRI	AP tumor diameter	212	0.82
I	MRI	Tumor volume	212	0.81
I	MRI	TV tumor diameter	212	0.78
I	MRI	CC tumor diameter	212	0.76
II	MRS	Tumor tCho/Noise	77	0.61
II	MRS	Tumor tCho/Creatine	75	0.59
II	MRS	Tumor tCho/Water	77	0.56
III	MRTA	Tumor ADC_Entropy6	175	0.81
III	MRTA	Tumor T1c_Entropy0	178	0.80
IV	CTTA	Tumor ceCT_Entropy6	153	0.71
IV	CTTA	Tumor ceCT_Kurtosis3	153	0.71
		Lymph node metastases		
I	MRI	CC tumor diameter	181	0.76
I	MRI	Tumor volume	181	0.70
I	MRI	AP tumor diameter	181	0.68
I	MRI	TV tumor diameter	181	0.67
II	MRS	Tumor tCho/Noise	70	0.61
II	MRS	Tumor tCho/Creatine	68	0.61
II	MRS	Tumor tCho/Water	70	0.49
III	MRTA	Tumor T1c_Entropy6	154	0.73
III	MRTA	Tumor ADC_Entropy0	151	0.71
IV	CTTA	Tumor ceCT_Kurtosis5	131	0.69
IV	CTTA	Tumor ceCT_Entropy2	131	0.66

Texture features are annotated with number indicating spatial scale filter (SSF).

ADC, apparent diffusion coefficient (map); AP, anteroposterior; AUC, area under curve (i.e. receiver operator characteristic curve); CC, craniocaudal; ceCT, contrast-enhanced CT; CT, computed tomography; CTTA, CT texture analysis; MRI, magnetic resonance imaging; MRS, MR spectroscopy; MRTA, MR texture analysis; T1c, contrast-enhanced T1-weigted (images); tCho, total choline containing metabolites; TV, transverse.

Table 8. Prognostic value of imaging markers based on univariable Cox regression analysis.

		Recurrence- and progression-free survival			
Paper	**Method**	**Predictor**	**n**	**HR**	**p**
I	MRI	AP tumor diameter (mm)	212	1.04	<0.001
I	MRI	CC tumor diameter (mm)	212	1.03	<0.001
II	MRS	Tumor tCho/Noise	77	1.14	0.33
II	MRS	Tumor tCho/Creatine	75	0.99	0.84
II	MRS	Tumor tCho/Water	77	0.93	0.49
III	MRTA	Tumor T1c_Kurtosis2	180	1.7	<0.001
III	MRTA	Tumor ADC_Entropy6	177	2.0	<0.001
III	MRTA	Tumor T1c_Entropy6	180	2.1	<0.001
IV	CTTA	Tumor ceCT_Kurtosis5	155	1.2	<0.001
Paper	**Method**	**Predictor *with cutoff****	**proportion**	**HR**	**p**
I	MRI	AP diameter > 20 mm	72/212	2.9	<0.001
I	MRI	CC diameter > 40 mm	69/212	2.4	0.005
I	MRI	AP > 20 mm and CC > 40 mm	52/212	3.4	<0.001
II	MRS	No significant predictor	-	-	-
III	MRTA	T1c_Kurtosis2 ≥ median	91/180	3.2	<0.001
III	MRTA	ADC_Entropy6 ≥ median	89/177	2.5	0.005
III	MRTA	T1c_Entropy6 ≥ 75-percentile	45/180	3.0	<0.001
IV	CTTA	ceCT_Kurtosis5 ≥ 75-percentile	39/155	2.9	0.002

*Cutoffs for tumor size are based on highest possible Youden index for prediction of deep myometrial invasion and lymph node metastases, respectively. Cutoffs for tumor texture features are based on Kaplan-Meier analyses, in which consecutive groups (quartiles) with similar survival are merged.

Texture features are annotated with number indicating spatial scale filter (SSF).

ADC, apparent diffusion coefficient (map); AP, anteroposterior; CC, craniocaudal; ceCT, contrast-enhanced CT; CT, computed tomography; CTTA, CT texture analysis; HR, hazard ratio; MRI, magnetic resonance imaging; MRS, MR spectroscopy; MRTA, MR texture analysis; T1c, contrast-enhanced T1-weigted (images); tCho, total choline containing metabolites.

7 Conclusions

Tumor size can be measured on preoperative conventional MRI with very low interobserver variability. Large tumor size predicts deep myometrial invasion, lymph node metastases and poor outcome in endometrial cancer. Using the cutoff values AP diameter >2 cm and CC diameter >4 cm may improve preoperative risk stratification (**Paper I**).

High choline levels, as measured by preoperative in vivo 1H-MR spectroscopy, differentiates tumor tissue from normal tissue in endometrial cancer patients. In endometrioid tumors, tCho/Water ratio increases with higher histological grade. tCho/Creatine ratio is correlated with MRI-measured tumor volume. However, choline levels do not seem to be associated with recurrence- and progression-free survival (**Paper II**).

MRI-derived tumor texture parameters predict deep myometrial invasion, high-risk histological subtype, and reduced recurrence- and progression-free survival in endometrial cancer (**Paper III**). CT-derived tumor texture features predict deep myometrial invasion and cervical stroma invasion in endometrial cancer, and also tend to predict high-risk histological subtype and survival (**Paper IV**). The image texture features entropy, kurtosis and MPP seem to reflect tumor heterogeneity and may serve as supplementary imaging biomarkers for more refined preoperative risk assessment that may ultimately enable better tailored treatment strategies in endometrial cancer (**Paper III and IV**).

8 Future perspectives

The studies in this thesis have aimed at identifying robust and accurate imaging biomarkers that may aid in the preoperative staging and risk stratification in endometrial cancer. The explored imaging features have all been quantitative in nature. The proposed tumor size cutoffs (**Paper I**) for identification of high-risk endometrial cancer, were *a posteriori* applied and optimized for the current dataset, which is adequate as an initial study. Given the promising results in **Paper I**, a future validation study with tumor size cutoffs *a priori* defined for an independent cohort, would be very interesting. The idea of replacing MRI-based depth-of-myometrial-invasion scoring with tumor size measurement could also be pursued. With recent advances of ultrasound technology, updated head-to-head studies comparing TVUS and MRI in terms of tumor size measurements and tumor invasion assessments, would also be interesting.

The paucity of significant findings in **Paper II** might discourage future research on MR spectroscopy in endometrial cancer. Still, the method is indisputably intriguing, as it – at least theoretically – has the potential to reveal a metabolic tumor profile, which eventually may become relevant in future targeted therapies. It is worth mentioning that all currently available studies on MR spectroscopy in endometrial cancer, including our study, are relatively small. A larger study at 3T (or higher field) with exploration of a wider range of metabolites (not limited to choline as in our study) would definitely be interesting – especially if methodological refinements could help to overcome some of the obstacles of spectroscopic imaging of the uterus in vivo.

Image texture analysis is largely unexplored in endometrial cancer. The promising results of MR- and CT texture analysis in **Paper III and IV**, accompanied by a few other endometrial cancer studies reporting texture analysis of MRI (68) and PET (69) as promising tools for preoperative risk stratification, should encourage future studies in this field. Our findings need validation across observers, institutions and software platforms. In general, texture analysis can be considered as one out of many elements

of radiomics, the science of high-throughput extraction of quantitative features from radiological imaging data. Future perspectives of radiomics include machine learning, and probably also approaches related to artificial intelligence. Our annotated endometrial cancer dataset (including clinical, imaging, histological and molecular data) is well suited for further radiomic studies. During recent years we also have examined a substantial number of endometrial cancer patients at 3T MRI. With increased image quality, the potential for texture analysis might also be increased. Eventually, some degree of standardization is needed to establish image texture analysis as a risk stratification tool in a true prospective setting and in clinical practice. Development of future risk stratification models would probably also benefit from a more multimodal and integrative approach, not limiting models to imaging markers. Thus, multidisciplinary research with radiology playing a key role, will hopefully yield further progress in endometrial cancer research.

9 References

1. Ferlay J, Soerjomataram I, Dikshit R, et al. Cancer incidence and mortality worldwide: sources, methods and major patterns in GLOBOCAN 2012. Int J Cancer 2015; 136:E359-E386.

2. Morice P, Leary A, Creutzberg C, Abu-Rustum N, Darai E. Endometrial cancer. Lancet 2016; 387:1094-1108.

3. Cancer Registry of Norway. Cancer in Norway 2017 - Cancer incidence, mortality, survival and prevalence in Norway. Oslo: Cancer Registry of Norway, 2018.

4. Wartko P, Sherman ME, Yang HP, Felix AS, Brinton LA, Trabert B. Recent changes in endometrial cancer trends among menopausal-age U.S. women. Cancer Epidemiol 2013; 37:374-377.

5. Abeler VM, Royne O, Thoresen S, Danielsen HE, Nesland JM, Kristensen GB. Uterine sarcomas in Norway. A histopathological and prognostic survey of a total population from 1970 to 2000 including 419 patients. Histopathology 2009; 54:355-364.

6. Koivisto-Korander R, Martinsen JI, Weiderpass E, Leminen A, Pukkala E. Incidence of uterine leiomyosarcoma and endometrial stromal sarcoma in Nordic countries: results from NORDCAN and NOCCA databases. Maturitas 2012; 72:56-60.

7. Bender D, Buekers T, Leslie K. Hormones and receptors in endometrial cancer. Proc Obstet Gynecol 2011; 2:1.

8. Bokhman JV. Two pathogenetic types of endometrial carcinoma. Gynecol Oncol 1983; 15:10-17.

9. Kandoth C, Schultz N, Cherniack AD, et al. Integrated genomic characterization of endometrial carcinoma. Nature 2013; 497:67-73.

10. Randall LM, Pothuri B. The genetic prediction of risk for gynecologic cancers. Gynecol Oncol 2016; 141:10-16.

11. Tan MH, Mester JL, Ngeow J, Rybicki LA, Orloff MS, Eng C. Lifetime cancer risks in individuals with germline PTEN mutations. Clin Cancer Res 2012; 18:400-407.

12. Lu KH, Daniels M. Endometrial and ovarian cancer in women with Lynch syndrome: update in screening and prevention. Fam Cancer 2013; 12:273-277.

13. Mahdi H, Mester JL, Nizialek EA, Ngeow J, Michener C, Eng C. Germline PTEN, SDHB-D, and KLLN alterations in endometrial cancer patients with Cowden and Cowden-like syndromes: an international, multicenter, prospective study. Cancer 2015; 121:688-696.

14. Amant F, Moerman P, Neven P, Timmerman D, Van LE, Vergote I. Endometrial cancer. Lancet 2005; 366:491-505.

15. Kurman RJ, Carcangui ML, Herrington CS, Young RH (Eds.). WHO classification of tumours of the female reproductive organs. 4th ed. Lyon: IARC, 2014.

16. Gilks CB, Oliva E, Soslow RA. Poor interobserver reproducibility in the diagnosis of high-grade endometrial carcinoma. Am J Surg Pathol 2013; 37:874-881.

17. Han G, Sidhu D, Duggan MA, et al. Reproducibility of histological cell type in high-grade endometrial carcinoma. Mod Pathol 2013; 26:1594-1604.

18. Zaino RJ, Kauderer J, Trimble CL, et al. Reproducibility of the diagnosis of atypical endometrial hyperplasia: a Gynecologic Oncology Group study. Cancer 2006; 106:804-811.

19. Gredmark T, Kvint S, Havel G, Mattsson LA. Histopathological findings in women with postmenopausal bleeding. Br J Obstet Gynaecol 1995; 102:133-136.

20. Pennant ME, Mehta R, Moody P, et al. Premenopausal abnormal uterine bleeding and risk of endometrial cancer. BJOG 2017; 124:404-411.

21. Dijkhuizen FP, Mol BW, Brolmann HA, Heintz AP. The accuracy of endometrial sampling in the diagnosis of patients with endometrial carcinoma and hyperplasia: a meta-analysis. Cancer 2000; 89:1765-1772.

22. Trimble CL, Kauderer J, Zaino R, et al. Concurrent endometrial carcinoma in women with a biopsy diagnosis of atypical endometrial hyperplasia: a Gynecologic Oncology Group study. Cancer 2006; 106:812-819.

23. Touboul C, Piel B, Koskas M, et al. Factors predictive of endometrial carcinoma in patients with atypical endometrial hyperplasia on preoperative histology. Anticancer Res 2014; 34:5671-5676.

24. Werner HM, Trovik J, Marcickiewicz J, et al. A discordant histological risk classification in preoperative and operative biopsy in endometrial cancer is reflected in metastatic risk and prognosis. Eur J Cancer 2013; 49:625-632.

25. Smith-Bindman R, Kerlikowske K, Feldstein VA, et al. Endovaginal ultrasound to exclude endometrial cancer and other endometrial abnormalities. JAMA 1998; 280:1510-1517.

26. Fischerova D, Cibula D. Ultrasound in gynecological cancer: is it time for re-evaluation of its uses? Curr Oncol Rep 2015; 17:28.

27. Haldorsen IS, Salvesen HB. What Is the Best Preoperative Imaging for Endometrial Cancer? Curr Oncol Rep 2016; 18:25.

28. Grant P, Sakellis C, Jacene HA. Gynecologic oncologic imaging with PET/CT. Semin Nucl Med 2014; 44:461-478.

29. Basu S, Li G, Alavi A. PET and PET-CT imaging of gynecological malignancies: present role and future promise. Expert Rev Anticancer Ther 2009; 9:75-96.

30. Kitajima K, Murakami K, Yamasaki E, Kaji Y, Sugimura K. Accuracy of integrated FDG-PET/contrast-enhanced CT in detecting pelvic and paraaortic lymph node metastasis in patients with uterine cancer. Eur Radiol 2009; 19:1529-1536.

31. Baser E, Gungor T, Togrul C, Turkoglu O, Celen S. Preoperative prediction of poor prognostic parameters and adjuvant treatment in women with pure endometrioid type endometrial cancer: what is the significance of tumor markers? Eur J Gynaecol Oncol 2014; 35:513-518.

32. Hsieh CH, ChangChien CC, Lin H, et al. Can a preoperative CA 125 level be a criterion for full pelvic lymphadenectomy in surgical staging of endometrial cancer? Gynecol Oncol 2002; 86:28-33.

33. Kim HS, Park CY, Lee JM, et al. Evaluation of serum CA-125 levels for preoperative counseling in endometrioid endometrial cancer: a multi-center study. Gynecol Oncol 2010; 118:283-288.

34. Todo Y, Okamoto K, Takeshita S, Sudo S, Kato H. A patient group at negligible risk of para-aortic lymph node metastasis in endometrial cancer. Gynecol Oncol 2016; 141:155-159.

35. Salvesen HB, Haldorsen IS, Trovik J. Markers for individualised therapy in endometrial carcinoma. Lancet Oncol 2012; 13:e353-e361.

36. Staff AC, Trovik J, Eriksson AG, et al. Elevated plasma growth differentiation factor-15 correlates with lymph node metastases and poor survival in endometrial cancer. Clin Cancer Res 2011; 17:4825-4833.

37. Guntupalli SR, Zighelboim I, Kizer NT, et al. Lymphovascular space invasion is an independent risk factor for nodal disease and poor outcomes in endometrioid endometrial cancer. Gynecol Oncol 2012; 124:31-35.

38. Suehiro Y, Okada T, Okada T, et al. Aneuploidy predicts outcome in patients with endometrial carcinoma and is related to lack of CDH13 hypermethylation. Clin Cancer Res 2008; 14:3354-3361.

39. Wik E, Raeder MB, Krakstad C, et al. Lack of estrogen receptor-alpha is associated with epithelial-mesenchymal transition and PI3K alterations in endometrial carcinoma. Clin Cancer Res 2013; 19:1094-1105.

40. Tangen IL, Werner HM, Berg A, et al. Loss of progesterone receptor links to high proliferation and increases from primary to metastatic endometrial cancer lesions. Eur J Cancer 2014; 50:3003-3010.

41. Bosse T, Nout RA, Stelloo E, et al. L1 cell adhesion molecule is a strong predictor for distant recurrence and overall survival in early stage endometrial cancer: pooled PORTEC trial results. Eur J Cancer 2014; 50:2602-2610.

42. Salvesen HB, Iversen OE, Akslen LA. Prognostic significance of angiogenesis and Ki-67, p53, and p21 expression: a population-based endometrial carcinoma study. J Clin Oncol 1999; 17:1382-1390.

43. Birkeland E, Wik E, Mjos S, et al. KRAS gene amplification and overexpression but not mutation associates with aggressive and metastatic endometrial cancer. Br J Cancer 2012; 107:1997-2004.

44. Colombo N, Creutzberg C, Amant F, et al. ESMO-ESGO-ESTRO Consensus Conference on Endometrial Cancer: diagnosis, treatment and follow-up. Ann Oncol 2016; 27:16-41.

45. Frei KA, Kinkel K. Staging endometrial cancer: role of magnetic resonance imaging. J Magn Reson Imaging 2001; 13:850-855.

46. Kinkel K, Forstner R, Danza FM, et al. Staging of endometrial cancer with MRI: guidelines of the European Society of Urogenital Imaging. Eur Radiol 2009; 19:1565-1574.

47. Sala E, Rockall AG, Freeman SJ, Mitchell DG, Reinhold C. The added role of MR imaging in treatment stratification of patients with gynecologic malignancies: what the radiologist needs to know. Radiology 2013; 266:717-740.

48. Barwick TD, Rockall AG, Barton DP, Sohaib SA. Imaging of endometrial adenocarcinoma. Clin Radiol 2006; 61:545-555.

49. Kinkel K, Kaji Y, Yu KK, et al. Radiologic staging in patients with endometrial cancer: a meta-analysis. Radiology 1999; 212:711-718.

50. Lin G, Ng KK, Chang CJ, et al. Myometrial invasion in endometrial cancer: diagnostic accuracy of diffusion-weighted 3.0-T MR imaging--initial experience. Radiology 2009; 250:784-792.

51. Shen SH, Chiou YY, Wang JH, et al. Diffusion-weighted single-shot echo-planar imaging with parallel technique in assessment of endometrial cancer. AJR Am J Roentgenol 2008; 190:481-488.

52. Takeuchi M, Matsuzaki K, Nishitani H. Diffusion-weighted magnetic resonance imaging of endometrial cancer: differentiation from benign endometrial lesions and preoperative assessment of myometrial invasion. Acta Radiol 2009; 50:947-953.

53. Inada Y, Matsuki M, Nakai G, et al. Body diffusion-weighted MR imaging of uterine endometrial cancer: is it helpful in the detection of cancer in nonenhanced MR imaging? Eur J Radiol 2009; 70:122-127.

54. Kilickesmez O, Bayramoglu S, Inci E, Cimilli T, Kayhan A. Quantitative diffusion-weighted magnetic resonance imaging of normal and diseased uterine zones. Acta Radiol 2009; 50:340-347.

55. Husby JA, Salvesen OO, Magnussen IJ, et al. Tumour apparent diffusion coefficient is associated with depth of myometrial invasion and is negatively correlated to tumour volume in endometrial carcinomas. Clin Radiol 2015; 70:487-494.

56. Leach MO, Morgan B, Tofts PS, et al. Imaging vascular function for early stage clinical trials using dynamic contrast-enhanced magnetic resonance imaging. Eur Radiol 2012; 22:1451-1464.

57. Haldorsen IS, Stefansson I, Gruner R, et al. Increased microvascular proliferation is negatively correlated to tumour blood flow and is associated with unfavourable outcome in endometrial carcinomas. Br J Cancer 2014; 110:107-114.

58. Haldorsen IS, Gruner R, Husby JA, et al. Dynamic contrast-enhanced MRI in endometrial carcinoma identifies patients at increased risk of recurrence. Eur Radiol 2013; 23:2916-2925.

59. Harry VN, Semple SI, Parkin DE, Gilbert FJ. Use of new imaging techniques to predict tumour response to therapy. Lancet Oncol 2010; 11:92-102.

60. Takeuchi M, Matsuzaki K, Harada M. Differentiation of benign and malignant uterine corpus tumors by using proton MR spectroscopy at 3T: preliminary study. Eur Radiol 2011; 21:850-856.

61. Zhang J, Cai S, Li C, et al. Can magnetic resonance spectroscopy differentiate endometrial cancer? Eur Radiol 2014; 24:2552-2560.

62. Han X, Kang J, Zhang J, et al. Can the signal-to-noise ratio of choline in magnetic resonance spectroscopy reflect the aggressiveness of endometrial cancer? Acad Radiol 2015; 22:453-459.

63. Takeuchi M, Matsuzaki K, Harada M. Carcinosarcoma of the uterus: MRI findings including diffusion-weighted imaging and MR spectroscopy. Acta Radiol 2016.

64. Okada T, Harada M, Matsuzaki K, Nishitani H, Aono T. Evaluation of female intrapelvic tumors by clinical proton MR spectroscopy. J Magn Reson Imaging 2001; 13:912-917.

65. Rockall AG, Sohaib SA, Harisinghani MG, et al. Diagnostic performance of nanoparticle-enhanced magnetic resonance imaging in the diagnosis of lymph node metastases in patients with endometrial and cervical cancer. J Clin Oncol 2005; 23:2813-2821.

66. Fortuin AS, Bruggemann R, van der Linden J, et al. Ultra-small superparamagnetic iron oxides for metastatic lymph node detection: back on the block. Wiley Interdiscip Rev Nanomed Nanobiotechnol 2018; 10.

67. Sala E, Mema E, Himoto Y, et al. Unravelling tumour heterogeneity using next-generation imaging: radiomics, radiogenomics, and habitat imaging. Clin Radiol 2017; 72:3-10.

68. Ueno Y, Forghani B, Forghani R, et al. Endometrial Carcinoma: MR Imaging-based Texture Model for Preoperative Risk Stratification-A Preliminary Analysis. Radiology 2017; 284:748-757.

69. De Bernardi E, Buda A, Guerra L, et al. Radiomics of the primary tumour as a tool to improve (18)F-FDG-PET sensitivity in detecting nodal metastases in endometrial cancer. EJNMMI Res 2018; 8:86.

70. Ng F, Ganeshan B, Kozarski R, Miles KA, Goh V. Assessment of primary colorectal cancer heterogeneity by using whole-tumor texture analysis: contrast-enhanced CT texture as biomarker of 5-year survival. Radiology 2013; 266(1):177-84.

71. Sandrasegaran K, Lin Y, Asare-Sawiri M, Taiyini T, Tann M. CT texture analysis of pancreatic cancer. Eur Radiol 2019; 29(3):1067-1073.

72. Ganeshan B, Goh V, Mandeville HC, Ng QS, Hoskin PJ, Miles KA. Non-small cell lung cancer: histopathologic correlates for texture parameters at CT. Radiology 2013; 266:326-336.

73. Smith AD, Gray MR, Del Campo AM et al. Predicting overall survival in patients with metastatic melanoma on antiangiogenic therapy and RECIST stable disease on initial posttherapy images using CT texture analysis. AJR 2015; 205:w283-w293.

74. Pecorelli S. Revised FIGO staging for carcinoma of the vulva, cervix, and endometrium. Int J Gynaecol Obstet 2009; 105:103-104.

75. Denschlag D, Reed NS, Rodolakis A. Fertility-sparing approaches in gynecologic cancers: a review of ESGO task force activities. Curr Oncol Rep 2012; 14:535-538.

76. Lu Q, Liu H, Liu C, et al. Comparison of laparoscopy and laparotomy for management of endometrial carcinoma: a prospective randomized study with 11-year experience. J Cancer Res Clin Oncol 2013; 139:1853-1859.

77. Takano M, Ochi H, Takei Y, et al. Surgery for endometrial cancers with suspected cervical involvement: is radical hysterectomy needed (a GOTIC study)? Br J Cancer 2013; 109:1760-1765.

78. Benedetti PP, Basile S, Maneschi F, et al. Systematic pelvic lymphadenectomy vs. no lymphadenectomy in early-stage endometrial carcinoma: randomized clinical trial. J Natl Cancer Inst 2008; 100:1707-1716.

79. Kitchener H, Swart AM, Qian Q, Amos C, Parmar MK. Efficacy of systematic pelvic lymphadenectomy in endometrial cancer (MRC ASTEC trial): a randomised study. Lancet 2009; 373:125-136.

80. Norsk gynekologisk forening. Veileder gynekologisk onkologi. https://legeforeningen.no/Fagmed/Norsk-gynekologisk-forening/Veiledere/Veileder-gynekologisk-onkologi/

81. Colombo N, Preti E, Landoni F, et al. Endometrial cancer: ESMO Clinical Practice Guidelines for diagnosis, treatment and follow-up. Ann Oncol 2013; 24 Suppl 6:vi33-vi38.

82. Chan JK, Kapp DS. Role of complete lymphadenectomy in endometrioid uterine cancer. Lancet Oncol 2007; 8:831-841.

83. Rossi EC, Kowalski LD, Scalici J, et al. A comparison of sentinel lymph node biopsy to lymphadenectomy for endometrial cancer staging (FIRES trial): a multicentre, prospective, cohort study. Lancet Oncol 2017; 18:384-392.

84. Khoury-Collado F, St CC, Abu-Rustum NR. Sentinel Lymph Node Mapping in Endometrial Cancer: An Update. Oncologist 2016; 21:461-466.

85. Nougaret S, Horta M, Sala E, et al. Endometrial Cancer MRI staging: Updated Guidelines of the European Society of Urogenital Radiology. Eur Radiol 2019; 29:792-805.

86. Eisenhauer EA, Therasse P, Bogaerts J, et al. New response evaluation criteria in solid tumours: revised RECIST guideline (version 1.1). Eur J Cancer 2009; 45:228-247.

87. Tirkes T, Hollar MA, Tann M, Kohli MD, Akisik F, Sandrasegaran K. Response criteria in oncologic imaging: review of traditional and new criteria. Radiographics 2013; 33:1323-1341.

88. Haldorsen IS, Salvesen HB. Staging of endometrial carcinomas with MRI using traditional and novel MRI techniques. Clin Radiol 2012; 67:2-12.

89. Haldorsen IS, Husby JA, Werner HM, et al. Standard 1.5-T MRI of endometrial carcinomas: modest agreement between radiologists. Eur Radiol 2012; 22:1601-1611.

90. Beddy P, Moyle P, Kataoka M, et al. Evaluation of depth of myometrial invasion and overall staging in endometrial cancer: comparison of diffusion-weighted and dynamic contrast-enhanced MR imaging. Radiology 2012; 262:530-537.

91. Fujii S, Matsusue E, Kigawa J, et al. Diagnostic accuracy of the apparent diffusion coefficient in differentiating benign from malignant uterine endometrial cavity lesions: initial results. Eur Radiol 2008; 18:384-389.

92. Sjobakk TE, Lundgren S, Kristoffersen A, et al. Clinical 1H magnetic resonance spectroscopy of brain metastases at 1.5T and 3T. Acta Radiol 2006; 47:501-508.

93. Todo Y, Okamoto K, Hayashi M, et al. A validation study of a scoring system to estimate the risk of lymph node metastasis for patients with endometrial cancer for tailoring the indication of lymphadenectomy. Gynecol Oncol 2007; 104:623-628.

94. Todo Y, Watari H, Okamoto K, et al. Tumor volume successively reflects the state of disease progression in endometrial cancer. Gynecol Oncol 2013; 129:472-477.

95. Naressi A, Couturier C, Devos JM, et al. Java-based graphical user interface for the MRUI quantitation package. MAGMA 2001; 12:141–152.

96. Vanhamme L, van den Boogaart A, Van HS. Improved method for accurate and efficient quantification of MRS data with use of prior knowledge. J Magn Reson 1997; 129:35–43.

97. Stanwell P, Russell P, Carter J, et al. Evaluation of ovarian tumors by proton magnetic resonance spectroscopy at three Tesla. Invest Radiol 2008; 43:745–751.

98. Miles KA, Ganeshan B, Hayball MP. CT texture analysis using the filtration-histogram method: what do the measurements mean? Cancer Imaging 2013; 13:400-406.

99. Gillies RJ, Kinahan PE, Hricak H. Radiomics: Images Are More than Pictures, They Are Data. Radiology 2016; 278:563-577.

100. Schink JC, Rademaker AW, Miller DS, Lurain JR. Tumor size in endometrial cancer. Cancer 1991; 67:2791-2794.

101. Mariani A, Webb MJ, Keeney GL, Lesnick TG, Podratz KC. Surgical stage I endometrial cancer: predictors of distant failure and death. Gynecol Oncol 2002; 87:274-280.

102. Shah C, Johnson EB, Everett E, et al. Does size matter? Tumor size and morphology as predictors of nodal status and recurrence in endometrial cancer. Gynecol Oncol 2005; 99:564-570.

103. Chattopadhyay S, Cross P, Nayar A, Galaal K, Naik R. Tumor size: a better independent predictor of distant failure and death than depth of myometrial invasion in International Federation of Gynecology and Obstetrics stage I endometrioid endometrial cancer. Int J Gynecol Cancer 2013; 23:690-697.

104. Glunde K, Jacobs MA, Bhujwalla ZM. Choline metabolism in cancer: implications for diagnosis and therapy. Expert Rev Mol Diagn 2006; 6:821-829.

105. Negendank W. Studies of human tumors by MRS: a review. NMR Biomed 1992; 5:303-324.

106. Podo F. Tumour phospholipid metabolism. NMR Biomed 1999; 12:413-439.

107. Ackerstaff E, Glunde K, Bhujwalla ZM. Choline phospholipid metabolism: a target in cancer cells? J Cell Biochem 2003; 90:525-533.

108. Rose CJ, Mills SJ, O'Connor JP, et al. Quantifying spatial heterogeneity in dynamic contrast-enhanced MRI parameter maps. Magn Reson Med 2009; 62:488-499.

109. Ahmed A, Gibbs P, Pickles M, Turnbull L. Texture analysis in assessment and prediction of chemotherapy response in breast cancer. J Magn Reson Imaging 2013; 38:89-101.

110. Wibmer A, Hricak H, Gondo T, et al. Haralick texture analysis of prostate MRI: utility for differentiating non-cancerous prostate from prostate cancer and differentiating prostate cancers with different Gleason scores. Eur Radiol 2015; 25:2840-2850.

111. Ganeshan B, Miles KA. Quantifying tumour heterogeneity with CT. Cancer Imaging 2013; 13:140-149.

112. Andor N, Graham TA, Jansen M, et al. Pan-cancer analysis of the extent and consequences of intratumor heterogeneity. Nat Med 2016; 22:105-113.

113. Morris LG, Riaz N, Desrichard A, et al. Pan-cancer analysis of intratumor heterogeneity as a prognostic determinant of survival. Oncotarget 2016; 7:10051-10063.

STUDY 1

OPEN

Preoperative Tumor Size at MRI Predicts Deep Myometrial Invasion, Lymph Node Metastases, and Patient Outcome in Endometrial Carcinomas

Sigmund Ytre-Hauge, MD,† Jenny A. Husby, MD,*† Inger J. Magnussen, MD,* Henrica M.J. Werner, MD, PhD,‡§ Øyvind O. Salvesen, MSc, PhD,|| Line Bjørge, MD, PhD,‡§ Jone Trovik, MD, PhD,‡§ Ingunn M. Stefansson, MD, PhD,¶# Helga B. Salvesen, MD, PhD,‡§ and Ingfrid S. Haldorsen, MD, PhD*†*

Objective: The aim of this study was to explore the relation between preoperative tumor size based on magnetic resonance imaging (MRI) and the surgical pathologic staging parameters (deep myometrial invasion, cervical stroma invasion, and metastatic lymph nodes) and to assess the prognostic impact of tumor size in endometrial carcinomas. Interobserver variability for the different tumor size measurements was also assessed.

Methods/Materials: Preoperative pelvic MRI of 212 patients with histologically confirmed endometrial carcinomas was read independently by 3 radiologists. Maximum tumor diameters were measured in 3 orthogonal planes (anteroposterior, transverse, and craniocaudal planes [CC]), and tumor volumes were estimated. Tumor size was analyzed in relation to surgical staging results and patient survival. The multivariate analyses were adjusted for preoperative risk status based on endometrial biopsy. Intraclass correlation coefficients and receiver operating characteristics curves for the different tumor measurements were also calculated.

Results: Anteroposterior tumor diameter independently predicted deep myometrial invasion ($P < 0.001$), whereas CC tumor diameter tended to independently predict lymph node metastases ($P = 0.06$). Based on receiver operating characteristic curves, the following tumor size cutoff values were identified: anteroposterior diameter greater than 2 cm predicted deep myometrial invasion (unadjusted odds ratio [OR], 12.4; $P < 0.001$; adjusted OR, 6.7; $P < 0.001$) and CC diameter greater than 4 cm predicted lymph node metastases (unadjusted OR, 6.2; $P < 0.001$; adjusted OR, 4.9; $P = 0.009$). Large tumor size was associated with reduced progression/recurrence-free survival ($P \leq 0.005$ for all size

*Department of Radiology, Haukeland University Hospital; †Section for Radiology, Department of Clinical Medicine, University of Bergen; ‡Department of Obstetrics and Gynecology, Haukeland University Hospital; §Center for Cancer Biomarkers, Department of Clinical Science, University of Bergen, Bergen; ||Unit for Applied Clinical Research, Department of Cancer Research and Molecular Medicine, Norwegian University of Science and Technology, Trondheim; ¶Center for Cancer Biomarkers, the Gade Institute, Department of Clinical Medicine, University of Bergen; and #Department of Pathology, Haukeland University Hospital, Bergen, Norway.

Address correspondence and reprint requests to Ingfrid S. Haldorsen, MD, PhD, Department of Radiology, Haukeland University Hospital, Jonas Liesvei 65, 5021 Bergen, Norway. E-mail: ingfrid.haldorsen@helse-bergen.no.

ISSN: 1048-891X
DOI: 10.1097/IGC.0000000000000367

Supported by the Western Norway Regional Health Authority; Research Funds at the Department of Radiology; Haukeland University Hospital; Norwegian Research Council; the University of Bergen; the Meltzer Foundation; the Norwegian Cancer Society (the Harald Andersen's legacy); MedViz (www.medviz.uib.no); a medical imaging and visualization research and development cluster in Western Norway founded by Haukeland University Hospital, University of Bergen, and Christian Michelsen Research; and Bergen Research Foundation.

Supplemental digital content is available for this article. Direct URL citation appears in the printed text and is provided in the HTML and PDF versions of this article on the journal's Web site (www.ijgc.net).

The authors declare no conflicts of interest.

parameters), and CC diameter had an independent impact on survival (adjusted hazards ratio, 1.04; $P = 0.009$). The interobserver variability for the different size measurements was very low (intraclass correlation coefficient, 0.78–0.85).

Conclusions: Anteroposterior tumor diameter greater than 2 cm predicts deep myometrial invasion, and CC tumor diameter greater than 4 cm predicts lymph node metastases. Tumor size is a strong prognostic factor in endometrial carcinomas. Preoperative tumor measurements based on MRI may potentially improve preoperative risk stratification models and thus enable better tailored surgical treatment in endometrial cancer.

Key Words: Endometrial carcinoma, Tumor size, Magnetic resonance imaging, Prognosis

Received October 24, 2014, and in revised form November 9, 2014.
Accepted for publication December 8, 2014.

(*Int J Gynecol Cancer* 2015;25: 459–466)

Endometrial cancer is the most common gynecologic malignancy in industrialized countries, and the incidence is increasing.[1] Surgical treatment is planned based on preoperative assessment of histological subtype, grade, and depth of myometrial invasion. Surgical International Federation of Gynecology and Obstetrics (FIGO) stage is documented to be the strongest prognostic factor in endometrial carcinoma, thus guiding adjuvant therapy in addition to the assessment of histologic subtype and grade in the hysterectomy specimen.[1–3]

Magnetic resonance imaging (MRI) has long been considered the diagnostic imaging method of choice for preoperative staging of endometrial carcinomas.[4–6] The presence of deep myometrial invasion and cervical stroma invasion could be visualized, and enlarged lymph nodes could be detected. However, conventional pelvic MRI has reportedly limitations in accuracy in the detection of the staging parameters, in particular for detecting lymph node metastases.[6,7] Interobserver variation between radiologists for all staging parameters also represents a source of inaccuracy.[8]

As opposed to the cervical cancer FIGO staging system,[6] FIGO staging for endometrial cancers does not include tumor size measurements. Nevertheless, large macroscopic tumor size, assessed in the hysterectomy specimen, has long been known to predict lymph node metastasis and poor survival in patients with endometrial carcinomas.[9–13] Recent publications support that tumor volume based on preoperative MRI predicts lymph node metastases and has prognostic impact in endometrial cancer.[14,15] However, the reproducibility of MRI-based tumor measurements has, to our knowledge, not yet been explored. Furthermore, the optimal cutoff value for risk assessment based on tumor size is not yet defined.

The primary objective of this study was to explore the relationship between different preoperative tumor size measurements using MRI and the surgical pathologic staging parameters deep myometrial invasion, cervical stroma invasion, and metastatic lymph nodes in endometrial carcinoma patients. The secondary objectives were to assess the interobserver variability for the different tumor measurements and to explore the value of these preoperative tumor size measurements to identify patients with poor outcome.

MATERIALS AND METHODS

Patient Series, Study Setting, and Clinical Outcome

This prospective study was conducted under institutional review board–approved protocols with informed consent from all patients. From April 2009 to November 2013, preoperative pelvic MRI was performed in 212 patients in whom the diagnosis of endometrial carcinoma was histologically verified at surgical staging. All patients were diagnosed and treated at the same university hospital serving a population of ~1 million inhabitants.

Follow-up data regarding recurrence, progression, and survival have been collected from patient records and from correspondence with the responsible primary physicians or gynecologists. The date of the last follow-up was July 2014, and the mean (range) follow-up for survivors was 25 (0–58) months.

Histological Diagnosis

All patients were surgically staged according to the 2009 FIGO staging criteria.[2] The responsible surgeon decided the extent of sampling, balancing preoperatively known histologic risk factors and the patient's comorbidity. The patient group without lymph node sampling is typically older with more myometrial invasion, otherwise not different from the sampled group.[16] Surgical specimens were sectioned along the longitudinal plane of the uterus, and myometrial invasion and cervical stromal invasion were estimated grossly and confirmed microscopically according to standard procedures.[17] Routine histopathology reports were generated without knowledge of preoperative MRI findings. The pathologists documented number and size of metastatic lymph nodes.

MRI Protocol

Contrast-enhanced (CE) MRI was performed on a 1.5-T Siemens Avanto Running Syngo MR B17 (Erlangen, Germany) using a 6-channel body coil[8] in accordance with the guidelines of European Society of Urogenital Imaging.[5] The mean (range) interval between MRI examination and surgical staging was 11.3 (0–98) days.

Data Analysis

All images were deidentified and read independently by 3 observers who were blinded for tumor stage, histological diagnosis, and patient outcome. Observer 1 and 2 are consultants with more than 10 years of experience with pelvic MRI. Observer 3 included 2 junior radiologists (both having more than 4 years of experience with pelvic MRI); one read the first 105 MRI examinations, and the other read the following 111 examinations.

All observers reported imaging findings on a standardized form. Presence of deep myometrial invasion (tumor invading half or more of the myometrial wall), cervical stroma invasion (disruption of the low-signal intensity cervical stroma on T2-weighted images), and enlarged pelvic or paraaortic lymph nodes (largest short-axis diameter >10 mm) were recorded. Maximum tumor diameters were measured in 3 orthogonal planes: anteroposterior (AP) and transverse (TV) diameters on axial CE T1-weighted oblique images (perpendicular to the long axis of the uterus) as well as craniocaudal (CC) diameters on sagittal T2-weighted images (Fig. 1). Tumor volume was then estimated based on these measurements of maximum tumor diameter in 3 orthogonal planes using the following equation: tumor volume = AP diameter × TV diameter × CC diameter/2.

To establish the overall imaging findings based on the recordings by all 3 observers, we also computed a new data set ("consensus reading") in which the value given by the majority of the observers was recorded for categorical variables, and the median value was recorded for continuous variables.

Statistical Analysis

Estimation of sample size was done by χ^2 test using software East4 2005 (Cytel Software Corp). To achieve 90% power of detecting a 20% higher occurrence of positive markers in patients with metastatic lymph nodes (5% vs 25%) at a 5% significance level, 101 patients were needed for inclusion, defining the minimum number of patients to be included in the MRI study. To reach 90% power detecting a 30% difference in 5-year survival (90% for patients with markers within reference range vs 60% with pathologic markers) at a 5% level of significance, 65 patients were needed, assuming a positive to negative ratio of the markers of 1:3.

Clinical and histopathology staging parameters were analyzed in relation to tumor size measurements using Mann-Whitney *U* test, Kruskal-Wallis H test, Jonckheere-Terpsta trend test, χ^2 test, and binary logistic regression analysis. Intraclass correlation coefficient was used to assess the consistency and reproducibility of tumor size measurements, and minimal detectable change (1.96 × standard error of the mean × square root of 2) for the measured diameters was also calculated.

Receiver operating characteristic (ROC) analysis was performed to evaluate the diagnostic value of the different tumor size measurements in identifying deep myometrial invasion, cervical stroma invasion, and lymph node metastases. The optimal cutoff values (rounded to centimeters) were determined for which the best separation in Youden index between groups was achieved.

Differences in time to recurrence (for patients considered cured by primary treatment) or progression (for patients known to have residual disease after primary treatment) were assessed by the Mantel-Cox (log-rank) linear trend test. The Cox proportional hazards model was used to study the effect on survival of continuous variables. The prognostic value of different tumor size categories was explored with univariate analyses using Kaplan-Meier, and groups with similar survival were merged. McNemar test was used for pairwise analysis for differences in sensitivity, specificity, and accuracy. The data were analyzed using SPSS 22.0 (Chicago, IL) and Stata 12.1 (College Station, TX). All reported *P* values were 2-sided and considered to indicate statistical significance when less than 0.05.

RESULTS

Patients

The median (mean) patient age in the study sample (n = 212) was 66 (66) years (range, 32-93), and 91% (193/212) of the patients were postmenopausal. Applying the FIGO 2009 staging criteria, 55% (116/212) were stage IA (<50%

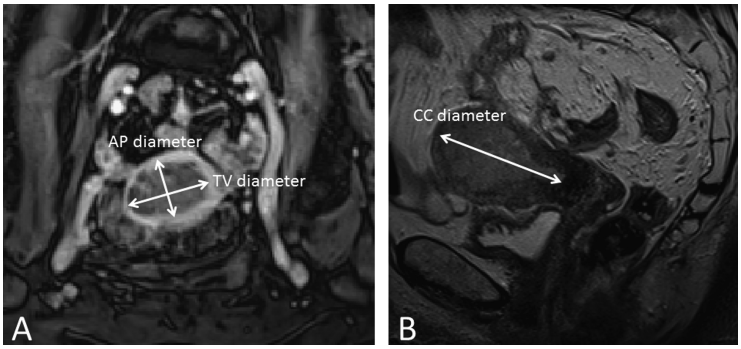

FIGURE 1. Axial oblique CE T1-weighted image (A) and sagittal T2-weighted image (B) for measurements of maximum tumor diameters in 3 orthogonal planes. AP and maximum TV diameters were measured on the axial oblique image (A), whereas CC diameters were measured on the sagittal image (B).

myometrial invasion), 23% (48/212) stage IB (≥50% myometrial invasion), 11% (23/212) stage II (cervical stroma invasion), 11% (24/212) stage III (local or regional tumor spread), and 0% (1/212) stage IV. The histological subtype was endometrioid in 81% (171/212) of which 50% (86/171) were grade 1, 29% (50/171) grade 2, and 17% (29/171) grade 3; whereas 4% (6/171) were ungraded. Clear cell histology was detected in 3% (6/212), serous in 10% (21/212), carcinosarcoma in 4% (9/212), and undifferentiated in 2% (5/212). Metastatic lymph nodes were more frequent in patients with deep myometrial invasion, cervical stroma invasion, high histologic grade, aneuploidy, and body mass index (BMI) greater than 25 (Table 1).

All patients were primarily treated with hysterectomy and bilateral salpingo-oophorectomy. Pelvic lymph node sampling was performed in 85% (181/212) as part of the routine surgical staging procedure. Adjuvant therapy was given to 33% (70/212), chemotherapy in 28% (59/212), pelvic radiation in 5% (10/212), and hormonal treatment in 0% (1/212).

Tumor Size Is Correlated to Surgicopathologic Findings

The mean (median, range) preoperative tumor diameters were 28 (26, 0–113) mm for axial TV diameter, 18 (16, 0–77) mm for axial AP diameter, and 35 (31, 0–102) mm for sagittal CC diameter. The mean (median, range) estimated tumor volume was 19 (6, 0–444) mL. Tumor volume was significantly higher in patients with deep myometrial invasion, cervical stroma invasion, and lymph node metastases at surgical staging and in patients with aneuploidy and high histologic grade (Table 2).

Tumor measurements in the 3 orthogonal planes and tumor volume did all predict the presence of deep myometrial invasion at surgical staging (unadjusted odds ratios [ORs], 1.06–1.13; $P < 0.001$ for all); however, AP tumor diameter was the only size variable independently predicting deep myometrial invasion (adjusted OR, 1.14; $P < 0.001$). Craniocaudal tumor diameter was the only variable predicting cervical stroma invasion (adjusted OR, 1.04; $P = 0.008$). Although all size parameters predicted lymph node metastases in the univariate analyses (unadjusted ORs, 1.02–1.05; $P \leq 0.004$ for all), only CC tumor diameter tended to independently predict lymph node metastases (adjusted OR, 1.04; $P = 0.06$).

Receiver operator characteristic curves for the different size parameters in the prediction of deep myometrial invasion (Fig. 2A), cervical stroma invasion (Fig. 2B), and lymph node metastases (Fig. 2C) showed that AP diameter had the highest area under the curve (AUC, 0.82) for deep myometrial invasion, whereas CC diameter had the highest AUC for cervical stroma invasion (AUC, 0.66) and for lymph node metastases (AUC, 0.76). Based on these ROC curves, the following cutoff values were identified: AP tumor diameter greater than 2 cm predicts deep myometrial invasion yielding sensitivity/specificity of 66%/86% and an OR of 12.4, and CC tumor diameter greater than 4 cm predicts lymph node metastases yielding sensitivity/specificity of 70%/73% and an OR of 6.2, whereas CC tumor diameter greater than 3 cm tends to predict cervical stroma invasion yielding sensitivity/specificity of 66%/51% and an

TABLE 1. Clinical characteristics and MRI findings in relation to the presence of metastatic lymph nodes at surgical staging in 181 endometrial carcinoma patients

		LN+	LN−	
		n = 20	n = 161	
Variable	**n**	**n (%)**	**n (%)**	***P****
Low-risk group†	72	0 (0)	72 (46)	**<0.001**
Intermediate-risk group†	51	10 (50)	41 (26)	
High-risk group†	54	10 (50)	44 (28)	
Myometrial invasion				**< 0.001**
<50%	109	4 (20)	105 (65)	
≥50%	72	16 (80)	56 (35)	
Cervical stroma invasion				**0.001**
Yes	27	8 (40)	19 (12)	
No	154	12 (60)	142 (88)	
Histologic subtype				0.14
Endometrioid	141	13 (65)	128 (80)	
Nonendometrioid	40	7 (35)	33 (20)	
Histological grade among endometrioid subtype				**0.007**
Grade 1	70	2 (15)	68 (55)	
Grade 2	42	5 (38)	37 (30)	
Grade 3	25	6 (46)	19 (15)	
Ploidy				**0.014**
Diploid	77	6 (50)	71 (82)	
Aneuploid	22	6 (50)	16 (18)	
Age, y				0.10
<66	95	7 (35)	88 (54)	
≥66	86	13 (65)	73 (45)	
BMI				**0.03**
<25	66	3 (15)	63 (40)	
≥25	113	17 (85)	96 (60)	
Tumor size at MRI				**<0.001**
AP ≤2 cm and/or CC ≤4 cm	136	8 (40)	128 (80)	
AP >2 cm and CC >4 cm	45	12 (60)	33 (20)	
Enlarged lymph nodes at MRI				**<0.001**
Enlarged lymph nodes	13	9 (45)	4 (2)	
Normal lymph nodes	168	11 (55)	157 (98)	

Significant P values are presented in boldface.

*χ^2 Test.

†Risk groups defined in European Society for Medical Oncology guidelines[26]: low risk, endometrioid grade 1/2 with myometrial invasion <50%; intermediate risk, endometrioid grade 1/2 with myometrial invasion ≥50% or endometrioid grade 3 with myometrial invasion < 50%; high risk, endometrioid grade 3 with myometrial invasion ≥50% or nonendometrioid histology

LN+, patients with lymph nodes metastases at surgical staging; LN−, patients without lymph node metastases at surgical staging.

TABLE 2. Tumor volume in relation to clinical and histologic characteristics in 212 endometrial carcinoma patients

Variable	n	Tumor Volume, mL Mean (95% CI)	P*
Myometrial invasion			**<0.001**
<50%	132	7.4 (5.2–9.7)	
≥50%	80	37.5 (23.4–51.6)	
Cervical stroma invasion			**0.049**
Yes	32	33.7 (5.2–62.2)	
No	180	16.1 (11.4–20.8)	
Lymph node metastases			**<0.004**
Yes	20	62.7 (12.0–113.5)	
No	161	13.9 (10.2–17.6)	
Histologic subtype			0.27
Endometrioid	171	13.4 (10.2–16.6)	
Clear cell	6	20.6 (0.0–50.4)	
Serous	21	21.0 (4.9–37.1)	
Carcinosarcoma	9	65.5 (0.0–135.8)	
Undifferentiated/others	5	107.8 (0.0–345.6)	
Histological grade among endometrioid subtype			**<0.001**
Grade 1	86	8.9 (5.6–12.1)	
Grade 2	50	14.7 (9.4–19.9)	
Grade 3	29	26.5 (13.2–39.8)	
Ploidy			**0.015**
Diploid	91	24.7 (12.8–36.7)	
Aneuploid	23	41.1 (21.4–60.7)	
Age, y			0.21
<66	106	15.6 (7.0–24.3)	
≥66	106	22.0 (14.2–29.8)	
BMI			0.38
<25	74	15.1 (9.1–21.1)	
≥25	134	20.9 (12.4–29.4)	

Significant *P* values are presented in boldface.
*Mann-Whitney *U* test for 2 categories and Kruskal-Wallis H test or Jonckheere-Terpsta trend test for multiple categories.
CI, confidence interval.

OR of 2.0 (Table 3). When adjusting for risk status based on preoperative endometrial biopsy and for conventional imaging findings (consensus reading) suggesting deep myometrial invasion, cervical stroma invasion, and lymph node metastases, respectively, AP diameter greater than 2 cm independently predicted deep myometrial invasion (adjusted OR, 6.7), and CC diameter greater than 4 cm independently predicted lymph node metastases (adjusted OR, 4.9), whereas CC diameter greater than 3 cm did not predict cervical stroma invasion (Table 3).

Tumor Size Predicts Progression/Recurrence-Free Survival

The 3 tumor diameter measurements and tumor volume did all predict progression/recurrence-free survival ($P \leq 0.01$ for all size parameters) in endometrial carcinoma patients. In a multivariate analysis including all size parameters and preoperative risk status based on endometrial biopsy, only CC tumor diameter had an independent impact on survival (Table 4, Supplemental Digital Content, http://links.lww.com/IGC/A270). When stratifying patient groups according to the proposed cutoff values for size variables defined by the ROC analyses, patients with AP tumor diameter greater than 2 cm and patients with CC tumor diameter greater than 4 cm had significantly reduced progression/recurrence-free survival ($P \leq 0.03$ for both; Figs. 3A, B). Combining these 2 size criteria yielded similar survival curves among patients with both or 1 size criterion below the cutoff values (the 2 survival curves are thus merged in Fig. 3C), whereas patients with both AP tumor diameter greater than 2 cm and CC tumor diameter greater than 4 cm had significantly reduced progression/recurrence-free survival ($P = 0.004$; Fig. 3C).

Interobserver Variability for Tumor Measurements

The interobserver variability for tumor diameter measurements by the 3 observers was low with intraclass correlation coefficients of 0.78 to 0.85 and minimum detectable change of 14 to 26 mm for the different tumor diameter measurements (Table 5, Supplemental Digital Content, http://links.lww.com/IGC/A270). Furthermore, the AUC values of the ROC curves for prediction of deep myometrial invasion, cervical stroma invasion, and lymph node metastases were not significantly different between observers (Figs. 2D-F).

DISCUSSION

In this large population-based study, we demonstrate a significant predictive value of preoperative tumor size measurements based on MRI to identify deep myometrial invasion and lymph node metastases. Furthermore, tumor size had a significant independent impact on survival also when adjusting for preoperative risk status based on endometrial biopsy. Based on the present study, we propose a risk model with cutoff values of AP tumor diameter greater than 2 cm indicating high risk for deep myometrial invasion and CC tumor diameter greater than 4 cm indicating high risk for lymph node metastases. Having established that the interobserver variability for these different tumor measurements at MRI was very low, we infer that these preoperative tumor measurements with corresponding cutoff values may represent robust biomarkers aiding in the preoperative risk stratification and in planning of tailored surgical treatment in endometrial cancer patients.

Presence of deep myometrial invasion in hysterectomy specimen at surgicopathological staging is associated with an increased risk of lymph node metastases, tumor recurrence, and distant relapse in endometrial carcinoma patients.[3,18] We found that all size parameters predicted deep myometrial invasion, which is in accordance with the findings of Todo et al[14] reporting high volume indexes (defined as the product

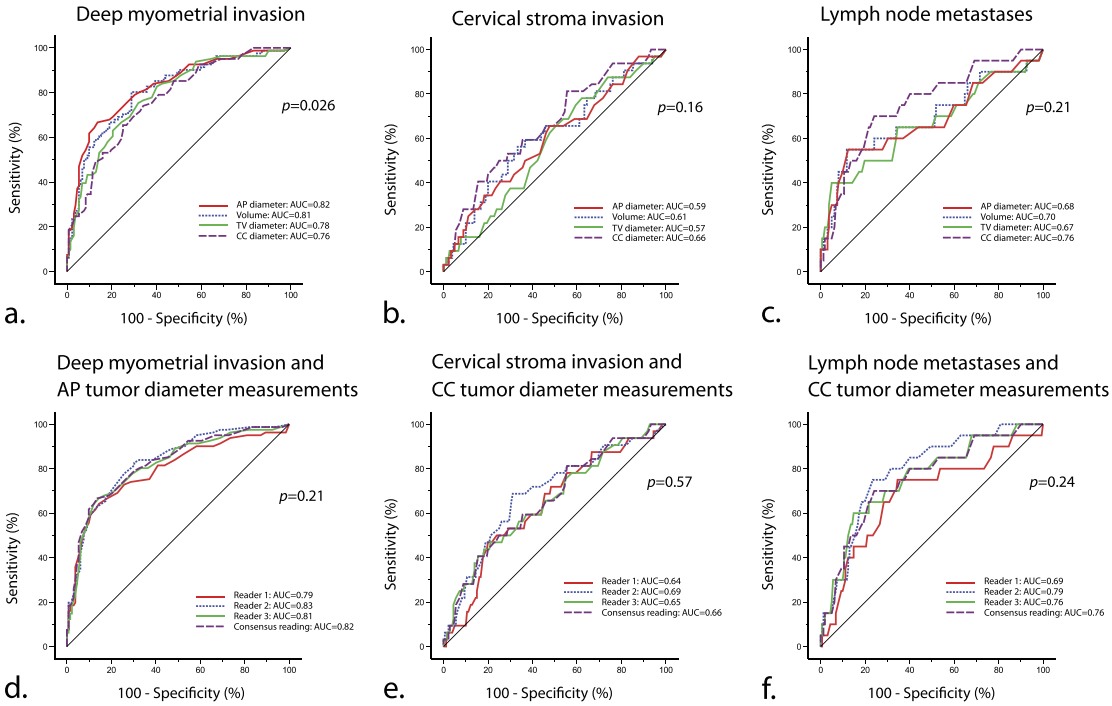

FIGURE 2. Receiver operator characteristic curves for the various tumor size measurements for identification of (A) deep myometrial invasion, (B) cervical stroma invasion, and (C) lymph node metastases and ROC curves for the different observers for (D) AP diameter to predict deep myometrial invasion, (E) CC diameter to predict cervical stroma invasion, and (F) CC diameter to predict lymph node metastases in patients with endometrial carcinoma. *P* values refer to the test of equal AUC values across tumor measurements.

TABLE 3. Sensitivity, specificity, LR+, LR−, and OR for the prediction of deep myometrial invasion (by AP tumor diameter >2 cm), cervical stroma invasion (by CC tumor diameter >3 cm), and lymph node metastases (by CC diameter >4 cm) using surgical staging as the criterion standard

	AP Tumor Diameter >2 cm and Deep Myometrial Invasion	CC Tumor Diameter >3 cm and Cervical Stroma Invasion	CC Tumor Diameter >4 cm and Lymph Node Metastases
Sensitivity, % (positive/total no. patients)	66 (53/80)	66 (21/32)	70 (14/20)
Specificity, % (positive/total no. patients)	86 (114/132)	51 (91/180)	73 (117/161)
LR+	4.9	1.5	2.6
LR−	0.39	0.68	0.41
Unadjusted and adjusted* OR (95% CI);	12.4 (6.3–24.5)	2.0 (0.9–4.3)	6.2 (2.2–17.2)
P value† for deep myometrial invasion/cervical stroma invasion/lymph node metastases based on size cutoff values	*P* < 0.001	*P* = 0.10	*P* < 0.001
	6.7 (3.1–14.4)	1.1 (0.4–2.7)	4.9 (1.5–15.8)
	P < 0.001	*P* = 0.85	*P* = 0.009

*Adjusted for risk status based on preoperative endometrial biopsy and conventional imaging findings (consensus reading) suggesting deep myometrial invasion, cervical stroma invasion, and lymph node metastases, respectively.

†Binary logistic regression analysis.

LR+, likelihood ratio for positive results: LR+ = sensitivity/(1 − specificity); LR−, likelihood ratio for negative results: LR− = (1 − sensitivity)/specificity.

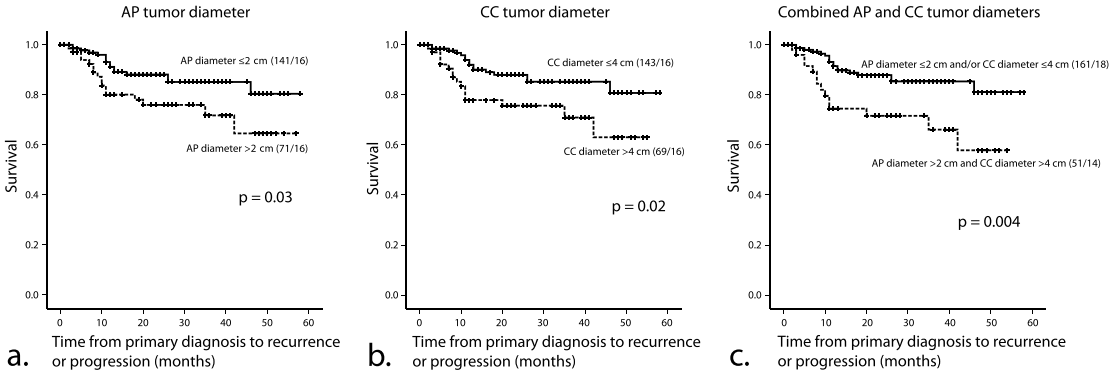

FIGURE 3. Kaplan-Meier survival curves depicting progression/recurrence-free survival according to (A) maximal AP tumor diameter (≤2 vs >2 cm), (B) maximal CC tumor diameter (≤4 vs >4 cm), and (C) a combination of AP and CC tumor diameters (AP ≤2 cm and/or CC ≤4 cm vs AP >2 cm and CC >4 cm). *P* values refer to the log-rank test for equality of survival distribution.

of maximum AP, TV, and CC tumor diameters at MRI) to be associated with deep myometrial invasion. As opposed to Todo et al,[14] we have also explored the independent impact of the different size variables in a multivariate model including preoperative risk status based on endometrial biopsy. Interestingly, AP diameter, which had the largest AUC (Fig. 2A), proved to be the only size variable independently predicting deep myometrial invasion.

Based on the ROC curve, the optimal cutoff value for prediction of deep myometrial invasion was AP diameter greater than 2 cm, and AP diameter greater than 2 cm independently predicted deep myometrial invasion even when adjusting for conventional imaging findings (consensus reading) suggesting the same. Interestingly, we found that AP diameter greater than 2 cm and MRI indicating deep myometrial invasion had comparable accuracy (sensitivity, specificity) for identification of deep myometrial invasion at surgical staging: 79% (66%, 86%) and 74% (70%, 77%), respectively, however, with significantly better specificity for AP diameter greater than 2 cm (86% vs 77%; $P = 0.015$, McNemar test). Thus, this relatively simple approach of measuring AP tumor diameter yields a diagnostic performance similar to or slightly better than conventional reading for prediction of deep myometrial invasion.

Several surgicopathological risk models for prediction of lymph node metastases have been proposed in endometrial cancer based on histologic grade, subtype, and tumor extent,[10,19,20] among which 1 model includes tumor greater than 2 cm based on the gross inspection of hysterectomy specimen.[10] These models are, however, limited by the fact that they rely on surgicopathological staging results, which are per definition not available preoperatively.

Tumor diameter greater than 2 cm in macroscopic fresh tissue has been reported to independently predict lymph node metastases and survival[9]; however, the independent impact on survival of tumor size greater than 2 cm has not been consistently reproduced in the literature.[10,13] Based on macroscopic gross inspection of the cut-up of the uterus, maximum tumor dimension greater than 3.75 cm was recently reported an independent predictor of deep myometrial invasion, distant recurrence, and death.[11] Because CC diameter was almost uniformly the largest tumor diameter in our study, our cutoff value for CC diameter greater than 4 cm seems to be in line with the proposed cutoff value of 3.75 cm. Direct comparison between tumor diameter measurements in macroscopic fresh tissue and preoperatively based on MRI is, however, difficult due to the differences in planes eligible for tumor measurements and the potential distortion and compression of tumor tissue in vivo compared with ex vivo. Thus, the optimal cutoff values for tumor size are not necessarily transferable from in vivo MRI-based assessment to the ex vivo gross section-based tumor measurements. Still, the metastatic potential and unfavorable prognostic impact of large tumor size in endometrial carcinomas is consistently supported by both in vivo and ex vivo studies.[9–15]

We found that the MRI-based parameters AP tumor diameter greater than 2 cm and CC tumor diameter greater than 4 cm both alone and combined are strongly associated with reduced progression/recurrence-free survival in endometrial carcinomas (Fig. 3). These tumor size parameters should in the future also be evaluated in relation to other preoperative biomarkers such as p53, hormone receptor, and DNA ploidy status in preoperative biopsies, prognostic markers assessed in blood samples,[21] and on functional imaging by MRI or PET/CT, which have been shown to yield prognostic information.[16,22–25]

For all risk stratification models, high accuracy and reproducibility of the variables included in the model are essential. To our knowledge, this is the first study assessing the interobserver variability for the different tumor size measurements at MRI in endometrial cancer. Interestingly, we found that tumor size was measured with very low interobserver variability and with no striking difference related to the readers' previous experience. Thus, tumor size measurements seem to represent robust biomarkers that are promising for potential inclusion in future risk stratification models in endometrial cancer.

This study has some limitations. First, the study was conducted in a single institution using a standardized imaging protocol. Thus, the potential impact of various imaging protocols on MRI-based tumor size measurements has not been assessed. However, our imaging protocol is based on the guidelines of the European Society of Urogenital Imaging and is thus expected to be quite similar to those applied at most centers treating endometrial cancer patients. Second, intraobserver variability was not assessed in this study. This is, however, expected to be lower than the observed interobserver variability, which was very low in this study, and the intraobserver variability is thus expected to be almost negligible.

In summary, tumor size assessed preoperatively by MRI predicts the presence of deep myometrial invasion and lymph node metastases and is a strong prognostic factor in endometrial carcinoma. Based on our findings, we propose cutoff values greater than 2 cm AP tumor diameter for predicting deep myometrial invasion and greater than 4 cm CC tumor diameter for predicting lymph node metastases, as well as poor survival for the combination of greater than 2 cm AP and greater than 4 cm CC tumor diameter. Preoperative tumor measurements at MRI may thus provide clinically relevant biomarkers for future risk stratification models guiding tailored surgical treatment in endometrial cancer.

REFERENCES

1. Amant F, Moerman P, Neven P, et al. Endometrial cancer. *Lancet*. 2005;366:491–505.
2. Pecorelli S. Revised FIGO staging for carcinoma of the vulva, cervix, and endometrium. *Int J Gynaecol Obstet*. 2009;105:103–104.
3. Salvesen HB, Haldorsen IS, Trovik J. Markers for individualised therapy in endometrial carcinoma. *Lancet Oncol*. 2012;13:e353–e361.
4. Frei KA, Kinkel K. Staging endometrial cancer: role of magnetic resonance imaging. *J Magn Reson Imaging*. 2001;13:850–855.
5. Kinkel K, Forstner R, Danza FM, et al. Staging of endometrial cancer with MRI: guidelines of the European Society of Urogenital Imaging. *Eur Radiol*. 2009;19:1565–1574.
6. Sala E, Rockall AG, Freeman SJ, et al. The added role of MR imaging in treatment stratification of patients with gynecologic malignancies: what the radiologist needs to know. *Radiology*. 2013;266:717–740.
7. Haldorsen IS, Salvesen HB. Staging of endometrial carcinomas with MRI using traditional and novel MRI techniques. *Clin Radiol*. 2012;67:2–12.
8. Haldorsen IS, Husby JA, Werner HM, et al. Standard 1.5-T MRI of endometrial carcinomas: modest agreement between radiologists. *Eur Radiol*. 2012;22:1601–1611.
9. Schink JC, Rademaker AW, Miller DS, et al. Tumor size in endometrial cancer. *Cancer*. 1991;67:2791–2794.
10. Mariani A, Webb MJ, Keeney GL, et al. Surgical stage I endometrial cancer: predictors of distant failure and death. *Gynecol Oncol*. 2002;87:274–280.
11. Chattopadhyay S, Cross P, Nayar A, et al. Tumor size: a better independent predictor of distant failure and death than depth of myometrial invasion in International Federation of Gynecology and Obstetrics stage I endometrioid endometrial cancer. *Int J Gynecol Cancer*. 2013;23:690–697.
12. Lee KB, Ki KD, Lee JM, et al. The risk of lymph node metastasis based on myometrial invasion and tumor grade in endometrioid uterine cancers: a multicenter, retrospective Korean study. *Ann Surg Oncol*. 2009;16:2882–2887.
13. Shah C, Johnson EB, Everett E, et al. Does size matter? Tumor size and morphology as predictors of nodal status and recurrence in endometrial cancer. *Gynecol Oncol*. 2005;99:564–570.
14. Todo Y, Watari H, Okamoto K, et al. Tumor volume successively reflects the state of disease progression in endometrial cancer. *Gynecol Oncol*. 2013;129:472–477.
15. Todo Y, Choi HJ, Kang S, et al. Clinical significance of tumor volume in endometrial cancer: a Japan-Korea cooperative study. *Gynecol Oncol*. 2013;131:294–298.
16. Trovik J, Wik E, Werner HM, et al. Hormone receptor loss in endometrial carcinoma curettage predicts lymph node metastasis and poor outcome in prospective multicentre trial. *Eur J Cancer*. 2013;49:3431–3441.
17. Silverberg SG, Kurman RJ, Nogales F. Tumors of the uterine corpus. In: Tavassoli FA, Devilee P, eds. *Tumours of the Breast and Female Genital Organs. World Health Organization Classification of Tumours. Pathology & Genetics*. Lyon, France: IACR Press Inc; 2003:217–258.
18. Werner HM, Trovik J, Marcickiewicz J, et al. Revision of FIGO surgical staging in 2009 for endometrial cancer validates to improve risk stratification. *Gynecol Oncol*. 2012;125:103–108.
19. Creasman WT, Morrow CP, Bundy BN, et al. Surgical pathologic spread patterns of endometrial cancer. A Gynecologic Oncology Group Study. *Cancer*. 1987;60:2035–2041.
20. Kang S, Lee JM, Lee JK, et al. How low is low enough? Evaluation of various risk-assessment models for lymph node metastasis in endometrial cancer: a Korean multicenter study. *J Gynecol Oncol*. 2012;23:251–256.
21. Staff AC, Trovik J, Eriksson AG, et al. Elevated plasma growth differentiation factor-15 correlates with lymph node metastases and poor survival in endometrial cancer. *Clin Cancer Res*. 2011;17:4825–4833.
22. Haldorsen IS, Gruner R, Husby JA, et al. Dynamic contrast-enhanced MRI in endometrial carcinoma identifies patients at increased risk of recurrence. *Eur Radiol*. 2013;23:2916–2925.
23. Haldorsen IS, Stefansson I, Gruner R, et al. Increased microvascular proliferation is negatively correlated to tumour blood flow and is associated with unfavourable outcome in endometrial carcinomas. *Br J Cancer*. 2014;110:107–114.
24. Njolstad TS, Engerud H, Werner HM, et al. Preoperative anemia, leukocytosis and thrombocytosis identify aggressive endometrial carcinomas. *Gynecol Oncol*. 2013;131:410–415.
25. Kang S, Kang WD, Chung HH, et al. Preoperative identification of a low-risk group for lymph node metastasis in endometrial cancer: a Korean gynecologic oncology group study. *J Clin Oncol*. 2012;30:1329–1334.
26. Colombo N, Preti E, Landoni F, et al. Endometrial cancer: ESMO Clinical Practice Guidelines for diagnosis, treatment and follow-up. *Ann Oncol*. 2013;24:vi33–vi38.

Table 4 (Suppl)
Unadjusted and adjusted hazard ratios for preoperative tumor size measurements at MRI and for preoperative endometrial biopsy suggesting high-risk* for the prediction of progression/recurrence-free survival in endometrial carcinomas

	Tumor size at MRI				
	Transverse diameter (mm)	Anterioposterior diameter (mm)	Craniocaudal diameter (mm)	Tumor volume (ml)	High-risk based on preoperative biopsy*
Unadjusted HR [95% CI] (*p*-value) ¶	**1.03 [1.01-1.05] (*p*=0.005)**	**1.03 [1.01-1.05] (*p*=0.01)**	**1.03 [1.01-1.04] (*p*<0.001)**	**1.01 [1.00-1.01] (*p*<0.001)**	**4.35 [2.13-8.89] (*p*<0.001)**
Adjusted HR [95% CI] (*p*-value) ¶	1.02 [0.97-1.07] (*p*=0.48)	0.93 [0.88-0.99] (*p*=0.03)	**1.04 [1.01-1.06] (*p*=0.009)**	1.01 [1.00-1.02] (*p*=0.09)	**4.13 [1.88-9.08] (*p*<0.001)**

* Preoperative endometrial biopsy indicating non-endometrioid subtype or endometrioid grade 3.
¶ Cox Proportional Hazard Model. The adjusted HR is based on multivariate analyses including all the variables listed on the same line.
CI, confidence interval; HR, hazard ratio; MRI, magnetic resonance imaging.

Table 5 (Suppl)
Interobserver variability for tumor diameter measurements by 3 observers

	Mean (mm)			Mean difference (SD) (mm)			ICC (95%CI)	MDC (mm)
	Obs 1	Obs 2	Obs 3	Obs 1/2	Obs 1/3	Obs 2/3		
Transverse diameter	32	26	27	6 (10)	4 (11)	2 (8)	0.78 (0.73-0.82)	21
Anterioposterior diameter	20	17	18	2 (7)	2 (8)	0 (6)	0.85 (0.81-0.88)	14
Sagittal diameter	38	33	34	5 (15)	4 (14)	1 (8)	0.78 (0.73-0.82)	26

ICC, intra-class correlation; MDC, minimal detectable change; SD, standard deviation

STUDY 3

ORIGINAL RESEARCH

Preoperative Tumor Texture Analysis on MRI Predicts High-Risk Disease and Reduced Survival in Endometrial Cancer

Sigmund Ytre-Hauge, MD,[1,2]* Julie A. Dybvik, MD,[1]
Arvid Lundervold, BSc, MD, PhD,[1,3] Øyvind O. Salvesen, MSc, PhD,[4]
Camilla Krakstad, PhD,[5,6] Kristine E. Fasmer, MSc ,[1,2]
Henrica M. Werner, MD, PhD,[5,6] Balaji Ganeshan, PhD,[7] Erling Høivik, PhD,[5,6]
Line Bjørge, MD, PhD,[5,6] Jone Trovik, MD, PhD,[5,6] and
Ingfrid S. Haldorsen, MD, PhD[1,2]

Background: Improved methods for preoperative risk stratification in endometrial cancer are highly requested by gynecologists. Texture analysis is a method for quantification of heterogeneity in images, increasingly reported as a promising diagnostic tool in various cancer types, but largely unexplored in endometrial cancer.
Purpose: To explore whether tumor texture parameters from preoperative MRI are related to known prognostic features (deep myometrial invasion, cervical stroma invasion, lymph node metastases, and high-risk histological subtype) and to outcome in endometrial cancer patients.
Study type: Prospective cohort study.
Population/Subjects: In all, 180 patients with endometrial carcinoma were included from April 2009 to November 2013 and studied until January 2017.
Field Strength/Sequences: Preoperative pelvic MRI including contrast-enhanced T_1-weighted (T_1c), T_2-weighted, and diffusion-weighted imaging at 1.5T.
Assessment: Tumor regions of interest (ROIs) were manually drawn on the slice displaying the largest cross-sectional tumor area, using the proprietary research software TexRAD for analysis. With a filtration-histogram technique, the texture parameters standard deviation, entropy, mean of positive pixels (MPP), skewness, and kurtosis were calculated.
Statistical Tests: Associations between texture parameters and histological features were assessed by uni- and multivariable logistic regression, including models adjusting for preoperative biopsy status and conventional MRI findings. Multivariable Cox regression analysis was used for survival analysis.
Results: High tumor entropy in apparent diffusion coefficient (ADC) maps independently predicted deep myometrial invasion (odds ratio [OR] 3.2, $P < 0.001$), and high MPP in T_1c images independently predicted high-risk histological subtype (OR 1.01, $P = 0.004$). High kurtosis in T_1c images predicted reduced recurrence- and progression-free survival (hazard ratio [HR] 1.5, $P < 0.001$) after adjusting for MRI-measured tumor volume and histological risk at biopsy.
Data Conclusion: MRI-derived tumor texture parameters independently predicted deep myometrial invasion, high-risk histological subtype, and reduced survival in endometrial carcinomas, and thus, represent promising imaging biomarkers providing a more refined preoperative risk assessment that may ultimately enable better tailored treatment strategies in endometrial cancer.
Level of Evidence: 2
Technical Efficacy: Stage 2

J. MAGN. RESON. IMAGING 2018;00:000–000.

View this article online at wileyonlinelibrary.com. DOI: 10.1002/jmri.26184

Received Feb 1, 2018, Accepted for publication Apr 17, 2018.

*Address reprint requests to: S.Y.-H., Department of Radiology, Haukeland University Hospital, Jonas Liesvei 65, 5021 Bergen, Norway. E-mail: sigmund.ytre-hauge@helse-bergen.no

From the [1]Department of Radiology, Haukeland University Hospital, Bergen, Norway; [2]Section for Radiology, Department of Clinical Medicine, University of Bergen, Norway; [3]Department of Biomedicine, University of Bergen, Norway; [4]Unit for Applied Clinical Research, Department of Cancer Research and Molecular Medicine, Norwegian University of Science and Technology, Trondheim, Norway; [5]Department of Obstetrics and Gynaecology, Haukeland University Hospital, Bergen, Norway; [6]Centre for Cancer Biomarkers, Department of Clinical Science, University of Bergen, Norway; and [7]Institute of Nuclear Medicine, University College London, London, UK

Additional supporting information may be found in the online version of this article.

Tumor heterogeneity is a key feature of malignant disease. Several pan-cancer analyses, comprising a variety of cancer types, have reported intratumor genetic heterogeneity to be associated with tumor aggressiveness and reduced survival.[1,2] Mechanisms proposed to explain the aggressive behavior of heterogeneous tumors include Darwinian selection among clones enabling tumor adaptation and drug resistance.[3]

Texture analysis (TA), a method for quantification of heterogeneity in images, has become an important element in the growing field of radiomics, the science of high-throughput extraction of quantitative features from radiological imaging data.[4] Although radiomics inherently operates at a more macroscopic level than genomics and histological markers, the method has proven useful in medical diagnostic imaging, especially in oncological imaging.[5] Magnetic resonance imaging (MRI)- and computed tomography (CT)-derived texture parameters have been proposed as tools for accurate diagnosis, preoperative risk stratification, or assessment of treatment response in several cancer types, eg, in the brain,[6] lung,[7] breast,[8] and prostate.[9] A recent preliminary study also reported MR texture analysis (MRTA) as a useful tool for preoperative risk stratification in endometrial cancer.[10]

Endometrial cancer is the most common gynecologic malignancy in industrialized countries, with an increasing incidence.[11] Treatment strategy and prognosis are traditionally based on the International Federation of Gynecology and Obstetrics (FIGO) stage and histological subtype and grade determined from the hysterectomy specimen.[12,13] To enable more individualized surgical treatment, improved methods for preoperative risk stratification methods are highly warranted.

MRI is widely used for preoperative assessment of endometrial cancer.[14–16] However, conventional MRI has confirmed shortcomings in predicting FIGO stage,[16,17] and interobserver variability between radiologists also represents a source of inaccuracy.[18] Advances in MRI technology have increasingly enabled quantitative and functional imaging. Diffusion-weighted imaging (DWI), reflecting tumor microstructure, dynamic contrast-enhanced (DCE)-MRI, and MR spectroscopy (MRS), reflecting tumor physiology and metabolism, may to an extent reduce the subjectivity in the assessment of endometrial cancers and yield novel biomarkers for preoperative risk stratification. Still, overtreatment at primary surgery (eg, unnecessary lymphadenectomy in low-risk patients) may represent a problem. In this regard, MRTA could potentially enhance the role of diagnostic imaging and refine the preoperative risk assessments.

This large, population-based study aimed to explore whether the staging parameters deep (≥50%) myometrial invasion (DMI), cervical stroma invasion (CSI), and lymph node metastases (LNM), high-risk histological subtype, and clinical outcome in endometrial cancer patients are reflected in MRTA parameters.

Materials and Methods

Study Setting

This prospective study was conducted under Institutional Review Board approval with written informed consent from all patients. From April 2009 to November 2013, preoperative pelvic MRI was performed in a population-based cohort of 252 patients with suspected endometrial cancer. The final histological diagnosis based on hysterectomy specimen did not confirm endometrial cancer in 36 patients and these were excluded. Thus, 216 consecutive patients with endometrial cancer, histologically verified at subsequent staging, were included in the study cohort. All patients were diagnosed and treated at the same university hospital, which is a European Society of Gynaecological Oncology accredited center. The last follow-up was in January 2017 and mean follow-up time for the group of patients without recurrence or progression was 51 months (range 0–85).

Imaging Protocol

MRI was performed on a 1.5T Siemens Avanto running Syngo MR B17 (Erlangen, Germany) using a six-channel body coil. Prior to imaging, 20 mg butylscopolamine bromide (Buscopan, Boehringer, Ingelheim, Germany) was administered intravenously.

Based on the Guidelines of the European Society of Urogenital Imaging (ESUR),[15] the MRI protocol included pelvic sagittal and axial oblique (perpendicular to the long axis of uterus) T_2-weighted images and axial oblique T_1-weighted images obtained before and after intravenous contrast administration (Dotarem, Guerbet, Villepinte, France: 0.1 mmol gadolinium per kg of body weight, 3 ml/s injection speed) using a 2-minute delay.[18] T_2 images were acquired using 2D spin echo sequences (repetition time (TR) / echo time (TE) = 6310/95 msec [for sagittal images TR/TE = 4920/95], matrix = 256 × 256, field of view [FOV] = 180 × 180 mm^2, section thickness = 3 mm, averages = 2 [for sagittal images averages = 3]) yielding a voxel size of 0.7 × 0.7 × 3.0 mm. T_1 images were acquired using a 3D volumetric interpolated breath-hold (VIBE) gradient echo sequence with fat saturation (TR/TE = 7.23/2.55 msec, matrix = 192 × 192, FOV = 250 × 250 mm^2, section thickness = 2 mm, averages = 1) yielding a voxel size of 1.3 × 1.3 × 2.0 mm.

Pelvic DWI was acquired using an axial oblique 2D spin-echo echo planar imaging sequence with b-values of 0 and 1000 s/mm^2 (TR/TE = 3100/79 msec, matrix = 128 × 128, FOV = 300 × 300 mm^2, section thickness = 5 mm, averages = 12). Apparent diffusion coefficient (ADC) maps were generated with voxel size 2.3 × 2.3 × 5 mm.

Histological Diagnosis

Mean (range) interval between MR examination and surgical staging was 11 (0–98) days.

The preoperative biopsy was graded as either low-risk (endometrioid grade 1–2) or high-risk (endometrioid grade 3 or nonendometrioid) endometrial cancer. From preoperative endocervical

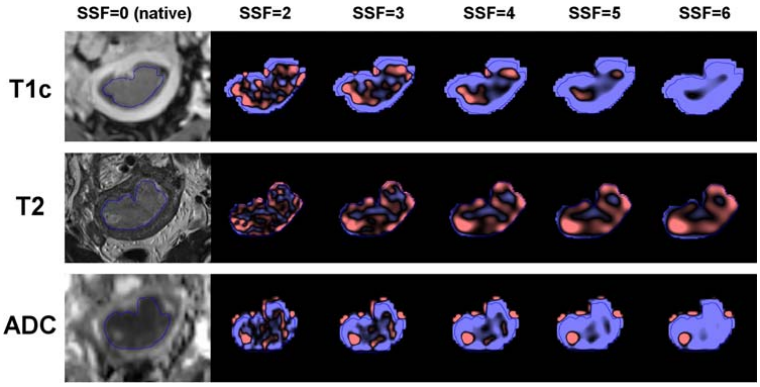

FIGURE 1: Endometrial carcinoma manually segmented (blue line) on contrast-enhanced T_1-weighted (T_1c) image (upper row), T_2-weighted (T_2) image (middle row), and ADC-map (lower row) from the same 52-year-old postmenopausal woman diagnosed with stage 1b endometrial cancer (endometrioid, grade 1). Successive filtered images (spatial scale of filtration [SSF] 2–6) to the right of each native image.

curettage, an assessment of cervical tumor involvement was also performed.

All patients were surgicopathologically staged according to the 2009 FIGO staging system.[12] Hysterectomy specimens were sectioned along the longitudinal plane of the uterus, and myometrial invasion and cervical stromal invasion were estimated grossly and confirmed microscopically according to standard criteria.[19]

Image Analysis

One radiologist (SYH, with 5 years of experience in pelvic MRI), blinded for clinical and histological data, assessed the eligibility of the images for MRTA. Of the 216 scanned patients, 33 were excluded due to small or poorly defined tumors, and three due to major image artifacts. Thus, 180 patients were included for MRTA; three of these had major artifacts on DWI only. Contrast-enhanced T_1-weighted images (T_1c, $n = 180$), T_2-weighted images (T_2, $n = 180$), and ADC-maps ($n = 177$) were exported to the commercially available research software TexRAD (TexRAD, part of Feedback, Cambridge, UK). Median (range) region of interest (ROI) sizes were in T_1c images 169 (24–1760) voxels, in T_2 images 593 (45–4970) voxels, and in ADC maps 73 (10–654) voxels.

Results from conventional MRI (assessment of tumor size, myometrial and cervical invasion and presence of lymph node metastases) were recorded as consensus opinion from three radiologists (median values for continuous variables and majority for categorical variables) having independently read the same MR images in a prior study.[20]

Texture Analysis

In TexRAD, one radiologist (SYH) manually drew ROIs separately on T_1c images, T_2 images, and ADC-maps, aiming at including all viable tumor tissue on the slice displaying the largest cross-sectional tumor area (Fig. 1). The ROIs were processed using a filtration-histogram technique based on Laplacian of Gaussian spatial bandpass filtering, in which image elements of different sizes were enhanced corresponding to spatial scale filter (SSF) from 2–6 mm, ie, fine (2 mm), medium (3–5 mm), and coarse texture (6 mm) (Fig. 1). Based on texture quantification in tumor ROIs, the parameters mean intensity, standard deviation (SD), entropy, mean of positive pixels (MPP), skewness, and kurtosis were calculated. The mean intensity does not reflect heterogeneity per se, and thus, this feature was omitted in further analyses. MPP in unfiltered MR images (SSF = 0) equals mean intensity and was also omitted. Thus, the total number of texture parameters included in the statistical analyses was 87 (combinations of T_1c/T_2/ADC-map, SD/entropy/skewness/MPP/kurtosis at SSF 0/2/3/4/5/6). A condensed notation is used in this article, eg, ADC_Entropy6, indicating tumor ROI entropy in ADC-map at SSF 6.

Statistical Analysis

The majority of texture parameters did not have normal distribution, thus nonparametric tests were used. Mann–Whitney *U*-test assessed the ability of texture parameters to predict DMI, CSI, LNM, and high-risk histological subtype (endometrioid grade 3 or nonendometrioid). The texture parameters were subsequently ranked according to lowest *P*-value, and the best predictors selected for receiver operator characteristic (ROC) curve analyses and univariable and multivariable logistic regression. In the multivariable analyses, we adjusted for MRI-measured tumor volume, conventional MRI reading results, and preoperative biopsy risk status. When comparing the diagnostic performance of texture variables with conventional MRI reading results, McNemar's test was used. In this analysis, cutoffs for texture variables were determined by ROC curve analysis selecting the highest Youden index. Spearman's bivariate correlation test was used to explore correlations.

Survival analysis was performed for each of the texture parameters separately in univariable Cox regression analysis for predicting recurrence- and progression-free survival (RPFS), ie, time to recurrence (for patients considered to be cured by primary treatment) or progression (for patients known to have residual disease after primary treatment). Ranked according to lowest *P*-value, the best predictor was selected to be included in a multivariable analysis also including MRI-measured tumor volume and preoperative

TABLE 1. Patient and Tumor Characteristics for 180 Endometrial Carcinoma Patients Studied

Age, mean (range)	67 (41–93)
BMI, mean (range)	28 (16–50)
Postmenopausal, *n* (%)	166 (93%)
FIGO stage, *n* (%)	
IA	87 (48%)
IB	45 (25%)
II	21 (12%)
IIIB	3 (2%)
IIIC1	13 (7%)
IIIC2	7 (4%)
IVA	1 (1%)
IVB	3 (2%)
Histologic subtype, *n* (%)	
Endometrioid	142 (79%)
Clear cell	6 (3%)
Serous	19 (11%)
Carcinosarcoma	9 (5%)
Undifferentiated/others	4 (2%)
Histological grade in endometrioid tumors, *n* (%)	
Grade 1	64 (45%)
Grade 2	46 (32%)
Grade 3	30 (21%)

FIGO stage refers to the International Federation of Gynecology and Obstetrics stage according to 2009 criteria. BMI, body mass index.

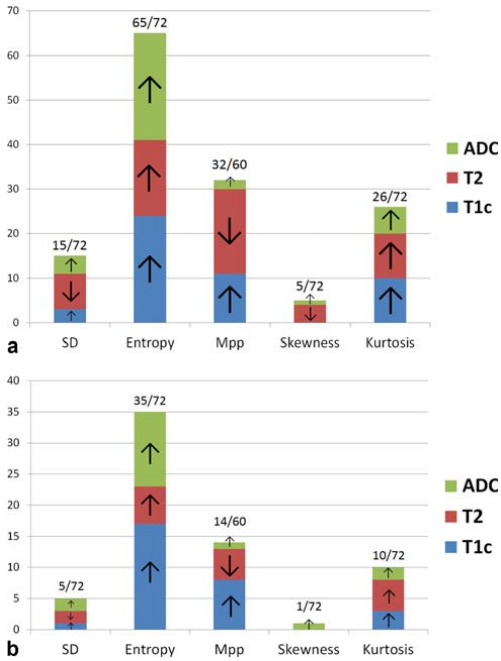

FIGURE 2: Proportions of the respective texture parameters predicting presence of deep myometrial invasion, cervical stroma invasion, lymph node metastases, and high-risk histological subtype at significance level of 0.05 (a) and at significance level of 0.002 (b) are given in the bars. Up arrows indicate that high values for the respective texture parameter predict high-risk cancer (positive staging parameters/high-risk histology), whereas down arrows indicate that low values for the respective texture parameters predict high-risk cancer. Notice the consistency and high proportion of entropy- and kurtosis-based parameters being significant predictors of high-risk cancer. The feature MPP also yielded a high proportion of significant predictors. Low values of MPP in T_2 images predicting high-risk cancer, as opposed to high values in T_1c images and ADC-maps, is explainable by the reciprocal nature of different MRI sequences. ADC, apparent diffusion coefficient (maps); MPP, mean of positive pixels; MRI, magnetic resonance imaging; SD, standard deviation; T_1c, contrast-enhanced T_1-weighted (images); T_2, T_2-weighted (images).

biopsy risk status. For the top-ranked texture parameters, differences in RPFS were assessed by the Mantel–Cox test and Kaplan–Meier plots.

Based on the findings of extensive correlations among the 87 texture parameters (Suppl. Tables 1–3), a customized modification of Bonferroni correction was applied, in which the number of effective tests was arbitrarily estimated at 25, yielding a significance level of 0.002. In the multivariable analyses a traditional significance level of 0.05 was used. The data were analyzed using SPSS 23.0 (IBM, Armonk, NY).

Results

Patients

Mean patient age at primary treatment in the study sample ($n = 180$) was 67 years (Table 1). Primary surgical treatment included bilateral salpingo-oophorectomy and hysterectomy for 98% (177/180), tumor reduction surgery for 1/180, and curettage only for 2/180. Lymphadenectomy was performed in 86% (154/180), pelvic only in 126 patients, and pelvic and para-aortic in 28 patients. In patients who underwent lymphadenectomy, the mean number of resected nodes was 18 (range 1–54). Adjuvant therapy was given to 39% (70/180); comprising chemotherapy in 83% (58/70), radiotherapy (external or internal) in 16% (11/70), and hormonal treatment in 1% (1/70). Further details on patient and tumor characteristics are given in Table 1.

Overall Evaluation of Texture Parameters

A summary of the texture features SD, entropy, MPP, skewness, and kurtosis significantly predicting high-risk endometrial cancer is given in Fig. 2, depicting the number of texture variables (combinations of T_1c/T_2/ADC-map at SSF

0/2/3/4/5/6) predicting DMI, CSI, LNM, and high-risk histological subtype. Entropy, followed by MPP and kurtosis, had the highest proportion of significant predictors, whereas skewness and SD yielded fewer significant predictors. For the feature SD there was also inconsistency in terms of both high values (T_1c images and ADC-maps) and low values (T_2 images) predicting high-risk cancer. High values of entropy and kurtosis (in T_1c images, T_2 images, and ADC maps) consistently predicted high-risk cancer, whereas low values of MPP and skewness in T_2 images predicted high-risk cancer, as opposed to high values in T_1c images and ADC maps (Fig. 2, arrows). The top-ranked texture parameters for prediction of deep myometrial invasion, cervical stroma invasion, lymph node metastases, high-risk histological subtype, and recurrence- and progression-free survival, respectively, are given in Table 2.

The texture parameters based on the same MRI sequence and texture feature, ie, only differing in filter level, were highly correlated (Suppl. Tables 1–3). For entropy, this was particularly striking, with correlation coefficients ranging from 0.86 to 1.00.

Prediction of Deep Myometrial Invasion (DMI)

Of the 87 texture parameters assessed, 44 significantly ($P < 0.002$) predicted DMI in univariable analysis. The majority of these comprised the parameters entropy, MPP and kurtosis, among which the top 10 all comprised entropy (Suppl. Table 4). The top-ranked predictor of DMI, entropy in ADC-maps at filter level 6 (ADC_Entropy6), using a cutoff value of 4.49, yielded significantly higher accuracy and specificity than conventional MRI reading (0.78 vs. 0.70, $P = 0.015$ and 0.84 vs. 0.69, $P = 0.004$, respectively) (Table 3). In a multivariable analysis, ADC_Entropy6 independently predicted DMI with an odds ratio of 3.2 (95% confidence interval 1.7–6.1, $P < 0.001$) when adjusting for high-risk status based on preoperative biopsy (endometrioid grade 3 or nonendometrioid), conventional MRI reading suggesting DMI, and MRI-measured tumor volume (Table 4). The ROC curve yielded an area under the ADC_Entropy6 ROC-curve (AU-ROC) of 0.81 ($P < 0.001$) (Fig. 3a) for prediction of DMI.

Prediction of Cervical Stroma Invasion (CSI)

For prediction of CSI in univariable analysis, none of the 87 texture parameters reached the significance level of 0.002. The top-ranked predictor of CSI, MPP in T_2 images at filter level 4 (T_2_MPP4), using a cutoff value of 137, yielded lower accuracy and specificity than conventional MRI reading (0.74 vs. 0.82, $P < 0.001$ and 0.78 vs. 0.93, $P < 0.001$, respectively) (Table 3). Furthermore, T_2_MPP4 did not independently predict CSI when adjusting for preoperative endocervical curettage indicating cervical tumor invasion, conventional MRI reading suggesting CSI, and MRI-measured tumor volume (Table 4). The corresponding AU-ROC for T_2_MPP4 was 0.64 ($P = 0.01$) (Fig. 3b) for prediction of CSI.

Prediction of Lymph Node Metastases (LNM)

Five out of 87 texture parameters were significant ($P < 0.002$) predictors of LNM in univariable analysis, all five parameters being entropy in T_1c images at different filter levels (Suppl. Table 4). However, the top-ranked parameter, entropy in T_1c images at filter level 6 (T_1c_Entropy6), using a cutoff value of 5.31, had lower accuracy and specificity than conventional MRI reading (0.72 vs. 0.90, $P < 0.001$ and 0.73 vs. 0.97, $P < 0.001$) (Table 3). In the multivariable analysis, T_1c_Entropy6 did not independently predict LNM, when adjusting for high-risk status in preoperative biopsy, conventional MRI reading suggesting LNM and MRI-measured tumor volume (Table 4). The corresponding AU-ROC for T_1c_Entropy6 was 0.73 ($P = 0.001$) (Fig. 3c) for prediction of LNM.

Prediction of High-Risk Histological Subtype

Sixteen of the tested 87 texture parameters were significant ($P < 0.002$) predictors of high-risk histological subtype (endometrioid grade 3 and nonendometrioid tumors) in univariable analysis. The majority of these parameters comprised entropy, and the remaining MPP (Suppl. Table 4). The top-ranked predictor, MPP in T_1c images at filter level 4 (T_1c_MPP4), independently predicted high-risk histological subtype with an odds ratio of 1.01 (1.00–1.01, $P = 0.004$) when adjusted for high-risk status based on preoperative biopsy and MRI-measured tumor volume (Table 4). The corresponding AU-ROC for T_1c_MPP4 was 0.66 ($P < 0.001$) (Fig. 3d) for prediction of high-risk histological subtype.

Survival Analysis

Thirteen out of 87 texture parameters significantly ($P < 0.002$) predicted RPFS in univariable Cox regression analysis (Suppl. Table 4). The top-ranked prognostic texture parameter, kurtosis in T_1c images at filter level 2 (T_1c_Kurtosis2), independently predicted reduced survival with a hazard ratio of 1.5 (1.2–2.0, $P < 0.001$) when adjusted for high-risk status based on preoperative biopsy and MRI-measured tumor volume (Table 5). Significantly different RPFS was observed in patients based on the two highest-ranked tumor texture parameters in the Cox analysis: T_1c_Kurtosis2 and ADC_Entropy6 (also the best predictor of DMI) when grouping patients according to the textural tumor parameter being below or at/above median value (Fig. 4a,b). The proportion of patients given adjuvant treatment was higher in the poor outcome groups: 51% received adjuvant treatment among patients with T_1c_Kurtosis2 at or above the median value (poor outcome group, Fig. 4a). Only 27% received adjuvant treatment among patients with

TABLE 2. Top-Ranked MRI-Derived Texture Parameters In Relation to Clinical and Histological Characteristics in 180 Endometrial Carcinoma Patients

	ADC_Entropy6[b]			T2_MPP4[c]			T1c_Entropy6[d]			T1c_MPP4[e]			T1c_Kurtosis2[f]		
Variable	***n***	**Median (95% CI)**	***P*[a]**	***n***	**Median (95% CI)**	***P*[a]**	***n***	**Median (95% CI)**	***P*[a]**	***n***	**Median (95% CI)**	***P*[a]**	***n***	**Median (95% CI)**	***P*[a]**
Myometrial invasion			**<0.001**			**<0.001**			**<0.001**			**<0.001**			**0.001**
<50%	99	3.8 (3.6–4.0)		100	242 (200–260)		100	4.5 (4.3–4.8)		100	92 (71–110)		100	0.04 (–0.22–0.26)	
≥50%	76	4.7 (4.6–5.0)		78	140 (124–160)		78	5.4 (5.2–5.6)		78	141 (121–170)		78	0.42 (0.24–0.67)	
Cervical stroma invasion			0.02			0.01			0.03			0.10			0.01
No	144	4.1 (3.9–4.3)		146	192 (173–212)		146	4.9 (4.6–5.0)		146	110 (92–122)		146	0.14 (0.00–0.28)	
Yes	31	4.7 (4.4–5.0)		32	135 (105–221)		32	5.3 (4.8–5.6)		32	138 (94–186)		32	0.55 (0.31–0.91)	
Lymph node metastases			0.004			0.01			**0.001**			0.13			0.03
No	132	4.2 (4.0–4.4)		135	190 (174–205)		135	4.9 (4.6–5.0)		135	111 (94–124)		135	0.16 (0.00–0.30)	
Yes	19	5.1 (3.9–5.5)		19	133 (105–223)		19	5.8 (4.7–6.2)		19	141 (92–186)		19	0.58 (0.06–1.12)	
Histological type/grade			**0.001**			0.01			**<0.001**			**<0.001**			0.02
E1 + 2	109	4.0 (3.9–4.3)		110	192 (173–239)		110	4.8 (4.5–5.0)		110	98 (81–118)		110	0.07 (–0.11–0.28)	
E3+NE	66	4.6 (4.3–4.9)		68	162 (132–192)		68	5.3 (4.9–5.5)		68	143 (112–174)		68	0.46 (0.26–0.62)	
Age			0.21			0.03			0.17			0.01			0.07
<67	90	4.1 (4.0–4.4)		90	193 (173–228)		90	4.9 (4.6–5.0)		90	99 (81–114)		90	0.13 (–0.10–0.33)	
≥67 (median and above)	87	4.4 (4.0–4.6)		90	173 (143–200)		90	5.0 (4.8–5.3)		90	127 (112–150)		90	0.29 (0.13–0.58)	
BMI			0.63			0.89			0.61			0.83			0.70
<25	50	4.4 (3.9–4.7)		50	177 (160–207)		50	4.9 (4.6–5.3)		50	115 (82–146)		50	0.29 (–0.10–0.48)	
≥25 (overweight)	124	4.2 (4.0–4.4)		126	185 (158–205)		126	4.9 (4.7–5.1)		126	113 (100–134)		126	0.22 (0.03–0.35)	

[a]Mann-Whitney *U* -test.
[b]Highest ranked texture parameter for prediction of myometrial invasion.
[c]Highest ranked texture parameter for prediction of cervical stroma invasion.
[d]Highest ranked texture parameter for prediction of lymph node metastases.
[e]Highest ranked texture parameter for prediction of histological type/grade.
[f]Highest ranked texture parameter for prediction of recurrence- and progression-free survival. Significant *P* values after modified Bonferroni correction (< 0.002) are given in **bold**. ADC, apparent diffusion coefficient (maps); BMI, body mass index; CI, confidence interval; E1-3, endometrioid grade 1-3; MPP, Mean of positive pixels; MRI, magnetic resonance imaging; NE, nonendometrioid; T1c, contrast enhanced T1-weighted (images); T2, T2-weighted (images).

TABLE 3. Diagnostic Performance of Top-Ranked Tumor Texture Parameters Using Cutoffs and of Conventional MRI Readings for Assessment of Key Staging Parameters in Endometrial Cancer

		Sensitivity	Specificity	Accuracy
Deep myometrial invasion	ADC_Entropy6[a] > 4.49	0.70 (53/76)	0.84 (83/99)	0.78 (136/175)
	MRI reading DMI+	0.72 (55/76)	0.69 (68/99)	0.70 (123/175)
		[$P = 0.82$]	[$\boldsymbol{P = 0.004}$]	[$\boldsymbol{P = 0.015}$]
Cervical stroma invasion	T2_MPP4[b] < 137	0.53 (17/32)	0.78 (114/146)	0.74 (131/178)
	MRI reading CSI+	0.31 (10/32)	0.93 (136/146)	0.82 (146/178)
		[$P = 0.12$]	[$\boldsymbol{P < 0.001}$]	[$\boldsymbol{P < 0.001}$]
Lymph node metastases	T1c_Entropy6[c] > 5.31	0.68 (13/19)	0.73 (99/135)	0.72 (112/154)
	MRI reading LNM+	0.42 (8/19)	0.97 (131/135)	0.90 (139/154)
		[$P = 0.13$]	[$\boldsymbol{P < 0.001}$]	[$\boldsymbol{P < 0.001}$]

[a]Highest ranked texture parameter for prediction of myometrial invasion.
[b]Highest ranked texture parameter for prediction of cervical stroma invasion.
[c]Highest ranked texture parameter for prediction of lymph node metastases. Cutoffs for texture variables are determined by ROC-curve analysis selecting the highest Youden index. Significant differences in diagnostic performance ($P < 0.05$) are given in **bold**. *P*-values refer to McNemar's test. ADC, apparent diffusion coefficient (maps); CSI, cervical stroma invasion; DMI, deep myometrial invasion; LNM, lymph node metastases; MPP, mean of positive pixels; MRI, magnetic resonance imaging; ROC, receiver operator characteristics; T1c, contrast-enhanced T1-weighted (images); T2, T2-weighted (images).

T_1cKurtosis2 below the median value. Similarly, for patients with ADC_Entropy6 at or above the median value, 51% received adjuvant treatment compared to 26% among patients with ADC_Entropy6 below the median value.

Discussion

In this large, population-based study we demonstrated that texture parameters derived from preoperative MRI are significantly associated with high-risk disease and reduced survival in endometrial cancer. Our findings suggest that tumor texture analysis yields clinically relevant imaging markers that may aid in the preoperative staging and risk assessment.

Surgical staging and subsequent histological assessment have traditionally been the primary basis for treatment and prognostication in endometrial cancer, thereby allowing only limited risk stratification prior to surgery. In this study, we link novel MRI features to established risk factors in endometrial cancer, and identify tumor texture parameters that noninvasively and accurately predict high-risk status preoperatively. Compared to conventional anatomical MRI interpretation, the top-ranked texture parameter ADC_Entropy6 has significantly higher accuracy for prediction of DMI. Also in multivariable analyses, when adjusting for other relevant markers available preoperatively, the texture parameters remain significant and independent predictors of DMI (ADC_Entropy6) and high-risk histological subtype (T_1c_MPP4). Similarly, in the survival analysis the top-ranked texture parameter, T_1c_Kurtosis2, is a significant and independent predictor of RPFS, comparable to MRI-measured tumor volume, which has previously been reported as a strong prognostic factor.[21] Differences in adjuvant treatment in the study population could theoretically influence survival, since adjuvant treatment expectedly improves survival. However, since adjuvant treatment was more frequently administered in the poor outcome group when stratifying patients according to the highest-ranked texture features (Fig. 4), this seems highly unlikely to have biased our results.

Interestingly, a recent preliminary MRI study using TexRAD in endometrial cancer[10] found that a subset of 11 texture parameters jointly predicted DMI with an AU-ROC of 0.84. Similarly, in our study the top-ranked single parameter, ADC_Entropy6, predicted DMI with an AU-ROC of 0.81. For prediction of high-grade tumor, a subset of 16 texture parameters jointly yielded an AU-ROC of 0.83,[10] whereas the top-ranked single parameter in our study, T_1c_MPP4, yielded an AU-ROC of 0.66. However, in spite of being based on somewhat different approaches, both studies suggest a very promising role of MRI texture analysis for better preoperative risk assessment in endometrial cancer.

In our study, comprising tumor texture analysis of T_1c images, T_2 images, and ADC-maps, we found the parameters entropy, MPP, and kurtosis to be associated with high-risk endometrial cancer to a larger extent than SD and skewness. As the texture features are pure mathematical descriptors of histogram shape, their biological correlates are somewhat unclear, and very few publications have tried to translate these features into structural or physiological tissue characteristics.[22]

TABLE 4. Univariable and Multivariable Logistic Regression for Prediction of Deep Myometrial Invasion, Cervical Stroma Invasion, Lymph Node Metastases, and High-Risk Histological Subtype at Surgical Staging

		Univariable		Multivariable	
Dependent variable (based on surgical staging/pathology)	**Predicting variable (from preoperative imaging and biopsy)**	**Unadjusted OR (95% CI)**	***P***	**Adjusted OR (95% CI)**	***P***
Deep myometrial invasion	ADC_Entropy6	4.7 (2.8–7.8)	**<0.001**	3.2 (1.7–6.1)	**<0.001**
	MRI tumor volume	1.05 (1.03–1.07)	**<0.001**	1.01 (0.99–1.03)	0.36
	MRI reading DMI+	5.3 (2.8–10.1)	**<0.001**	2.0 (0.9–4.4)	0.08
	High-risk biopsy[a]	1.2 (0.6–2.2)	0.66	0.7 (0.3–1.6)	0.41
Cervical stroma invasion	T2_MPP4	0.995 (0.99–1.00)	0.03	0.996 (0.99–1.00)	0.11
	MRI tumor volume	1.006 (1.00–1.01)	0.02	0.999 (0.99–1.01)	0.77
	MRI reading CSI+	6.2 (2.3–16.6)	**<0.001**	4.5 (1.4–14.3)	**0.01**
	Biopsy Cervix+	2.2 (1.2–3.9)	0.01	2.0 (1.1–3.9)	**0.03**
Lymph node metastases	T1c_Entropy6	3.1 (1.5–6.6)	0.003	1.7 (0.7–4.3)	0.26
	MRI tumor volume	1.02 (1.01–1.03)	0.007	1.01 (0.99–1.03)	0.43
	MRI reading LNM+	23.8 (6.2–91.8)	**<0.001**	14.0 (3.2–61.0)	**<0.001**
	High-risk biopsy[a]	3.0 (1.1–8.0)	0.03	1.6 (0.5–5.2)	0.45
High-risk histological subtype[a]	T1c_MPP4	1.01 (1.00–1.01)	**0.001**	1.01 (1.00–1.01)	**0.004**
	MRI tumor volume	1.02 (1.01–1.04)	**<0.001**	1.02 (1.00–1.04)	**0.02**
	High-risk biopsy[a]	22.7 (9.5–54.4)	**<0.001**	24.6 (9.6–63.5)	**<0.001**

The top-ranked texture parameter is included in each category.
[a]High-risk histological subtype is defined as endometrioid grade 3 or nonendometrioid subtype as opposed to low-risk histological subtype defined as endometrioid grade 1 and 2. Similarly, high-risk biopsy is defined as endometrioid grade 3 or nonendometrioid subtype.
Cervical tumor involvement in the preoperative endocervical curettage is notated Biopsy Cervix+.
Significant *P* values (after modified Bonferroni correction in univariable analysis ($P < 0.002$) and $P < 0.05$ in multivariable analysis) are given in **bold.**
ADC, apparent diffusion coefficient (maps); CI, confidence interval; CSI, cervical stroma invasion; LNM, lymph node metastases; MPP, mean of positive pixels; MRI, magnetic resonance imaging; OR, odds ratio; T1c, contrast-enhanced T1-weighted (images); T2, T2-weighted (images).

However, entropy reflects textural irregularity and is clearly linked to tissue heterogeneity. MPP is a TexRad specific feature, which in MRI is relevant only in filtered images, ie, when pixels are recoded into a range of positive values or negative values according to their native values. Consequently, MPP reduces the impact of dark objects in the image (eg, nonenhancing fluid collections in T_1c images), as elaborated in a review by Miles et al.[23] Kurtosis reflects the shape of the histogram in terms of pointedness, taking into account the relation between centrum and periphery, ie, high kurtosis typically reflects frequent extreme deviations, as opposed to frequent modestly sized deviations yielding lower kurtosis values. When applied to T_1c images, T_2 images, and ADC maps, the texture parameters in particular reflect heterogeneity in terms of neoangiogenesis, cellular distribution, and cellular density, respectively.[22] The TexRad-specific filtering algorithm is hypothesized to enhance the biologically relevant information in medical images.[23] Among our high-ranked predictors, we found texture parameters of all filter levels, often highly correlated. We did not see a clear pattern in which certain filter levels had a better predictive or prognostic performance than others. This observation complies with previous TexRad-based publications, including the previous endometrial cancer study, in which no specific filter level has proven general superiority.[10] Our findings also illustrate some of the diversity and complexity of radiomics; characterizing cancers of different origin, type, subtype, and grade, using images originating from different modalities and protocols and employing image analyses being inherently software- and operator-dependent.

In routine clinical practice, conventional MRI is widely established as a useful tool in the preoperative assessment of endometrial cancer. Adding texture analysis does not increase scan time, nor patient-related side effects.

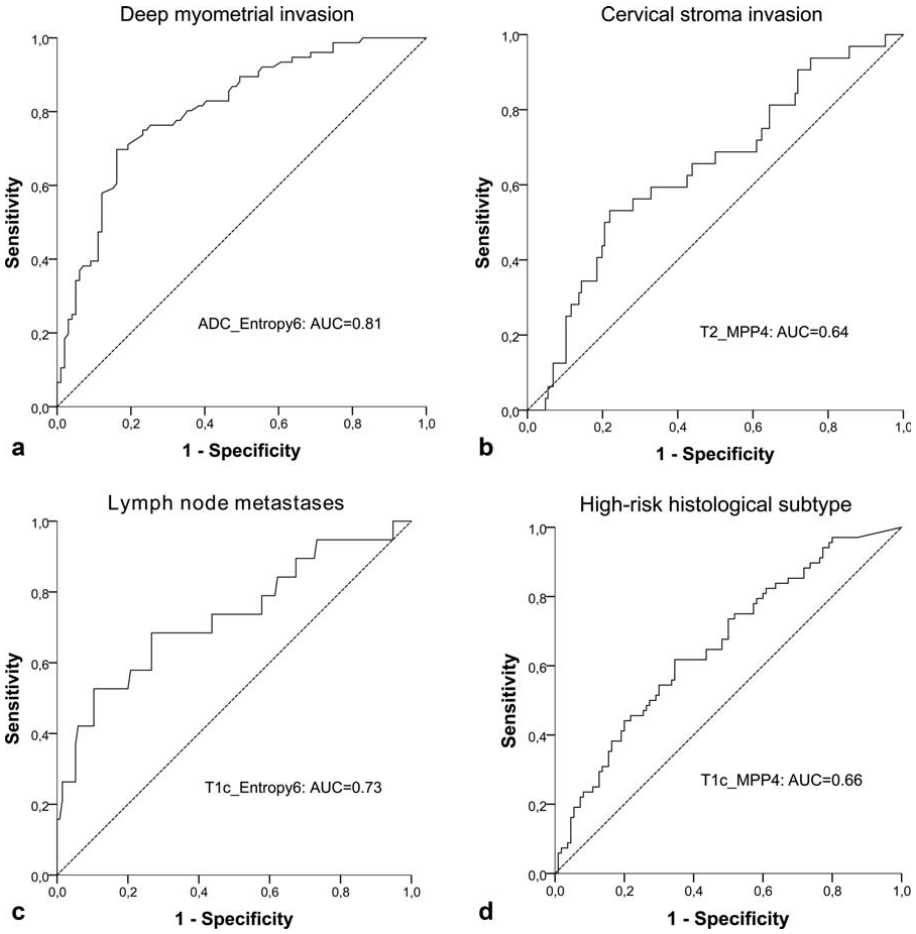

FIGURE 3: Receiver operator characteristics (ROC) curves visualizing the diagnostic performance of the top-ranked texture parameters for predicting presence of the staging parameters deep myometrial invasion (a), cervical stroma invasion (b), lymph node metastases (c), and for high-risk histological subtype (d). ADC_entropy6 yielded an area under the curve (AUC) of 0.81 ($P < 0.001$) for prediction of deep myometrial invasion (a), T_2_MPP4 an AUC of 0.64 ($P = 0.01$) for prediction of cervical stroma invasion (b), T_1c_Entropy6 and AUC of 0.73 ($P = 0.001$) for prediction of lymph node metastases (c), and T_1c_MPP4 and AUC of 0.66 ($P < 0.001$) for prediction of high-risk histological subtype (d). *P*-values refer to the test of equal areas under the diagonal and the ROC-curve.

With a PACS-integrated software, texture analysis can be executed with only a few minutes operator time per case. The decisive steps are image selection and tumor segmentation, which in our study were done manually. With advances in technology, semiautomated and automated tumor segmentation is increasingly available. However, this approach was not within the scope of our study. Extending the analysis from a 2D approach (largest cross-sectional tumor area) to a 3D approach (whole tumor) would also be more feasible based on automatic segmentation. One publication on CT texture analysis of colorectal cancer compared the 2D to 3D approach and found 3D analysis to be slightly more representative of tumor heterogeneity and yielded better prognostic information.[24] This was, however, a relatively small ($n = 55$) and retrospective study, and the benefit of the 3D approach should be further evaluated—also taking into account its time-consuming nature.

Our study has some limitations. First, the study was conducted in a single institution using a standardized imaging protocol. Thus, our results are not necessarily generally applicable to different scanners or patient populations. However, the imaging protocol was largely based on ESUR guidelines and would be expected to be similar in clinical practice elsewhere. Second, intra- and interobserver

TABLE 5. Univariable and Multivariable Cox Regression Analysis for Prediction of Recurrence- and Progression-Free Survival

Variables included in analyses		Univariable		Multivariable	
		Unadjusted HR (95% CI)	*P*	Adjusted HR (95% CI)	*P*
Three highest-ranked texture parameters	T1c_Kurtosis2	1.7 (1.3–2.3)	**<0.001**	1.6 (1.2–2.1)	**0.003**
	T1c_Entropy6	2.1 (1.4–3.2)	**<0.001**	0.7 (0.2–2.5)	0.61
	ADC_Entropy6	2.0 (1.4–2.9)	**<0.001**	2.1 (0.7–6.3)	0.17
Top-ranked texture parameter and other preoperative markers	T1c_Kurtosis2	1.7 (1.3–2.3)	**<0.001**	1.5 (1.2–2.0)	**<0.001**
	MRI tumor volume	1.01 (1.00–1.01)	**<0.001**	1.01 (1.00–1.01)	**0.007**
	High-risk biopsy[a]	4.3 (2.3–8.0)	**<0.001**	3.4 (1.8–6.4)	**<0.001**

[a]Categorical variable. High-risk biopsy is defined as endometrioid grade 3 or nonendometrioid subtype as opposed to low-risk comprising endometrioid grades 1 and 2.
Significant *P* values (after modified Bonferroni correction in univariable analysis ($P < 0.002$) and $P < 0.05$ in multivariable analysis) are given in **bold**.
ADC, apparent diffusion coefficient (maps); CI, confidence interval; HR, hazard ratio; MRI, magnetic resonance imaging; T1c, contrast-enhanced T1-weighted (images).

variability for the texture measurements was not assessed in this study, which was based on manual segmentation. Valid, automated tumor segmentation tools could potentially overcome interobserver variability, and this should be explored in future research. Lastly, the histogram-based approach in TexRAD does not cover all aspects of texture analysis. Our findings should encourage future research with even more sophisticated image texture analysis.

In summary, preoperative tumor texture analysis from MRI independently predicts high-risk disease and reduced survival in endometrial cancer. This approach using texture analysis to yield prognostic biomarkers may ultimately guide tailored treatment in endometrial cancer. However, the value of image texture analysis in endometrial cancer needs to be further evaluated and validated across observers, centers, and platforms prior to potential implementation in the clinic.

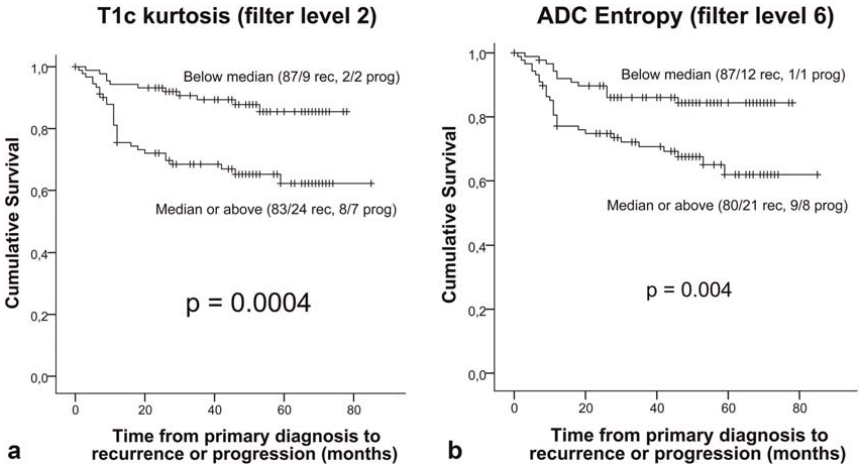

FIGURE 4: Kaplan–Meier curves depicting significantly different patient survival for the two highest-ranked tumor texture parameters: T_1c_Kurtosis2 (a) and ADC_Entropy6 (b). High tumor values for T_1c_Kurtosis2 (a) and for ADC_Entropy6 (b) were significantly associated with reduced recurrence- and progression free survival ($P = 0.0004$ and $P = 0.004$, respectively). *P*-values refer to the Mantel–Cox (log-rank) test.

Conflict of Interest

B.G. is a director, part-time employee of TexRAD Ltd, and shareholder of Feedback Plc (Cambridge, England, UK), the company owns TexRAD Ltd and develops and markets the TexRAD texture analysis algorithm described in this article.

Acknowledgment

Contract grant sponsor: Western Norway Regional Health Authority; Contract grant sponsor: University of Bergen; Contract grant sponsor: Bergen Research Foundation; Contract grant sponsor: MedViz, a medical imaging and visualization R&D cluster in Western Norway.

References

1. Andor N, Graham TA, Jansen M, et al. Pan-cancer analysis of the extent and consequences of intratumor heterogeneity. Nat Med 2016; 22:105–113.
2. Morris LG, Riaz N, Desrichard A, et al. Pan-cancer analysis of intratumor heterogeneity as a prognostic determinant of survival. Oncotarget 2016;7:10051–10063.
3. Gerlinger M, Rowan AJ, Horswell S, et al. Intratumor heterogeneity and branched evolution revealed by multiregion sequencing. N Engl J Med 2012;366:883–892.
4. Gillies RJ, Kinahan PE, Hricak H. Radiomics: Images are more than pictures, they are data. Radiology 2016;278:563–577.
5. Sala E, Mema E, Himoto Y, et al. Unravelling tumour heterogeneity using next-generation imaging: Radiomics, radiogenomics, and habitat imaging. Clin Radiol 2017;72:3–10.
6. Rose CJ, Mills SJ, O'Connor JP, et al. Quantifying spatial heterogeneity in dynamic contrast-enhanced MRI parameter maps. Magn Reson Med 2009;62:488–499.
7. Ganeshan B, Goh V, Mandeville HC, Ng QS, Hoskin PJ, Miles KA. Non-small cell lung cancer: histopathologic correlates for texture parameters at CT. Radiology 2013;266:326–336.
8. Ahmed A, Gibbs P, Pickles M, Turnbull L. Texture analysis in assessment and prediction of chemotherapy response in breast cancer. J Magn Reson Imaging 2013;38:89–101.
9. Wibmer A, Hricak H, Gondo T, et al. Haralick texture analysis of prostate MRI: utility for differentiating non-cancerous prostate from prostate cancer and differentiating prostate cancers with different Gleason scores. Eur Radiol 2015;25:2840–2850.
10. Ueno Y, Forghani B, Forghani R, et al. Endometrial carcinoma: MR imaging-based texture model for preoperative risk stratification-A preliminary analysis. Radiology 2017;284:748–757.
11. Amant F, Moerman P, Neven P, Timmerman D, Van LE, Vergote I. Endometrial cancer. Lancet 2005;366:491–505.
12. Pecorelli S. Revised FIGO staging for carcinoma of the vulva, cervix, and endometrium. Int J Gynaecol Obstet 2009;105:103–104.
13. Salvesen HB, Haldorsen IS, Trovik J. Markers for individualised therapy in endometrial carcinoma. Lancet Oncol 2012;13:e353–e361.
14. Frei KA, Kinkel K. Staging endometrial cancer: Role of magnetic resonance imaging. J Magn Reson Imaging 2001;13:850–855.
15. Kinkel K, Forstner R, Danza FM, et al. Staging of endometrial cancer with MRI: Guidelines of the European Society of Urogenital Imaging. Eur Radiol 2009;19:1565–1574.
16. Sala E, Rockall AG, Freeman SJ, Mitchell DG, Reinhold C. The added role of MR imaging in treatment stratification of patients with gynecologic malignancies: What the radiologist needs to know. Radiology 2013;266:717–740.
17. Haldorsen IS, Salvesen HB. Staging of endometrial carcinomas with MRI using traditional and novel MRI techniques. Clin Radiol 2012;67:2–12.
18. Haldorsen IS, Husby JA, Werner HM, et al. Standard 1.5-T MRI of endometrial carcinomas: modest agreement between radiologists. Eur Radiol 2012;22:1601–1611.
19. Silverberg RJ, Kurman RJ, Nogales F. Tumors of the uterine corpus. In: Tavassoli FA, Devilee P (eds.). Tumours of the breast and female genital organs. World Health Organization Classification of Tumours. Pathology & Genetics. Lyon, France: IACR Press, 2003;217–258.
20. Ytre-Hauge S, Husby JA, Magnussen IJ, et al. Preoperative tumor size at MRI predicts deep myometrial invasion, lymph node metastases, and patient outcome in endometrial carcinomas. Int J Gynecol Cancer 2015;25:459–466.
21. Todo Y, Watari H, Okamoto K, et al. Tumor volume successively reflects the state of disease progression in endometrial cancer. Gynecol Oncol 2013;129:472–477.
22. Just N. Improving tumour heterogeneity MRI assessment with histograms. Br J Cancer 2014;111:2205–2213.
23. Miles KA, Ganeshan B, Hayball MP. CT texture analysis using the filtration-histogram method: What do the measurements mean? Cancer Imaging 2013;13:400–406.
24. Ng F, Kozarski R, Ganeshan B, Goh V. Assessment of tumor heterogeneity by CT texture analysis: Can the largest cross-sectional area be used as an alternative to whole tumor analysis? Eur J Radiol 2013;82:342–348.

Suppl. table 1
Spearman correlation coefficients (r_s) for the top ranked texture parameters in table 2 at different filter levels (SSF 0-6).

		ADC_Entropy [a]						T2_MPP [b]						T1c_Entropy [c]						T1c_MPP [d]						T1c_Kurtosis [e]					
SSF		0	2	3	4	5	6	0	2	3	4	5	6	0	2	3	4	5	6	0	2	3	4	5	6	0	2	3	4	5	6
0																															
2	r_s	>0.99 **						0.41 **						0.96 **						0.38 **						0.42 **					
3	r_s	>0.99 **	>0.99 **					0.43 **	0.96 **					0.96 **	>0.99 **					0.42 **	0.86 **					0.45 **	0.71 **				
4	r_s	>0.99 **	>0.99 **	>0.99 **				0.44 **	0.90 **	0.97 **				0.96 **	>0.99 **	>0.99 **				0.38 **	0.57 **	0.80 **				0.51 **	0.53 **	0.81 **			
5	r_s	>0.99 **	>0.99 **	>0.99 **	>0.99 **			0.44 **	0.83 **	0.92 **	0.97 **			0.96 **	>0.99 **	>0.99 **	>0.99 **			0.33 **	0.35 **	0.59 **	0.88 **			0.56 **	0.39 **	0.45 **	0.76 **		
6	r_s	>0.99 **	>0.99 **	>0.99 **	>0.99 **	>0.99 **		0.44 **	0.74 **	0.82 **	0.89 **	0.97 **		0.96 **	>0.99 **	>0.99 **	>0.99 **	>0.99 **		0.27 **	0.22 *	0.45 **	0.75 **	0.93 **		0.48 **	0.28 **	0.20 *	0.43 **	0.84 **	

* Correlation is significant at the 0.05 level (2-tailed).
** Correlation is significant at the 0.002 level (2-tailed).

[a] ADC_Entropy6 was the highest ranked texture parameter for prediction of myometrial invasion.

[b] T2_MPP4 was the highest ranked texture parameter for prediction of cervical stroma invasion.

[c] T1c_Entropy6 was the highest ranked texture parameter for prediction of lymph node metastases.

[d] T1c_MPP4 was the highest ranked texture parameter for prediction of histological type/grade.

[e] T1c_Kurtosis2 was the highest ranked texture parameter for prediction of recurrence- and progression-free survival.

ADC, apparent diffusion coefficient (maps); MPP, mean of positive pixels; SSF, spatial scale of filtration; T1c, contrast enhanced T1-weighted (images); T2, T2-weighted (images).

Suppl. table 2
Range of Spearman correlation coefficients (r_s) among texture parameters of different filter levels (SSF 0-6).

	Standard deviation	Entropy	Skewness	MPP	Kurtosis
	r_s	r_s	r_s	r_s	r_s
T1c	0.35 – 0.91	0.96 – 1.00	0.00 – 0.87	0.22 – 0.93	0.20 – 0.84
T2	0.50 – 0.95	0.86 – 0.99	0.14 – 0.88	0.41 – 0.97	0.32 – 0.87
ADC	0.60 – 0.96	0.99 – 1.00	0.18 – 0.90	0.29 – 0.91	0.29 – 0.91

ADC, apparent diffusion coefficient (maps); MPP, mean of positive pixels; SSF, spatial scale of filtration; T1c, contrast enhanced T1-weighted (images); T2, T2-weighted (images).

Suppl. table 3
Range of Spearman correlation coefficients (r_s) among texture parameters from MR images (T1c/T2/ADC) at the same filter level (SSF).

	Standard deviation	Entropy	Skewness	MPP	Kurtosis
	r_s	r_s	r_s	r_s	r_s
T1c/T2/ADC	0.18 – 0.46	0.76 – 0.95	-0.17 – 0.30*	-0.48 – 0.35**	0.10 – 0.37

* Lowest absolute value: 0.00

** Lowest absolute value: 0.02

ADC, apparent diffusion coefficient (maps); MPP, mean of positive pixels; MR, magnetic resonance; SSF, spatial scale of filtration; T1c, contrast enhanced T1-weighted (images); T2, T2-weighted (images).

Suppl. table 4

Top 10 ranked MRI derived texture parameters for predicting clinical and histological characteristics and survival in 180 endometrial carcinoma patients.

	Deep myometrial invasion (Yes/No)		Cervical stroma invasion (Yes/No)		Lymph node metastases (Yes/No)		Histological grade (E1+E2 vs E3+NE)		Recurrence- and progression-free Survival	
Rank	Texture parameter	p*	Texture parameter	p*	Texture parameter	p*	Texture parameter	p*	Texture parameter	p+
1	ADC_Entropy6	**3.02×10^{-12}**	T2_MPP4	0.0119	T1c_Entropy6	**0.00114**	T1c_MPP4	**0.000297**	T1c_Kurtosis2	**0.000027**
2	ADC_Entropy4	**3.59×10^{-12}**	T2_MPP3	0.0125	T1c_Entropy5	**0.00144**	T1c_MPP5	**0.000692**	ADC_Entropy6	**0.000148**
3	ADC_Entropy3	**3.66×10^{-12}**	ADC_Entropy4	0.0131	T1c_Entropy2	**0.00150**	T1c_Entropy0	**0.000741**	ADC_Entropy4	**0.000149**
4	ADC_Entropy2	**3.82×10^{-12}**	T1c_Kurtosis2	0.0139	T1c_Entropy3	**0.00147**	T1c_Entropy6	**0.000786**	ADC_Entropy2	**0.000150**
5	ADC_Entropy5	**3.99×10^{-12}**	ADC_Entropy2	0.0139	T1c_Entropy4	**0.00167**	T1c_MPP3	**0.000821**	ADC_Entropy3	**0.000155**
6	ADC_Entropy0	**5.32×10^{-12}**	ADC_Entropy3	0.0144	ADC_Entropy0	0.00314	T1c_Entropy3	**0.000834**	ADC_Entropy5	**0.000168**
7	T1c_Entropy0	**6.01×10^{-12}**	ADC_Entropy5	0.0149	T1c_Entropy0	0.00315	T1c_Entropy2	**0.000848**	ADC_Entropy0	**0.000308**
8	T1c_Entropy6	**1.43×10^{-11}**	ADC_Entropy6	0.0151	ADC_Entropy2	0.00322	T1c_Entropy5	**0.000867**	T1c_Entropy6	**0.000446**
9	T1c_Entropy5	**2.37×10^{-11}**	T2_MPP2	0.0170	ADC_Entropy4	0.00325	T1c_Entropy4	**0.000876**	T1c_Entropy5	**0.000581**
10	T1c_Entropy2	**3.81×10^{-11}**	T1c_Entropy0	0.0174	ADC_Entropy3	0.00331	ADC_Entropy5	**0.001125**	T1c_Entropy4	**0.000626**

* Mann-Whitney U Test.

+ Univariable Cox regression analysis.

Texture parameters differing only in filter level (SSF 0-6) are grouped by colors.

Significant p values after modified Bonferroni correction (<0.002) are given in **bold**.

ADC, apparent diffusion coefficient (maps); E1-3, endometrioid grade 1-3; MPP, mean of positive pixels; MRI, magnetic resonance imaging; NE, non-endometrioid; SSF, spatial scale of filtration; T1c, contrast enhanced T1-weighted (images); T2, T2-weighted (images).

Appendix

MR registration form in endometrial cancer

Patient number	Images read by (initials)
Date of reading	

Lesions are numbered consecutively according to decreasing size and primary location is specified: Fundus, **F**, Corpus **CO**, Istmus **I**, Cervix **CE**.

Lesions Number: **No**	**Localis.**	Ax on uterus: (transverse diam rel. to uterus x AP) (mm) (VIBE+k)	Sag on uterus: CC diam (mm) (T2)	Maximum infiltr. depth myometr (mm) (VIBE+k)	Minimum distance tumor – serosa (mm) (VIBE+k)	ADC-value	SD ADC-value	ROI (ADC-value) (mm^2)	Tumor limited to uterus (Y/N)
			ADC-values in normal myometrium:						

Lesions **No cont.**	Tumor limited to endometrium (E) / <50 % of myometrium (A) ≥ 50 % of myometrium (B)	Tumor in cervix (Y/N)	If Yes: Endo-cervix (E) Stroma (S)	If Yes: ADC-value cervix	Tumor growth serosa (Y/N)	Tumor growth adnex (Y/N)	Tumor growth vagina (Y/N)	Parailiac or paraaortic lymphadenopathy (largest short-axis diam ≥ 8 / 10 mm)(Y/N)

Lymph-nodes Numbered in decreasing size	Largest short-axis diam (mm)	Right (R)/ Left (L)/ Midline (M)	Close to ilica ext. (Y/N)	Close to ilica int. (Y/N)	Close to ilica comm. (Y/N)	Para-aortic (Y/N)	ADC-value	SD ADC-value	ROI (ADC-value) (mm^2)

Lymph-nodes cont.	Ratio short axis/ long axis >0.8 (Y/N)	Shape regular (R)/ irregular (I)	Central necrosis (Y/N)

Tumor expansion:	Tumor growth bladder (Y/N)	Tumor growth rectum (Y/N)	Distant metastases (Y/N); if yes, where

Free intraperitoneal fluid (Y/N)	If Yes: Small (↓) Moderate (→) Large (↑) quantities of fluid	Myomas (Y/N)	If Yes: Myomas > 1 cm axial diameter (Y/N)	Nabothi Cysts (Y/N)	Ovarian lesions (Y/N)	Adenomyosis (islands of ectopic endometrium in the myometrium) (Y/N)	If Yes: Thickest junctional zone (mm)	Other findings:

Graphic design: Communication Division, UiB / Print: Skipnes Kommunikasjon AS

uib.no

ISBN: 9788230843796 (print)
9788230865828 (PDF)